submitted Nov. 1 1994 to *JGR* special issue 011 UARS data validation]]

# Validation of UARS MLS Ozone Measurements

1,. Froidevaux, W. G. Read, '1'. A. Lungu, R. E. Cofield, E. F. Fishbein, I), A. 1I' 1OWCI, IL II'. Jarnot, 11.1'. Ridenoure, Z. Shippony, J. W. Waters, J. J. Margitan, I. S. McDermid, R. A. Stachnik

Jet Propulsion Laboratory, California Institute of Technology, Pasadena, CA, U.S.A.

G. E. Peckham

1 leriot- Watt University, Edinburgh, Scotland

G. Braathen

Norsk Institutt for Luftforskning,, Oslo, Norway

'1'. Deshler

University of Wyoming, Laramie, WY, U.S.A.

J. Fishman

NASA Langley Research Center, Hampton, VA, U.S.A.

I). J. Hofmann, and S. J. Oltmans

NOAA CMADL, Boulder, CO, U.S.A.

Abstract

This paper describes the validation]] of ozone data from the Upper Atmosphere Research Satellite (UARS) Microwave Limb Sounder (MI, S). The MLS ozone retrievals arc obtained from the calibrated microwave radiances (emission spectra) in two separate bands, at frequencies near 205 and 183 GHz. Analyses described here focus on the MLS Version 3 data (the first set of files made publicly available). We describe results of simulations performed to assess the quality of the retrieval algorithms, in terms of both mixing; ratio and radiance closure. From actual MLS observations, the 205 GHz ozone retrievals give better closure (smaller radiance residuals) than that from 183 GHz measurements and should be considered more accurate from the calibration aspects. However, the 183 GHz data are less noise-limited in the mesosphere and can provide the most useful scientific results in that region. We compare the retrieved 205 GHz ozone profiles in the mid-to lower stratosphere to ozonesonde measurements at a wide range of latitudes and seasons. Ground-based lidar data from '1'able Mountain, California, provide a good reference for comparisons at higher altitudes. Based on these analyses, comparisons with balloon-borne measurements and others, as W C]] as a detailed budget of estimated uncertainties, MLS results appear to be generally of high quality, with some biases worth mentioning. Results for the lowermost stratosphere ($\sim$50 to 100 hPa) arc still in need of improvement. A set of estimated precision and accuracy values is derived for the M 1,S ozone datasets. We also comment on recent updates in the retrieval algorithms ant] their impact on ozone values.

## 1. Introduction

The Microwave Limb Sounder (MLS) aboard the Upper Atmosphere Research Satellite (UA RS) has been performing emission measurements of the upper atmosphere on a global scale, day and night, since late September 1991. 1 descriptions and analyses of these and other (JARS observations have been described in a variety of articles; in particular, special issues dealing with UARS results can be found in the *Geophys. Res. Lett.*, Vol. 20, No. 12, 1993, and the *J. Atmos. Sci.*, Vol. 51, No. 20, 1994.

This paper adresses the quality of MLS ozone data, their expected uncertainties (both random and systematic) as well as their demonstrated accuracy, based cm comparisons with other datasets. This information should be of use to those attempting to use MLS ozone data, whether for comparison with other datasets, for absolute values to be used for example in radiative calculations, or for temporal and spatial variations, where precision matters more than accuracy. Since M 1,S ozone measurements arc made from two independent radiometers (near frequencies of 205 GHz and 183 GHz), wc discuss the quality of both of these datasets. However, we focus on the more accurate 205 GHz results, at least in the intercomparisons with other datasets. Additional analyses of the 183 GHz ozone data in the mesosphere (where the measurement sensitivity is better than for 205 GHz) are presented in *Ricaud et al.* (1994), in relation to models and ground-based measurements. Several validation workshops have been held among UARS investigators since the launch of UARS, and the evolving resu Its from those workshops have been documented (see e.g. *Grose* and *Gille*, 1994). Some validation of the zonal mean ozone values from MLS has already been provided in comparisons with TOMS total column data (*Froidevaux et* aL, 1994), where spatial and temporal variations are generally in good agreement. This includes for example the observed development of the ozone hole over Antarctica during southern winter and spring (see also *Manney et al.*, 1993; *Waters et* rd., 1993). Another, less direct type of validation exists in the form of observed ozone variations or waves (e.g. *Canziani et* al., 1994, *Elson et* al., 1994, Ray *et* cd., 1994), to the extent that such variations can be understood, modeled, or "duplicated" in other datasets (current or past).

In this special issue on validation of UARS data, we describe in more detail certain aspects of the M 1,S ozone measurements (section 2), data processing and retrieval specifics (section 3 and Appendix), radiances and closure for both simulated datasets and actual data (section 4), estimated uncertainties based on expected sources of error (section 5), and comparison results (section 6). The comparisons here focus on non-UARS datasets, because for ozone at least, there exists a large amount of accurate correlative data. We comment only briefly here on other existing satellite datasets (see section 6); note that a significant source of validation for MLS ozone can be found in *Cunnold et* al. (1 994a) (see also *Grose* and *Gille*, 1994), where statistical comparisons are made with coincident ozone profiles from the Stratospheric Aerosol and Gas Experiment (SAGE) II ozone data. Also, comparisons of UARS ozone meas urements to each other and to other datasets can be found in *Grose and Gille* (1994) and also in *Cunnold et al.* (1994 b). Wc provide a summary of accuracy and single profile precision values (see section 7) for tile MIS Version 3 ozone datasets currently available. Updated results and plans for continuing improvements arc described in section 8, before the concluding summary. Wc note that this special issue of *J. Geophys. Res.* contains validation papers for other atmospheric parameters from M LS, namely tangent pressure and temperature (*Fishbein et* al., 1994), chlorine monoxide ( *Waters et* al., 1994), and water vapor (*Lahoz et al.*, 1994). In addition, *Jarnot et* al. (1 994) discuss the calibration of MLS radiances, a topic of much relevance to the validation of atmospheric parameters. Furthermore, a detailed description of the forward model used to calculate radiances which are tabulated and used as part of the retrieval process is forth icoming (*Read et* al., in preparation).

## 2. Measurements

UARS M 1,S measurements are obtained from observations of millimeter-wavel ength thermal emission as the instrument field-of-view (FOV) is vertically scanned through the atmospheric limb. A general description of microwave limb sounding and its features is given by *Waters* (1 989, 1993), and the UARS MLS instrument is described by *Barath et* al. (1993).

Each of the 3 MLS radiometers (named "63 GHz", "205 GHz", and "[l 83 G] lz" radiometers because of the frequency near which they operate) receives emission - simultaneously - in a set of filter banks, each spanning 510 MHz in frequency space with 15 contiguous channels of varying width (see *Barath et* al., 1993, *Jarnot et* rd., 1994). The 63 GHz radiometer

measurements (M 1,S baud 1 ) provide tangent pressure and temperature information from $0_2$ emission spectra, the 205 GHz radiometer provides chlorine monoxide - ClO - (bands 2 aucl 3) and ozone (band 4), while the 183 GHz radiometer measures emission lines of water vapor (band 5) and ozone (band 6). In this paper, we will commonly refer to the 205 aud 183 GHz ozone data, following the above radiometer designation. The ozone lines are centered at 206.13205 GHz (1 .45 mm wavelength) aud 184.37782 GHz (1.63 mm wavelength), as listed in *Pickett et* rd. (1992). This spectral data cat alogue and the references therein arc the basis for the spectroscopic calculations used to model the ozone emission, along with the linewidth measurement by *Oh and Cohen* (1 992). The MLS instrument uses double-sideband heterodyne radiometers: signals from two sidebands, equally-sllaccd about the local oscillator frequency, are combined (with slightly unequal weights) into a single measurement. The weights, or sideband ratios, are measured for each channel as part of pre-launch instrument calibration (see *Jarnot et* al., 1 994). The primary sideband measures an atmospheric species of interest; the other is referred to as the image sideband. Fig. 1shows calculated radiances in the spectral domain covered by the 205 GHz radiometer, where ozone and ClO emission arc the primary M LS targets, for typical upper and lower stratospheric signals. Both primary and image sidebands arc shown in Fig. 1, for the MLS bands 2, 3, aud 4 mentioned above. Useful information on other species that emit in this region has also been obtained; this includes $SO_2$ from the Mount Pinatubo eruption (*Read et al.*, 1993), $HNO_3$ (*Santee et* al., 1994), and tropospheric $H_2O$ (*Read et* al., 1994). Other contributions include emission from the wing of a $N_20$ line outside the target bandpass, whit]] becomes significant only in the lowermost stratosphere, and very small emission features from $HO_2$ and a heavy (symmetric $O^{18}OO$ isotope) ozone line. A figure similar to Fig. 1 is shown in *Lahoz et* al. (1 994) regarding the emission features relevant to the 183 GHz radiometer, which includes the other primary ozone line as well as the $H_2O$ line targeted by MLS. The 183 GHz ozone line is four times stronger than the 205 GHz line, and thus provides better signals for the mesospheric region. It is essentially free of contaminant species, except for the lowermost stratosphere, where $H_2O$ continuum emission is present. Also, excess radiation (in comparison to model radiances) is measured by MLS in the essentially "lil]c-free" spectral domain of band 3 below about 30 km tangent height, even in very dry regions of the atmosphere. A contribution from the collision-induced spectrum of molecular nitrogen and oxygen is probabl y responsible, and this continuum, referred to as "dry air continuum", has been fitted empirically and included in the calculated radiances for all MLS bands. Wc discuss in section 5 the potential contribution to ozone mixing ratio errors (systematics) of inaccurate knowledge of the various aforementioned parameters, which can contribute to emission in the ozone band region.

It can be shown ( *Waters*, 1993) that the relative contribution to the measured limb emission, for optically-thin situations, has a Gaussian distribution along the observation path, with center at the tangent point and width equal to the resolution along the line of sight - perpendicular to the UARS velocity -, namely ~400 km. MLS, under normal operations, performs a complete limb scan with radiometric calibrations every 65.536s - a "MIS major frame" during which onc atmospheric profile is retrieved for each species of interest. The limb scan used in normal operations (see *Jarnot et* al., 1994) consists of discrete steps between about 90 and O km tangent, heights, with step spacing for the scan varying between ~1 km in the lower stratosphere to ~5 km in the mesosphere; individual spectra are measured during 1.8s dwells ("MLS minor frames") between steps. Calibration of the radiances occurs during each limb scan, when the MLS switching mirror "switches" to views of the internal blackbody target or space (at a temperature of 2.7 K). The UARS orbital motion (7 km/s) during the limb scan smears the profile measurements over ~400 km in a direction perpendicular to the MLS line-of-sight. The FOV vertical extent at the tangent point for the ozone measurements is ~3 km, the approximate inherent vertical resolution of the measurements. As discussed below, the MLS Version 3 data are produced on a vertical grid with points spaced each factor of $10^{1/3}$ (or 2.15) change in atmospheric pressure, giving a vertical resolution of 5.4 km (for a 7 km pressure scale height). Atmospheric pressure at the tangent point of the observation path is simultaneously measured by observations of thermal emission from molecular oxygen, and this provides the vertical coordinate for the profile retrievals.

The measurement latitudinal coverage is from 34° on onc side of the equator to 80° on the other. UARS performs a yaw maneuver at ~36 day intervals (a "UARS month"), when MLS high-latitude cover-

age switches between north and south. Within each UARS month, the UARS orbit plane precesses slowly with respect to the earth-sun line. The orbit precession causes the measurements to sweep through essentially all local solar times during the course of a UARS month, becoming 20 minutes earlier each day at a fixed latitude.

## 3. Data Processing

Here, we give a description of the general technique used for all MLS Version 3 retrievals, with some mathematical details given in the Appendix. We also present specifics of the retrievals for Version 3 ozone, which is the focus of most of the remainder of this paper. Retrieval specifics for the other primary MLS products are in companion papers by *Fishbein et* al. (1994) for tangent pressure and temperature, *Waters et al.* (1 994) for ClO, and *Lahoz et al.* (1994) for $H_2O$.

MLS data processing produces individual files containing measurements made over a 24 hour period, from O to 24 hours UT on each day. "1'here are two major steps to the processing. 'he first converts raw engineering ( "Level O") data from the instrument telemetry into calibrated radiances and other engineering diagnostics, and produces a "Level 1" file. *Jarnot et* al. (1 994) describe the MLS Level 1 processing. The second processing step converts calibrated radiances from daily level 1 files into geophysical data, producing "l, .evel 2" files (geophysical parameters and estimated uncertainties on a vertical grid chosen by the instrument team). The Level 2 processing step for MIS also produces '(level 3A" files, which are geophysical parameters (one file per parameter) on a vertical grid common to all UARS instruments producing atmospheric profiles. There are two sets of Level 3A files: (1) Level 3AT which has profiles equally spaced in time intervals of 65,536s, and (2) Level 3AL which has profiles equally spaced in latitude intervals of 4 degrees. There are typically 1318 or 1319 profiles in each MLS Level 3AT file, and about 840 profiles in each MLS Level 3AL file. Additional processing of Level 3AL files, described by *Reber and Huang* (1 994), produces Level 3B files which contain data commonly gridded in the horizontal for all UARS instruments producing Level 3A], data; these files can be used to generate "synoptic" fields of mean ozone and its wave components, but various investigators are producing their own version of such fields (e.g. see *Elson* and *Froidevaux*, 1993). Finally, each daily set of M LS Level 3AT and Level 3AL files has an associated Level 3PT and Level 3PL file (named Level 3 parameter files); these files contain additional information, such as diagnostics of the quality of the retrievals for each band, and the overall status of each major frame of M 1,S data. It is strongly recommended that the latter flag be monitored and used to discard bad data (also detectable by checking the sign and/or magnitude of the estimated uncertainties available in Level 3 files, as described below); although bad data are a rare occurrence on a typical day of MLS data, there are certain days/P eriods when certain or all MLS measurements are bad or unavailable, yet climatological (a priori) information can still be found in the data files. A brief summary of some of the above issues and other caveats specific to the currently available MLS data files, as well as a complete description) of the MLS file contents, is in the Standard Formatted Data Units documentation available from the NASA Goddard Space Flight Center Distributed Access Archive Center (DAAC).

### Retrievals

Jig. 2 is a schematic of the UARS MLS measurement geometry. Although not shown in the figure, there are 3 separate radiometers, each viewing at slightly different elevation angles (due to optical design constraints) for a given scan position reference point, given by the 63 GHz radiometer field of view (FOV) direction. These angular differences (measured prior to launch, see *Jarnot et al.*, 1994) are referred to here as $\delta\chi$ and $\delta\chi'$ for the 205 GHz and 183 GHz to 63 GHz FOV elevation differences; they correspond to about -290 m and +50 m in tangent altitude difference, respectively.rl'he equation of radiative transfer is used to calculate tile radiances originating from various tangent points (e.g. $P_1$ and $P_2$ in the figure), as the antenna FOV scans the atmosphere at different elevation angles ( e.g. $\chi_1$ and $\chi_2$). The calculated limb radiance values are then convolved over the antenna pattern and the channel filter response (see *Jarnot et* al., 1994; *Read et al.*, paper in preparation).

The approach used here for retrieving geophysical parameters of interest, such as tangent pressure ($P_{tan}$), temperature ($T$), and mixing ratios ($f$) from the MLS calibrated radiances (Level 1 data) is based 011 sequential estimation, as first applied to limb sounding by *Rodgers* (1976). This technique combines a priori information (such as climatological profiles with an associated error covariance) with rnea-

surement information, to produce a solution for the desired parameters, or state vector $x$ and associated error covariance matrix S. The a priori "state vector" is used to stabilize the solution in regions of poor sensitivity, and to provide some continuity. For example, tangent pressure a priori values in regions of poor measurement sensitivity are obtained from the hydrostatic equation relating changes in pressure to changes in height (h); $h$ is given by $(R_S cos\chi/n) - R_E$, where $R_S$ is the earth center to satellite distance, $R_E$ is the earth radius at the sub-tangent point, and n is the index of refraction at the tangent point. The angular change between $\chi_1$ and $\chi_2$ in Fig. 2 is largely caused by the antenna scan motion between measurements at different minor frames, but also by the spacecraft roll component. These calculations serve as estimates of tangent pressure at heights below 22 hPa (for Version 3 data), where the 63 GHz $O_2$ line is close to saturation, as well as in the top portion of the atmosphere, where M LS retrievals of $P_{tan}$ and $T$ are not currently reliable (see *Fishbein et* al., 1994). Independent parameters such as $R_S$ and $R_E$ are therefore part of the state vector, via their effect on the a priori mode] (or virtual measurement model). The above methodology can be viewed as a combination of the a priori information and the weighted least-squares solution to the linearized equation relating measurements and state vector (see Appendix for a simple derivation).

The update of state vector $x$ is obtained using the following sequence of equations (see *Rodgers*, 1976), for each channel radiance $y_i$ in a given band (or bands), and from top to bottom of the atmosphere:

$$\hat{x}_i = \hat{x}_{i-1} + \frac{\hat{S}_{i-1}K_i\,(y_i - y^c_{i-1})}{K_i^T\hat{S}_{i-1}K_i + \epsilon_i^2 + \omega_i^2}, \qquad (1)$$

$$\hat{S}_i = \hat{S}_{i-1} - \frac{\hat{S}_{i-1}K_iK_i^T\hat{S}_{i-1}}{K_i^T\hat{S}_{i-1}K_i + \epsilon_i^2 + \omega_i^2} \qquad (2)$$

with starting points given by the a priori values $\hat{x}_0 = x_a$ and $S_0 = S_a$; column vector $K_i$ is given by the $i$th row of the weighting function matrix $K = \partial y^c/\partial x$, $\epsilon_i^2$ is the $i$th diagonal element of the measurement error covariance matrix (assumed diagonal for the above equations), and $\omega_i$ is an additional error term discussed below. The calculated radiances $y_i^c$ and their derivatives $K_i$ are obtained by table lookup (for speed of evaluation) from climatological conditions; these values are tabulated for 10 different months (one per "UARS month"), 8 latitude bins (from 70S to 70N in 20 degree increments), 43 tangent pressures (cm the UARS 1.3 grid), and for ascending or descending sides of the orbit (for Doppler shift correction purposes). Radiances are interpolated with respect to tangent pressure using cubic splines and with respect to other variables via the linearized form (bared on tabulated radiances $\overset{*}{y}^c$ and state vector $\overset{*}{x}$) so that the calculated radiances in equation (1) are given by

$$y^c_{i-1} = \overset{*}{y}{}^c{}_{i-1} + K\,(\hat{x}_{i-1} - \overset{*}{x}) \qquad (3)$$

Given that this tabulated linear model is not as accurate as the complete radiative transfer model - so closure may not be as optimum as desired -, we have increased the radiance uncertainties $\epsilon_i$ by an "inflator" factor equal to 1 % of the radiances + 0.75 K for band 1 (see *Fisbein et* rd.,] 994), and by 3% of the radiances for bands 4 through 6; the factor was deemed unnecessary for ClO (bands 2 and 3), since the root mean square (rms) noise is large compared to the radiances in general in that case. Moreover, the term $\omega_i^2$ also includes contributions from variables which can affect the state vector components being retrieved for a particular band, but which are constrained to values $x^c$, with error covariance SC. These uncertainties, some of which may not be purely random, will contribute an additional factor $K_{ci}^T\hat{S}_{i-1}K_{ci}$ as part of $\omega_i^2$ above. For example, temperature and tangent pressure uncertainties - after their evaluation from band J retrievals - have their uncertainties propagated to mixing ratio estimates in this way; also, uncertainties arising from velocities (Doppler shifts) along the FOV direction are treated in this fashion, with no values retrieved, but with the (a priori) uncertainty estimates included in the equations for mixing ratio updates. In terms of the estimated error covariance (whose diagonal elements give the uncertainties in the M LS data files), we note that the retrieval software produces uncertainties which are flagged as negative under conditions of poor measurement sensitivity (see discussion in next sub-section for more details).

The order of the retrievals is chosen as band 1 ($P_{tan}$ and $T$), since $P_{tan}$ is needed first as a vertical coordinate for geophysical parameters and $T$ is used in the radiance calculations for other bands, band 5 ($1\ 1_20$) because of its potential impact on other species -, band 6 (ozone), Lane] 4 (ozone), and bands 2 and 3 (ClO). Table 1 provides a list of the state vector components which are either retrieved or constrained, as a function of band (listed in the above processing order). Among the parameters not mentioned yet are $B$, which represents magnetic field, for its Zeeman splitting effects 011 the $O_2$ line in band ], particularly in the center channels and in the mesosphere

(see *Fishbein et* al., 1994). Also, wc retrieve a set of baseline offsets $y^{off}$ and (for bands 2 and 3) linear coefficients $y^{lin}$, with one component for each minor frame; the a priori values for these are based on the previous minor frame (but with conservatively large a priori uncertainties). Correlations among these coefficients (and for $P_{tan}$ as well) are not rigorously accounted for, since the software overwrites each of these variables after each minor frame; a fuller treatment will be undertaken in future algorithms if necessary, although the effects on mixing ratios are not expected to be very large (based on tests already performed). There are also some parameters which we have not explicitly included in the "J'able, but which are implicitly included in the forward model, or the a priori model. These include the elevation angle $\chi$ and satellite roll angle, which enter in the a priori tangent pressure equation (described above), geometric quantities needed to perform transformations between the UARS MLS reference frames and the earth-centered frame, as well as assumptions for $N_2O$, dry air continuum and a few other trace species in the (tabulated) forward model radiances. We note also that $HNO_3$ emission contribution in band 4 was included as part of the tabulated forward model radiances (based on climatology), but no $HNO_3$ retrievals were attempted in Version 3 data.

No attempt is made to include "memory" from one scan profile (or retrieval) to the next (see *Rodgers*, 1976), except through the a priori (tangent pressure evaluation and climatological geophysical parameters). This was done to preserve independence between consecutive profiles (and to minimize propagation of '%ad"rctrievals), and because it was not obvious from test results that such smoothing (filtering) along the tangent track would give rise to significantly better retrievals. Another important feature of the M 1,S retrievals used in the production of Version 3 data is the use of an "opacity criterion", which eliminates rad iances corresponding to large optical depths along the line-of-sight, because of non-linearity concerns (given the non-iterative linear scheme used so far). This is not used for band 1, since a ]Ioll-linear calculation of radiances is used for this band. For all other bands, if one ignores the image sideband contribution to the radiance, a particular radiance at frequency $\nu$ can be written (approximately) as

$$y(\nu) = g_p(\nu)\, T_{tan}\, (1 - e^{-\tau_p(\nu)}) \qquad (4)$$

where $g_p(\nu)$ is the primary sideband gain factor, $T_{tan}$ is the tangent point temperature, and $\tau_p(\nu)$ is the optical depth along the line of sight. This leads to an estimate of the optical depth, given an estimate of $T_{tan}$ - from band 1 retrievals -, and the measurement $y(\nu)$, namely

$$\tau_p(\nu) = -ln(1 - y(\nu)/g_p(\nu)\, T_{tan}) \qquad (5)$$

When this estimated optical depth is greater than unity, the radiance is ignored in the sequential estimate update equations.

Some of the software features described above are expected to change in future iterative non-linear retrieval algorithms, where more optimum use can be made of the MLS radiances, with essentially no radiance cut-of' criterion, and a reevaluation of the radiance error inflator factors as part of the plans.

## Version 3 Data

The constituent profiles used in Level 2 files for tile M LS Version 3 data are represented as piecewise-linear in mixing ratio versus logarithm of atmospheric pressure, with breakpoints at pressure surfaces of $1000 \times 10^{-n/3}$ hPa where $n$ is an integer. For ozone, the starting and ending values of n arc 1 and 19, which corresponds to pressures of 464 ancl 4.6 x 10-4 hPa, respectively; these fixed boundaries were chosen very conservatively. A subset of this vertical range, most useful for scientific analyses, will be recommended later in this paper. The UARS Level 3 pressure grid ($1000 \times 10^{-n/6}$ hPa values) is twice as fine as the MIS Level 2 grid, and we have simply averaged the adj a-cent Level 2 grid values to fill in the Level 3 grid on the "odd" UARS surfaces. This leads to a reduction in the variability (e.g. about the zonal mean) for these odd pressure surfaces, compared to the even surfaces, since the averaging process reduces random noise.

The error factor added to the radiances (see the sub-section on retrievals above) to account for some of the forward modeling uncertainties was set at 3% of the radiances in both ozone bands. The opacity criterion used to discard radiances because of non-linearity effects was set to unity. Finally, it was found from simulations that better retrievals were obtained if radiances arising from tangent pressures larger than 100 hPa were not included, at least for the non-iterative retrievals used to produce Version 3 data. A more optimum usc of all channels will be sought in future software upgrades.

An example of the a priori values used for ozone is given in Fig. 3, for the month of September. The ozone climatology file was provided by members of

the UARS community, based on values given by *Keating et al.* (1 989a, 1 989b), with extrapolations for the poorly represented lower stratosphere (at pressures larger than 20 hi%). Model values from the Lawrence Livermore National laboratory 2-D model were used to fill in the tropospheric "climatology"; remaining missing data in the mesosphere and above were filled in with standard middle latitude values from the Caltech/JPL 1-D photochemical model. A priori uncertainties are generally chosen conservatively (i.e. large values are used) in order to minimize possible biases. For ozone, a 3 ppmv a priori uncertainty is used in the stratosphere down to 50 hPa, with a 2 ppmv uncertainty at, 100 h l's, and significantly tighter constraints in the troposphere, where no attempt is currently being made to retrieve ozone (climatological fields are found there in the MLS data files). A priori uncertainties decrease smoothly with decreasing pressure in the mesosphere, until about ().2 hPa, above which an uncertainty of 1 ppmv is assumed. Based on sensitivity tests of the influence of a priori values, we find that the 205 GHz ozone retrievals are affected in a non-negligible way by the a priori for pressures near 100 h]'a and above about 0.46 hPa; for the 183 GHz retrievals, these boundaries occur near 46 hI'a and above about 0.046 hPa. The use of a "global" a priori uncertainty is clearly an oversimplification of the variability of the real atmosphere. The possibility of larger-tlia]l-appro]miatc estimated uncertainties in the retrieved profiles exists as a result of this approach, for regions like the lowermost stratosphere where poorer measurement sensitivity exists (see section 5); however, this is a safer approach than the use of a priori uncertainties which are too small, since this can lead to undesirable biases with unrealistically small estimated uncertainties.

As mentioned in the previous sub-section, a diagnostic of the relative sensitivity of measurements and a priori can be obtained by considering the ratio of estimated uncertainty (in the retrieval product) to the a priori uncertainty. Typical (average) values of this "error ratio" arc shown in Fig. 4 for both ozone retrievals at two selected latitudes, on September 17, 1992. This function is characterized by values near unity where no measurement information exists, values close to zero (about 0.1 to 0.3 here) where significant measurement information exists, and a steep gradient in the transition regions where an increasing contribution comes from the a priori. Fig. 4 shows that, below $\sim$ 1 hPa, ozone from the 205 GHz radiometer provides a slightly more sensitive measurement than the 183 GHz data (for Version 3 results). Above 1 h] 'a, the 183 GHz ozone measurements become increasingly more sensitive in comparison to the 205 GHz retrievals; thus, the 183 GHz data are recommended for studies of mesospheric ozone, even if the expected accuracy is less than for the 205 GHz ozone (see section 5).

The "error ratio" is used to qualify retrieved values in the MLS data files. When the error ratio is greater than 0.5 (a fairly conservative value, within the steeply increasing region of Fig. 4), which means that the a priori contributes more than 25% to the result and the measurement-related uncertainty is more than $1/\sqrt{3}$ (or 0.58) times the a priori uncertainty, the estimated uncertainties are flagged with a negative sign. This alerts the user that poorer measurement sensitivity is expected, and the use of data values in these regions is cautioned against, since essentially no MLS measurement information exists beyond the flagged boundaries. The Version 3 data show variations in error ratio versus latitude, particularly for the 183 GHz ozone results, because more channels are being discarded from the retrieval process near the equator in the lllid-stratosphere. Future algorithms will avoid this by iterating over the retrieval process until convergence is reached, thereby allowing all channels to be used to their fullest potential. Such issues are less critical in Version 3 205 GHz results, since essentially all channels are always being used in the current algorithms; however, some improvements may be obtained via more accurate retrievals of other parameters (such as tangent pressure, temperature, and $H_2O$) which can have some impact on the ozone values (see section 5).

A veraging kernels are another, more formal, expression of measurement sensitivity used in the description of error characterization (see *Rodgers*, 1990; *Marks and Rodgers*, 1993). The rows of the averaging kernel matrix represent height-dependent weighting factors by which the true atmospheric profile is multiplied to give the retrieved profile. These functions arc given in Fig. 5 for MLS ozone retrievals representative of Version 3 data, in both frequency bands. The kernels provide a measure of profile sensitivity to changes in the true profiles, and arc equal to unity if no a priori influence exists; their vertical widths give a measure of vertical resolution (smoothing of the true profiles). These figures confirm the information provided above, regarding the relative sensitivity of 205 and 183 GHz retrievals in the current MLS algorithms. Some degradation in measurement sensi-

tivity can be seen in the lower mesosphere and at 100 hPa for the 205 GHz ozone data. The sensitivity is slightly worse for the 183 GHz results at 100 hPa and also at altitudes somewhat above this (for example in equatorial regions - see Fig. 4 -; note that the kernels in Fig. 5 are for ~nid-latitudes). 'The larger values of averaging kernels for the 183 GHz data in the mesosphere imply greater sensitivity in that region than for the 205 GHz data (see also Fig. 4).

## 4. Radiances and Closure

In this section, wc examine the MLS ozone radiances, both from simulations performed in an identical fashion to those producing Version 3 data, and from the actual data. The issue of closure is discussed by analyzing radiance residuals (observed or simulated radiances minus radiances calculated from the retrieved profiles), as well as diagnostics related to the goodness of fit for these radiances. Furthermore, profile residuals can also provide information on retrieval quality, in the case of simulations. For the production retrievals, we discuss known artifacts and caveats (with more information in section 6, based on comparisons with other datasets).

### Simulation results

This subsection describes results of simulation studies, in order to understand "numerical errors" arising from the software used to create the Version 3 data files. Wc do not expect this software to be completely optimum, since it is based on assumptions of linearity and does not fully utilize the complete set of measurements, which leads to some limitations (particularly in the lowermost stratosphere). More computer-intensive retrievals are needed for a fully iterative (non-linear) retrieval scheme - now in preparation.

#### Radiances and Residuals

Radiance residuals have been calculated based on a set of profiles obtained by smoothing actual MI, S-retrieved values for September 17 1992, a day with "ozone hole" conditions in the southern polar regions. The simulation uses the operational MLS scan sequence.

Results from a full day of radiance residuals nave been examined in 10 degree latitude bins as a function of pressure, and a typical subset, for 40 S (latitudes 45 S to 35 S) is shown in Fig. 6. The results are similar in other latitude bins. We see that closure exists at a level of 1 % (of radiances) or better (i.e. less than ~ 0.2 K), except at the lowermost pressure shown (100 hPa), where the calculated radiances arc systematically higher by about 1K than the "observed" radiances (which are of order 20 to 60 K). While this is not a large percentage difference in radiances, retrievals of ozone in the lowermost stratosphere depend more heavily on radiances (or radiance differences) in the outside (wing) channels, and spectral differences introduced between model and observed radiances have the potential to significantly impact ozone values near 100 hPa. As mentioned in section 3, the measurement information - relative to the a priori - is decreasing in the lowermost stratosphere, and this has an impact on the poorer radiance fits obtained there. Better closure has been obtained with test retrievals using a fully iterative method and improved algorithms. The quality of simulated ozone profiles is discussed further below. Figure 7 is similar to Fig. 6, but for the 183 GHz ozone results. Although reasonably good radiance fits arc also evident in these simulations, they arc somewhat worse than those for 205 GHz. The fit at 100 hPa is not an accurate reflection of the actual sensitivity, because we know that the current retrieval scheme has poor sensitivity at that level for the 183 GHz data; as climatology is basically input (from the smoothed, Previously "retrieved" fields at that level) arid the retrieved fields arc similar to the inputs because of non-optimal use of channels, an overly optimistic quality of fit is arrived at.

One can define diagnostics of goodness of fit by using the chi-square ($\chi^2$) concepts from statistical analysis (see *e.g. Bevington*, 1969). We have calculated values of

$$\chi^2_{ma} = \frac{1}{N} \sum \frac{(y_i - y_i^c)^2}{\epsilon_i^2} \qquad (6)$$

for each major frame (set of 32 minor frames). The variables $y_i$, $y_i^c$, and $\epsilon_i$ refer to measured radiance, calculated radiance (linear model used in the retrievals), and random (rms) radiance uncertainty. N is given by the number of degrees of freedom, namely the total number of observations (radiances) minus the number of parameters being retrieved. The above diagnostic is referred to as a reduced chi-square; in the algorithms used to produce Version 3 data files, index $i$ runs over all radiances from the top of the atmosphere to 46 hPa tangent pressure, to avoid too much emphasis 011 the less well-characterized regions in the lowermost stratosphere (wc may carry these

diagnostics down to 100 bl'a in future production algorithms). Too large (or too small) a value of $\chi^2_{ma}$ indicates a poor fit and/or a problem of some kind in the retrievals or measurements. Based on statistics from idealized Gaussian distributions, we have determined that $\chi^2_{ma}$ values above about 2, given the number of degrees of freedom available for each MLS major frame, are cause for concern and truly indicate poor fits. A similar quantity is also calculated for each minor frame, with index $i$ running over all 15 channels (14 for ozone at 183 GHz since one of the wing channels is not reliable and is not used); we denote this diagnostic by $\chi^2_{mi}$. The $\chi^2_{mi}$ values are marginally significant, since the number of measurements is fairly small, but we view these diagnostics as qualitatively useful nevertheless, especially in a relative sense (from minor frame to minor frame, or for different, software runs). Zonal mean values of $\chi^2_{ma}$ and $\chi^2_{mi}$ are given in Fig. 8 for the simulation run mentioned above; radiances with noise similar to the actual instrument noise were used, for a meaningful calculation of $\chi^2$ diagnostics. From the $\chi^2_{mi}$ values, we observe that the quality of radiance fits degrades in the lowermost stratosphere, particularly in the south polar vortex (south of 60 S). Also, the 183 GHz ozone radiance fits are of relatively poorer quality than the 205 GHz fits, especially near 46 hPa, consistent with the radiance fit quality observed in previous figures. The values of $\chi^2_{ma}$ in the bottom panels of Fig. 8 follow the average latitudinal trends of the $\chi^2_{mi}$ values, as expected. Values of $\chi^2_{ma}$ between 1 and 2 are typical for 205 GHz ozone results (average value is near 1 .2). Values between 1.5 and 2 are more typical for 183 GHz ozone, with extrema slightly above 3 (although some larger values exist near the latitude extremes). These results give some lower bounds for the fit quality we may expect in terms of closure based on real data (discussed further below). We will improve upon the simulation results in future software algorithms.

Ozone abundances

The retrieved zonal mean 205 GHz ozone fields are compared to the input ("true") fields in Fig. 9. Zonal mean differences are shown to be $\sim$ 0.1 pprnv or less throughout most of the stratosphere. There is a tendency to underestimate the mixing ratios near 46 hPa and overestimate them at 100 hPa, especially at high latitudes (where the mean biases are of order -0.4 and 0.6 ppmv respectively). This translates into $\sim$ 20 % negative bias in the polar vortex at 46 hPa; at 100 hPa, percentage differences are large, but not as meaningful, because the mixing ratios can become very small - especially in the tropics, but we have to keep these retrieval biases in mind, particularly at high latitudes. We expect to better understand and remove much of these effects in a future data processing, since some of this is undoubtedly related to nonlinear effects (in ozone and/or other parameters which contribute to emission in the ozone band). However, between 0.46 and 22 hPa, the true and retrieved ozone fields differ by less than 2%. The retrieved values near 0.2 hPa become clearly influenced by the a priori values, based on our analyses (see also section 5 below).

Another method of examining the retrieval quality is in terms of the reproducibility of "horizontal" atmospheric features, namely via mapping (simple horizontal gridding in this case) of the Level 3AT ozone fields. We show "true" versus retrieved ozone maps in Fig. 10, for pressures of 46, 10, and 2 hPa; the retrievals are from radiances with simulated noise. The differences at these pressure levels arise from noise as well as underlying systematic (exemplified in the zonal mean differences of Fig. 9). General features and mixing ratio gradients (e.g. at the edge of the Antarctic vortex and in the sub-tropics) are very well reproduced. However, there are some features (especially near the boundaries of color contour values) which can loose some of their continuity or appear slightly different after small biases and noise effects are '(applied'] via the retrieval process. If data users are aware of the noise level and any artifacts or potential biases (as discussed throughout this paper), overinterpretation of maps or MLS results in general should not be a problem.

Figure 11 is similar to the zonal mean cross section comparisons of Fig. 9, but for the 183 GHz results. Overall, somewhat better closure is obtained (in comparison with the 205 GHz ozone retrievals) in the mesosphere, with some evidence for degradation (in percentage terms) at pressures less than 0.1 hPa. Less of a bias (than in Fig. 9) exists near 100 h} 'a, but we mentioned earlier that some of this may be an artificial result because of too tight a constraint towards the a priori (as not enough channels are used). Note that a similar percentage fit to ozone will result in a poorer (larger) value of the $\chi^2$ diagnostic defined above, because the rms radiance noise is comparable for both ozone bands, but the signal is roughly twice as strong for the 183 GHz line (leading to a factor of 4 difference in $\chi^2$ for a given percentage ozone fit). This is a reflection of the fact that the 183 GHz ozone data are inherently more precise, in a relative sense, and

therefore "harder to fit" to within the noise. Based on these results (and other studies not shown here), the upper limit for 183 GHz ozone data usefulness is near 0.05 hPa (see also section 5), and the recommended lower limit is 46 hPa.

## Version 3 Results

This sub-section deals with Version 3 results, and compares radiance residuals and other diagnostics to simulation values. Known artifacts arc also mentioned.

### Radiances and Residuals

Fig. 12 shows radiances and residuals for Sep. 17, 1992 at 40S (similar to the simulations of Fig. 6). Residuals are only slightly worse than those from the simulations. Given that the averaging of radiances leads to negligible (0.02 to 0.1 K) noise in the mean radiances, the residual differences are an indication of residual (systematic) errors. There is also some latitudinal variability in the residuals (more pronounced than in the simulation case). For example, we show in Fig. 13 some of the poorer fits in the lowermost stratosphere, for 10S and 70S. The systematic trends in the residuals at 46 and 100 hPa arc believed to be caused by inaccuracies in the emission features from $HNO_3$ (on the positive frequency end) and $N_20$ (on the negative frequency end); indeed, radiance fits have been found to be significantly improved when $HNO_3$ is retrieved (but this was not done in the Version 3 data). Also, imperfect knowledge of $N_20$ (and $H_2O$) in the lowermost stratosphere and upper troposphere will probably have some small effect on the radiance residuals. in summary, poorer radiance residuals are observed in the lowermost stratosphere, but improvements can be expected in future data versions.

Fig. 14 is similar to Fig. 12, but for 183 GHz *ozone* results for September 17, 1992 at 40S. The radiance residuals are of poorer quality than the 205 GHz ozone results for all pressure levels. At 100 hPa in particular, these plots confirm that little sensitivity exists and that we are attempting to fit climatological radiances (since the retrieval does not perturb the a priori state significantly) to observations. Also, the residual patterns are different than those of Fig. 12. Part of the systematic effects in the upper stratosphere (which appear to have a different origin than the asymmetric residuals in the lower stratosphere) may have to do with a slight lack of closure between the forward model runs used in the retrieval and calculated radiance programs. It would seem (from preliminary tests with a fully iterative retrieval scheme) that a significant part of the systematic effects observed here arc not caused by the linear retrieval scheme's limitations. Therefore, instrumental or forward model errors probably have to be invoked. Pig. 15 is also similar to the 205 GHz figure above (Fig. 13), for radiances and residuals at 10S and 70S in the lower stratosphere, at tangent pressures of 22 and 46 hPa. Residuals are maximized at high latitudes at 46 h} 'a. It would appear from these radiances that the retrieved values from 183 GHz ozone data are too large near 70S latitude, thus leading to too strong a calculated signal, compared to the measured radiances. The future use of all channels in band 6 should help alleviate some of these lower stratospheric issues for 183 GHz ozone data. Also, wc will see in section 8 that updated retrievals using newer spectroscopic data for $0_2$ (MLS band 1 ) reduce the radiance residuals.

Fig. 16 has the same format as Fig. 8 (simulations), and provides a measure of the mean goodness of fit ($\chi^2_{mi}$ and $\chi^2_{ma}$) for both ozone bands, on September 17, 1992. The 205 GHz band results arc only slightly worse than the simulation results, and while there is some room for improvement, the fits arc judged to be of overall high quality (with increasing problems in the lowermost stratosphere). For the 183 GHz ozone band, however, tile goodness of fit is clearly degraded with respect to both the 205 GHz data and the simulation results for 183 GHz ozone, as implied by the radiance residuals discussed above.

Fig. 17 shows the time evolution of the zonal mean goodness of fit diagnostic $\chi^2_{ma}$ as a function of latitude, over the first two years of MLS data acquisition. While we have not identified the cause for poorer residuals at all times and places, this should help caution the data user to be somewhat more careful when the fits are poorer. We believe that the poorer radiance fits in the tropics and mid-latitudes in November 1992 and a few other times in the following year are related to the generation of excess instrumental noise induced by the switching mirror movement at low UARS power supply voltages (a problem now circumvented); this also affects the ClO radiance fits (see *Waters et* rd., *1994*), and to a lesser extent, the 1 83 GHz radiometer data. Also, the 205 GHz ozone near 60S during June/July (early winter), possibly in relation to actual atmospheric variability (and horizontal gradients effects). Slightly poorer (than average) fits arc obtained in the tropics during the first 7 months of the UARS mission; this appears to cor-

relate with the poorer comparisons versus tropical ozonesondes in the time period closest to launch (see section 6). Whether these occurrences exist because of abnormal wave activity, or another atmospheric effect remains to be explained. The poorer quality (in an absolute sense) of radiance fits for the 183 GHz ozone data is again evident in Fig. 17 (bottom panels). The pattern of tropical and subtropical high ($\chi^2_{ma}$) values appears to follow the pattern of zonal mean ozone obtained in the 205 G}1 z data (see *Froidevaux et* cd., 1994). We interpret this to mean that the 183 GHz ozone retrievals cannot (for lack of sensitivity in the current scheme) track the ozone 205 GHz pattern, and this leads to poorer radiance closure.

Ozone abundances

Despite some remaining issues mentioned above, the overall behavior of ozone radiances for the 205 GHz data points to good quality in the results. To confirm this reasonableness issue, Fig. 18 shows zonal mean MLS ozone data (from the 205 GHz band) versus climatology, for January and July at various latitudes. The climatological changes in ozone with latitude and season are quite well reproduced by the MLS data, The main difference occurs at 60S, where the ozone minimum observed by MLS near 10 hPa during July is only a weak feature in the climatology; this may have to CIO with the different vertical resolution of datasets being compared here, and warrants further investigation (the MLS minimum is not an isolated incident and exists in 1992 and 1993, for example). More detailed comparisons with correlative data sets arc discussed in section 6, in order to assess (or confirm) the quality of MLS retrievals.

*Known artifacts in* V3 dater

1 lere, we give a summary of known artifacts associated with the M 1,S Version 3 ozone data (as also briefly mentioned by *Froidevaux et* al., 1994); further work is required to better understand these problems and deal with them.

Ozone at 100 hPa has been consistently difficult to retrieve very accurately, probably because of a combination of reduced spectral signature arising from this altitude region and the difficulty associated with modeling (or retrieving) the underlying bas eline. The poorer retrievals at 100 hPa are particularly evident during the! summer in the tropics, where negative zonal means (of order a fcw tenths of a ppmv) persist. SoI ne of these biases could be related to nonlinearity issues, or maybe to the difficulty associated with fitting an inverted profile with a set of coefficients spaced roughly every 5 km. Also, we have observed "bulges" in the mixing ratio at 100 hPa, where the mixing ratios can become unreasonably large (as much as 1 to 2 ppmv), even in a zonal mean - at high southern latitudes in particular. This effect is exemplified in Fig. 19, where wc give a map of the difference between the mixing ratio (from the 205 GHz ozone) at 46 hPa and 100 hPa; this difference should typically be positive , but the plots illustrate that there arc significant regions where the MLS data yield negative values for this quantity (tropics and high latitudes in particular). These occurrences, aud the possible underestimate which can follow at the 46 hPa level may be related to the regions of poor radiance closure (see Fig. 17 above). Correlative data comparisons confirm that such '(bulges" at 100 hPa are not reproduced by ozonesonde data for example in the southern polar vortex (see section 6).

The 100 hPa level also exhibits a UARS yaw-cycle dependence (see evidence in *Froidevaux et al.*, 1994), *i.e.*, the mixing ratios (and column values) tend to be larger in the middle of the UARS month. This oscillation (which can be of order a few tenths of a ppmv) may be related to similar effects observed in temperature (*Fishbein et* al., 1994) and could be affected by t angent pressure artifacts; such an effect is also observed in lower stratospheric $H_2O$ (Lahoz et al., 1994). Efforts to reduce or remove this artifact have not been successful so far, but a fully iterative retrieval scheme has not yet been applied. Also, as yet unexplained occasional "jumps" in mixing ratios exist across yaw days, particularly at the 100 hPa level. We are investigating these artifacts, which imply poorer measurement accuracy for this lowermost st ratospheric pressure (as expected from the error analysis in section 5).

Since the current 183 GHz ozone retrievals are not sensitive enough at 100 hPa, we arc not advertising this level as a useful one for those retrievals. The main systematic effect to note is the existence of larger ozone values in earlier (not publicly released) MLS data versions, compared to the 205 GHz values, for mid - to upper stratospheric heights. These differences were of order 10-1590 (see Fig. 20) in post-launch retrievals (pre-version 3 data). Although it has become clear that systematic error sources are much more likely for the 183 GHz ozone data (see section 5), and could in principle explain these differences, a full understanding of the actual sources of this discrepancy is not available yet. We also note that the 205 GHz

ozone data have consistently given better comparisons with other datasets (see below) than the 183 GHz results. Uncertainties in sideband ratios and 183 GHz radiometer pointing misalignment could in principle combine to account for a large portion of this effect. An independent analysis of radiometer pointing misalignments through the usc of moon scan analyses (see *Jarnot et.* al., 1 994) has led to the conclusion that a shift (possibly incurred during launch) exists in comparison to the pre-launch alignment determination. The M LS Version 3 data include a shift consistent with these findings, but not quite as large as the final result obtained from the moon scan analyses (possiMy because of compensating sideband ratio errors). Fig. 20 demonstrates the better agreement currently found between the two ozone retrievals, using a semiempirical FOV elevation adjustment to improve the agreement in Version 3 data, We stress that relative variations in 183 GHz ozone data should be emphasized rather than absolute values (for which the 205 GHz data are recommended). A reevaluation of the parameters which can affect the MLS ozone data is in progress, in light also of the newer $O_2$ spectroscopic data, which has affected the retrieved tangent pressures by $\sim 6\,\%$ in more recent analyses (SCC section 5 and *Fishbein et* al., 1994). A brief update concerning this topic is provided in section 8.

## 5. Estimated Uncertainties

In this section, an estimated error budget is formulated. Comparisons with other data sets can help detect biases, and wc will see in the next section how consistent those analyses are with the uncertainties presented here. A list of error sources (mostly systematic in nature) is given in Table 2, and the MIS ozone sensitivity to these factors is studied, primarily via a series of tests for onc day's retrievals. in principle, the error analysis method of Rodgers (1990) could be applied here instead of sensitivity tests, with equivalent results (WC did usc this approach for the measurement noise and a priori error contributions); however, issues like latitude dependence of errors and errors in forward model parameters can sometimes be more easily studied using the actual retrieval algorithms and their sensitivity.

First a comment is worthwhile, regarding the uncertainties listed in the Version 3 MLS data files. In general, the estimated rms uncertainties in these files arc somewhat larger than the actual atmospheric rms variability, particularly in the lowermost altitude range. Fig. 21 is an example of a relatively quiet day (from an atmospheric variability point of view), and shows the ratio of rms variability (about the zonal n leans) to estimated rms uncertainties (from Version 3 ozone results for 205 GHz radiometer data), contoured versus latitude and pressure. Ratios smaller than unity can occur in regions of poor measurement sensitivity, as occurs near the tropopause (especially for 183 GHz ozone), where the a priori constraint can artificially reduce the variability relative to the generally very conservative a priori uncertainty. Also, some error sources included in the retrieval code arc not random in nature (e.g. part of the a priori tangent pressure estimated error arising from pointing knowledge uncertainty, and its impact on ozone). Later in this section, we will compare the uncertainties from the MLS data files to the random and systematic error estimates derived below. We now turn to a discussion of the various error sources listed in Table 2 following the order listed in that Table. Resulting error estimates are given in Figs. 22 and 23 for the 205 and 183 GHz radiometer data respectively. Although plots cover the range 100 to 0.1 hPa, we caution that the recommended vertical range for useful scientific studies needs to be taken into account. Based on increasingly poor measurement sensitivity in the Version 3 data files and the error analyses (given tm-10W), 205 GHz ozone band data analyses for altitudes above 0.46 hPa or below 46 hPa arc not advised, nor arc those for 183 GHz band data at altitudes above 0.046 hPa or below 46 hPa. Some information is contained at the limiting levels indicated above (and even at Level 2 pressures above and below these), but the full capability of the measurements will need to be exploited better in a future MLS data version. Error contributions near and beyond the limits stated above will change somewhat with such new software. For example, particularly for 183 GHz ozone data in the lowermost stratosphere, a priori error contribution will go clown, but other error sources in this region are likely to go up because of their artificial "damping" by the a priori weighting (i.e. Fig. 23 characteristics in the lowermost stratosphere will change).

Radiance noise determines the precision (repeatability) of the retrieved profiles. Precision estimates based 011 the measurement noise contribution (calculated via the method discussed by *Rodgers, 1990)* arc shown in Figs. 22 and 23. These values arc C1OSC to - but (as expected) generally slightly lower than - those obtained from an empirical estimate of precision, i.e. based on observed variability during several summer

( "quiet") days near the orbit turn-around tangent points (latitudes of 34N or 34 S), where the densest sampling occurs, and several tropical data sets (where actual atmospheric variability is also expected to be near minimum). We have kept the theoretical estimates of precision as probably the better indicator of true precision (this could only be checked exactly if the same atmospheric parcel was monitored for many measurements, and if atmospheric variability was negligible).

Scaling errors in calibrated radiances can arise from three sources: radiometric calibration errors, sideband ratio errors, and spectroscopic errors in line strengths. The first two sources of error are discussed by *Jarnot et al.* (1 994). Based on this reference, we use a systematic error ("one sigma type") of 0.6% for the radiometric calibration of the 205 GHz and 183 GHz radiometers, which is assumed to correspond to about one third of the worst-case error expected; this error reflects mostly uncertainties in the characterization of losses through the M LS antenna and switching mirror. Note that a spectrally flat radiance offset across the band (s) is taken out by the retrieval software, which uses only spectral contrast to retrieve mixing ratio values. Radiances from the two sidebands are combined to yield total radiances for each ozone band. The relative weighting of each sideband is described by the sideband ratio values (see *Jarnot et* al., J 994), determined before launch. Based on the al bove reference, sideband ratio errors can lead to likely (one third of worst-case) radiance errors of 0.6% for the 205 GHz ozone band and 7% for the much poorer characterization of the 183 GHz ozone band. Finally, a systematic line strength error of 0.5% is used for the ozone lines considered here (H. Pickett, private communication, 1994); this is larger than the intrinsic contribution f r o m dipole moment measurement errors in the microwave region, but it includes uncertainties in the corrections made for centrifugal distortion effects. Taking the above three sources of error in consideration, we then use a combined (root sum squared) scaling error of about 1.0% and 7% f o r the 205 and 183 GHz ozone bands, respectively. Since we arc using radiances in a mostly optically-thin regime for Version 3 data files, the scaling errors above will translate to mixing ratio errors directly, to first-order, as can be seen in Figs. 22 and 23; for 205 GHz ozone retrievals, radiance scaling uncertainties lead to slightly more than 1 % error, whereas the 7 % radiance scaling error for the 183 GHz band can produce 8 to 10 % errors in ozone for pressures less than 22 hPa, with increasing (non-linear) effects at higher pressures. The 183 GHz ozone error budget is largely dominated by this potential radiance scaling error (arising from the poorer characterization of sideband ratios). Ozone abundances obtained from the 205 GHz radiometer should give a better indication of the actual systematic error to expect in the 183 GHz ozouc retrievals (see discussions later in this paper).

Each M LS channel has au associated filter shape (spectral response) and position. There is a potential source of error in the knowledge of filter shape (see *Jarnot et* al., 1994). Following the above reference, we have used an uncertainty of 0.03% per MHz slope on the existing filter transmission functions as a worst-case; this bias was applied for all channels on onc side of the ozone line and with a different sign on the other side, as a worst-cam scenario. Resulting errors arc essentially negligible, as exemplified in Figs. 22 and 23, where the plotted rms- type errors (worst-case divided by three) are barely visible in the lowermost stratosphere.

Errors in field of view (FOV) direction have to do with the uncertainty in knowledge of the true pointing direction of each radiometer. in the case of ozone, we arc interested in possible errors arising from any misalignment of the 205 GHz or 183 GHz radiometer FOV with respect to the 63 (;112 FOV (errors in absolute pointing of the 63 GHz FOV arc accounted for be-Jow as possible systematic errors in tangent pressure). Although post-launch moon viewing calibration data gave no indication of a need to reconsider the alignment of tile 205 GHz radiometer (to within the pre-launch errors), the 183 GHz radiometer data indicate the need for an alignment adjustment from the pre-launch value (see *Jarnot et* al., 1 994). Changes in the software parameters producing Version 3 data were made to accomodate a possible misalignment consistent with the moon calibration data as well as the observed differences in ozone between the independent radiometer data. The MLS Version 3 data used a misalignment value of 0.006° (about 290 m in tangent height), somewhat less than the ~noon-derived result of 0.0110 (finalized only after the software changes for Version 3 data production), albeit consistent within the errors of the alignment determination. Elevation alignment errors of 0.0016 and 0.012 degrees, for the 205 and 183 GHz radiometers respectively, were used as the basis for our estimates of in-ofilc errors arising from remaining (worst-case) misalignments in FOV direction; the first number corresponds to pre-

launch (worst-case) knowledge for the 205 GHz radiometer data, while the second number reflects the post-launch uncertainty based on moon calibration tests for the 183 GHz radiometer, since independent evidence on ozone abundances indicate that there is reason to place more confidence in the post-launch numbers for the 183 GHz radiometer. in fact, the 183 GHz uncertainty (in relative FOV direction) used here is a conservative number, since we have added the ( "3 sigma" ) uncertainty (0.007°) from moon scan analyses (see *Jarnot et al.*, 1994) to the possible alignment change required (0.005°) to best fit the moon scan results alone (not the 205 GHz ozone results). Results in Figs. 22 and 23 are based on these worst-case sensitivity tests and a factor of 3 reduction to provide rms-type uncertainties. The larger uncertainty for the 183 GHz radiometer FOV gives rise to the more significant potential systematic errors (a few %) seen in Fig. 23.

Errors in FOV shape were also considered, by assuming that an error in beamwidth (radiometer-dependent) can modify the retrievals, and so can an error in the pattern's sidelobe levels. For the 205 GHz radiometer, based on *Jarnot et al.* (1994), a worst-case beamwidth error of 0.003° was assumed. The spectral dependence of the field of view is less than the estimated accuracy in FOV beamwidth (0.0030), as mentioned in *Jarnot et al.* (1994). For the 183 GHz radiometer, somewhat larger errors are used, based on the fact that the post-launch determination of FOV misalignment for this radiometer would lead one to suspect a corresponding error in FOV shape as well (*i.e.* different from the measured shape, which assumed a different alignment). Using an estimate of the likely change in FOV shape from the worst-cam misalignment in 183 GHz radiometer FOV (0.0180), we have used an error in beamwidth of 0.005° as a worst-case possibility. The resulting ozone rms errors (worst-case divide by three) shown in Figs. 22 and 23 do not play a major role compared to other systematic error sources. Errors in antenna sidelobe knowledge are considered negligible for ozone retrievals in the stratosphere, given the small ( 1%) amount of lower atmospheric radiance contribution from the sidelobes and its even smaller spectral contribution. The relative error contribution from sidelobe level uncertainties should be a maximum when the antenna is pointing near 60-70 km, and the lower sidelobes arc receiving strong signals from the troposphere (with weaker signals arising from the tangent point).

Spectroscopy errors can clearly lead to retrieved profile errors. Errors in line strength have been included above as part of radiance scaling errors. Line positions are known extremely accurately at microwave wavelengths, and thus do not represent a significant error source. A related error could arise from imperfect knowledge of the Doppler shift of the emitted radiation, caused by line-of-sight velocity effects. Since the spacecraft and earth velocity components along the line of sight are quite well known and are accounted for in the retrieval algorithms, atmospheric wind will constitute the largest error source, with maximum effect in the lower mesosphere (arid for channels adjacent to the center channel). For a conservative line of sight velocity error of 50 m/s, the ozone radiances for the 205 GHz radiometer will be negligibly affected (less than a 0.05 K effect). For the 183 GHz ozone line, a 1-2% (0.2 K) effect on some radiances is possible, but this is a negligible effect in tile stratosphere, and we have already mentioned significantly larger error sources for these retrievals, in order to include possible errors in linewidths, a 3% error in the broadening function was used to estimate systematic errors in profiles arising from this source, based on the spectroscopic work of Oh and Cohen (1 992), who quote a 3% accuracy value. Corresponding ozone uncertainties (treated here conservatively as "one sigma" values) are given in Figs. 22 and 23; this error source is one of the more significant ones for the 205 GHz data.

Errors arising from retrieval numerics refer to the differences between the mixing ratio profiles used to create simulated noise-free radiances, and the subsequently retrieved ozone profiles, keeping other parameters (tangent pressure, temperature, etc... ) set to the "true?' (known) values. This error source is fairly small (see Figs. 22 and 23) .

The error contribution from the a priori has been evaluated using the formalism of Rodgers (1990) (see what was termed null space error in that paper) and is included in the middle panels of Figs. 22 and 23. As expected, this is small in the region of good measurement sensitivity (10 to 1 hPa in particular), but rises in the in the mesosphere and lower stratosphere; 205 GHz ozone data is dominated by a priori contribution in most of the mesosphere, where 183 GHz ozone data is more measurement-sensitive, whereas the current 183 GHz ozone retrievals loss sensitivity below the 10 hPa altitude more quickly than the 205 GHz ozone values. If all the measurement channels were included (as planned in a future software version), the a priori error contribution would be smaller

than shown here, especially for the 183 GHz data near 100 hPa.

Errors in tangent pressure can clearly give rise to errors in mixing ratios (which arc based 011 radiances at the retrieved tangent pressures). A possible systematic error in $P_{tan}$ of about 6% (see *Fishbein et al.*, 1994) is assumed here, corresponding to about 300 m in tangent height. This potential error can have a significant impact on ozone (5 to 15 % for altitudes at and above 46 hPa), and arises primarily from possible errors in the $0_2$ spectroscopic data base. Indeed, post-Version 3 MLS data updates will include the latest recommended spectroscopic data base by *Liebe et al.* (1 992), which leads to a 6% change in $O_2$ linewidth. A smaller (3%) error from this source may be more reasonable for updated M 1,S software, although other error sources can also have some impact on the tangent pressure determination (see *Fishbein et* al., 1994).

Sim ilarly, systematic biases in temperature can lead to biases in mixing ratios, since the radiances in the ozone band (s) depend somewhat on temperature; this is a linear function at microwave wavelengths, where the temperature dependence is much weaker than in the infrared or ultraviolet. Biases in temperature were taken to be 2K for non-polar latitudes and 5K for latitudes poleward of 60 degrees; these values are consistent with observed average differences between MLS and NMC temperatures (MLS giving lower results, see *Fishbein et* al., 1994). The effect of temperature biases was isolated by imposing these biases while tangent pressure and other parameters were constrained to "truth". Corresponding rms changes in mixing ratios were then used to give the ozone systematic errors plotted here (see Pigs. 22 and 23). Typically, ozone uncertainties arising from such potential biases are of order 2-3 %, and somewhat larger in the lowermost stratosphere; the 183 GHz results are slightly less sensitive to temperature than the 205 GHz results.

Error sources numbered 11 through 14 in Table 2 deal with imperfect knowledge of emission features in the ozone band(s). The dry air continuum is a semi-empirical contribution derived from the radiance data in wing channels of the 205 GHz non-o zone-emission regions. Errors arising from imperfect knowledge of this continuum are obtained by using a "worst case" scenario in the forward model, with no such continuum, and comparing retrieved profiles to the standard run.

Similarly, errors in other constituents such as $HNO_3$, $N_2O$, $11_20$, and $S0_2$ were considered, especially for the lower stratosphere. These error sources lead to profile errors primarily in the lower stratosphere. 1 $INO_3$ was not retrieved by M LS software until after Version 3 data were created, and here, we will use 11 $N0_3$ errors appropriate to this data version, The differences between ozone retrievals using climatological assumptions for H $N0_3$ versus M I, S-retrieved $HNO_3$ provide a basis for ozone errors arising from uncertain knowledge of $HNO_3$. This error source should be reduced in results from future MLS data processing.

$N_20$ is a contaminant. of the ozone data near 205 GHz because of a line outside the ozone band which provides a (sloping) continuum in the ozone band, primarily in the lower stratosphere. Given the lack of enough spectral contrast for retrieving $N_2O$, however, we assume climatological values, and errors in this assumption can lead to errors in ozone. A systematic bias of 2(I % has been used here as the basis for the $N_2O$ uncertainty effect on ozone retrievals. The same has been done for sensitivity to $H_2O$ (this species also enters as a continuum effect in the ozone bands); the effect of water vapor comes mostly from below the tropopause, however, where large increases and variability can occur. Although MLS data contain information on water vapor slightly below the tropopause (*Read et* al., 1 994), this is not part of routine MLS Version 3 processing and was not used (as a constraint) in the Version 3 ozone retrievals. The uncertainty results for poor knowledge of these species arc displayed in Figs. 22 and 23. It may be that certain times and places are more subject to these types of errors, and the values used here are only a guide. Generally, these effects arc to be considered smaller than the inexact knowledge of tangent pressure (and temperature, to a lesser degree).

Finally, the effect of $S0_2$ should have a small impact on ozone (at 205 GHz) only during enhanced conditions (e.g. following the Mt. Pinatubo eruption). To illustrate this here, we have used conditions of enhanced $SO_2$, at the 1 ppbv level in the lower stratosphere (more than ten times background, but ten times less than the highest Pinatubo effect observed by MLS, as discussed by *Read et* al., 1993). This type of $SO_2$ "contamination" can give rise to 5% ozone errors in the lowermost stratosphere, similar to the effects of $H_2O$ and $N_20$ mentioned above, in the 46 to 100 hPa range. However, under background conditions, such errors will not appear; also, a future retrieval scheme should account for the amounts

retrieved by M LS, especially under enhanced conditions.

We see from the right panels of Figs. 22 and 23 that uncertain knowledge of certain atmospheric parameters can have a significant impact on ozone accuracy, especially at the lowermost altitudes. Most of these factors play a minimal role, however, for altitudes above 46 hPa, and tangent pressure uncertainties tend to dominate other effects at most altitudes. Errors in minor constituents $O^{18}OO$ and $HO_2$ are negligible because of the small signal strengths arising from these molecules; the $O^{18}OO$ mixing ratio should be well enough constrained from the ozone retrieval values, based on the expected isotopic ratio.

Finally, there is a small residual spectral baseline in the MLS spectra, after an empirical (post-launch) set of channel-dependent offsets of order 0.1 K has been removed from the spectra, by using data at the highest tangent altitudes (*Jarnot et* al., 1994). Variations in this residual baseline (as well as small average changes determined since the Version 3 data were processed) can be used to ascertain the effect of this error source. Since these variations are of order a few hundredths of a degree or less, typically, this will have minimal (much less than 1%) impact on ozone retrievals, where signals are of order tens of degrees; other error contributions make this source of error negligible. A scan-dependent spectral baseline would not be detectable in normal operations, but analysis of radiances taken during satellite roll maneuvers shows this is insignificant (for individual retrievals). .

Figures 24 and 25 give the total estimated errors (random, systematic, and a priori contributions, along with the root sum square of these as total error) from the (root sum square) combination of the error sources discussed above, for the 205 GHz and 183 GHz retrievals, respectively. We can see from these figures that the 205 GHz ozone uncertainty is not dominated by the systematic effects (rms estimate of 10 to 15 %) which account for the main part of the 183 GHz error budget (in the 1 to 20 hPa region). Ozone results from the 183 GHz band will be most useful for mesospheric studies, especially those dealing primarily with relative changes (*e. g.* diurnal variation analyses asin *Ricaud et* al., 1994). The random (measurement) noise component plays a major role for 205 GHz ozone data from 0.5 to 10 hPa, with (rms) systematic effects possible also at the 2 to 9 % level. At 46 and 100 hPa, the a priori and systematic error contributions will dominate; this is evident in some of the comparisons discussed in the next section, as well as in the artifacts mentioned earlier, where averaging the profiles still leaves a systematic effect - for example the yaw cycle dependence at 100 h} 'a, The estimated uncertainties derived by the M 1,S software algorithms arc also indicated in Figs. 24 and 25, for comparison; these values are generally somewhat larger than the estimated precision in the profiles, from a few percent larger in the upper stratosphere to a factor of more than two at 100 hPa. Mid-to lower stratospheric Level 2 and 3 profile errors should therefore be looked at as being close to the total (random plus systematic - and a priori -) rms error for ozone results at 205 GHz, and as a lower bound to the total (rms) error for the 183 GHz ozone retrievals. Ideally, statistical quantities such as the estimated errors in average ozone (over a latitude region and/or a period of time) should also be handled with these facts in mind, namely that only the random part of the total uncertainty can be reduced by the averaging process; in principle, the a priori error contribution can also be removed (see e.g. *Connor et* al., 1994). Using in large part the figures above, we will summarize the estimated precision and accuracy values in tabular form in section 7.

We note that the optimum use of all channels (especially for 183 GHz ozone data) and the suppression of the radiance error inflator factor (see section 3) - which may not be unreasonable in the future - would lead to a reduction in estimated precision and a priori contribution. Tests with this in mind suggest that tile main change for the 205 GHz data would be a precision at 100 hPa closer to 0.25 ppmv, and a value of 0.1 ppmv for a priori error contribution at pressures between 100 and 1 h] 'a. For the 183 GHz ozone data, the a priori error contribution would be significantly less than 0.1 ppmv from 1 to 100 h} 'a, and the precision would still be ~0.1 ppmv for this region. in addition to this, systematic errors may not be as large as these estimates, which arc! not a definite statement about what biases actually exist. In fact, radiance residuals mapped onto parameter space lead us to believe that this "residual error" may typically be of order 0.2 ppmv for the 205 GHz ozone stratospheric data (using improved software algorithms); this is smaller than the systematic error estimate of Fig. 24 in the lower stratosphere, although this type of residual error cau only be looked at as a minimum systematic error (some errors, such as a line strength error, would not show up in the residuals). For ozone data from the 183 GHz band, however, residual errors in the lower stratosphere (even with an improved iterative retrieval) appear to be of order 0.5 ppmv or

more, and more work will be needed to understand the sources of systematic errors (and reduce them). Nevertheless, improved measurements of 100 hPa ozone mixing ratios from UARS MLS are likely in the future.

## 6. Comparisons with other Data Sets

In this section, comparisons between MLS ozone (205 GHz data) and other data sets are made. This should, in principle, give results which are compatible with the estimated accuracies given in section 5.

### Comparisons with ozonesonde data

Comparisons are made between MLS 205 GHz ozone and ozonesonde data from selected sites, in the 100 to 10 hPa range. The ozonesonde data used here generally include about a year of measurements and cover a range of latitudes: Boulder (40N, 254.7 E), Hilo (19.4N, 205.0E), Ascension Island (8.0S, 345.7E), Brazzaville (4.3S, 15.0E), Gardermoen (60.1 N, 11 .0E) and McMurdo (77.5S, 166.411). A search for possible biases in the MLS dataset is one goal of these analyses, assuming that the data used as comparison are sufficiently accurate; we think this is the case but the "true" atmosphere is difficult to characterize at the sub-five percent level of accuracy, and much work is required to prove that such a goal can be (or has been) met. As a guide, the error bar on the ozonesonde data presented here is taken to be 5 % of the ozone abundance, which is probably somewhat of an underestimate, particularly at 10 hPa, based on earlier analyses relating to this measurement technique (*Barnes et al.*, 1985; *Hilsenrath et* al., 1986); indeed, this "canonical" number may apply to precision as well as accuracy (separately), but we will consider enough profiles in the average comparisons below that the uncertainty in the mean will be dominated by the absolute knowledge (accuracy).

*Boulder site*

The fine resolution ozonesonde data taken at varying time and space '(locations" with respect to the coarser M 1,S profiles lend themselves better to statistical analyses, rather than individual comparisons. 1 lowever, for Boulder, we present a few examples of individual profile comparisons (see Fig. 26), one for each season in 1992. Changes as a function of time are similar for both sets of data (e.g. the spring maximum is observed in panel (b) of Fig. 26). We have deliberately chosen to show in panel (d) of this figure a poor comparison at 100 hPa, where the Version 3 M 1,S value significantly overestimates the ozonesonde Value.

A full year (1992) time series comparison for all of the coincidences between 1992 Boulder sonde and MLS profiles is given in Fig. 27, for the four MLS retrieval surfaces (10, 22, 46, and 100 hPa) within the ozonesonde stratospheric altitude range. The ozonesonde data are simply interpolated onto the MLS retrieval grid. We plan to investigate possible quantitative effects introduced by the different vertical resolutions of these instruments, but we feel that this will not change the main conclusions reached here. At 10 hPa, ozonesonde data are generally considered less reliable than at the higher pressures; however, the cyclic annual ozone variations at this level are observed to be similar in both datasets. The same appears to hold for the 22 and 46 hPa levels, where there is good tracking of the more complex temporal variations in these datasets. At 100 hPa, the MLS Version 3 values are not very useful, given the size of the estimated uncertainties, and a significant comparison of the variations is not meaningful. However, the average values at this level agree quite well; this is illustrated in Fig. 28, where average sonde and MLS profiles for the datasets shown in Fig. 27 are displayed, along with panels of mean and rms differences (in ppmv and percent) and other quantities discussed below. The mean differences at all (4) levels of interest are only a few percent, which is within the overall uncertainty (precision) of the average values obtained here (the size of these uncertainties is at most the full width of the squares used as symbols for the mean differences). Any remaining average differences would have to be attributed mainly to systematic errors in either or both datasets, although a component of this may come from the different vertical resolution of the instruments.

The standard deviation of the differences (between MLS and sonde data) is displayed in the bottom panels of Fig, 28 (open circles) for comparison with the estimated rms precision of the differences (solid circles), i.e. the root sum square of the typical MLS and sonde precision (see sections 5 and 7 for MLS ozone precision values). One would expect the standard deviation of the differences (which removes any average bias between the two datasets) to be equal to or larger than the rms precision estimate, and we see from Fig. 28 that this is the case, but the standard deviations can be a factor of two larger than the rms precision. This could have several ex]Ja~la-

tions: the possibly conservative 5% precision value for the. sonde data (especially at 10 hPa), true atmospheric variability between the profiles sampled at non-coincident locations and times, vertical and horizontal resolution differences between M 1,S and sonde profiles (fine scales not resolved by M 1, S), or other errors in the profile measurements. We plan to investigate the vertical resolution effects by vertically smoothing the sonde data to the MLS resolution . It is worth noting here that a large number of (smoothed) SAG E 11 ozone profiles have been compared to M 1,S ozone profiles (see *Cunnold et al.*, 1994a) and that the standard deviations of the differences between these datasets agrees well with the rms precision estimates for the combined (difference) data. The other quantity shown in the bottom panels of Fig. 28 is the rms difference between MLS and sonde profiles (this equals the root sum square of the average differences and the standard deviations of the differences); the rms differences obtained in this section are often dominated by the standard deviation of the differences (i.e. the bias is small compared to the standard deviation). These rms differences could be viewed as an absolute worst case total uncertainty in the M LS profiles.

*Hilo* site

Plots similar to Figs. 27 and 28, but for comparisons between MLS ozone and Hilo ozonesonde data during 1992, are shown in Figs. 29 ant] 30. The agreement at 10 and 22 hPa is almost as good as for Boulder at those levels (near 5% mean difference, with M 1,S slightly high, and 5 to 10% rms difference). A larger percentage difference is observed in the lower stratosphere, with M 1,S ozone lower than the average sonde value at 46 hPa by almost 0.5 ppmv ($\sim$ 20%), and larger than the sonde data at 100 hPa by $\sim$ 0.2 ppmv (which is a large percentage difference at the low values of ozone observed there). Excluding the 100 h]'a level, the ozone variations measured by the sondes as a function of time at the various pressure surfaces are well reproduced by changes in the M 1,S ozone retrievals (with biases as mentioned above). Although the biases are somewhat larger than for the Boulder sonde data, the standard deviations of the differences (see Fig. 30) are somewhat smaller, and the total (rms) differences are not very different from the values (in ppmv) shown in Fig. 28.

A *scension* Island and *Brazzaville* sites

The tropical ozonesonde data are of particular importance since the eruption of Mt. Pinatubo, and we examine next two datasets in the region just south of the equator. Comparison plots arc given in Figs. 31 and 32 for Ascension island, and in Figs. 33 and 34 for Brazzaville. The results from the two sites, for about one year of data (October 1991 to roughly September 1992) give consistent mean differences with MLS ozone. A 5 to 10% systematic overestimate of the sonde ozone values exists in the MIS abundances at 10 and 22 hPa, while a $\sim$20% underestimate occurs at 46 hPa. 'J'here seems to be somewhat better agreement in the later portion (summer) of 1992 than during the earlier time period shown in Figs. 31 and 33, at least at 22 and 46 h] 'a. There may be some improvement based upon newer retrievals (discussed later in this paper), which take into account the effect of $HNO_3$ on ozone - and include updated $O_2$ spectroscopic parameters, but full confirmation of this will have to await more reprocessing of MLS data. As can be seen in Figs. 32 and 34, the standard deviations of the differences are again about twice the estimated rms precision, in many instances, with implications as discussed above. Rms differences are overall not very different than those shown for the Boulder and Hilo sites.

*Gardermoen* site

Figs. 35 and 36 arc similar in format to the above comparisons, but they apply to the Norwegian site of G ardermoen. The ozonesonde data we obtained here cover about a year, but for 1993 (and one sounding in early 1994) as opposed to the earlier portion of the UARS mission. Also, although the total number of ozonesonde profiles is not much different than other comparisons above, these data are weighted fairly heavily towards the winter period. Although atmospheric variability and dynamics might be expected to play a bigger role for the comparisons at this site, especially in or near the winter polar vortex, the rms differences of Fig, 36 are similar to those obtained from the tropical and mid-latitude ozonesonde comparisons shown above. In fact, a significant part of these differences are systematic in nature, as can be seen by the $\sim$ 0.3 ppmv bias between MLS ozone and the sonde data (MLS values being higher); this amounts to a few to 10% overestimate by MLS, except at 100 hPa where the percentage difference is about 40%. Trends are generally well reproduced by both datasets, and the standard deviations of the differ-

ences are c.1osc to those shown above for other sites.

*McMurdo* site

The last ozonesonde dataset wc present is for McMurdo, Antarctica, where the period of most interest is during the occurrence of the ozone hole. The time span covered by the combined MLS and sonde observations over McMurdo for 1992 is from late August to mid-September, along with one coincidence in late October (see the time series comparison in Fig. 37). Rather good agreement is observed in the ozone values and variations at 10 and 22 hPa; in particular, the large increase in ozone abundances which has occurred by late October is tracked very closely by both MLS and sonde data (see also at 46 hPa). At 46 hPa, the September decline in ozone is seen in both datasets, although MLS values tend to be systematically lower than the sonde data. A consistent overestimate of the (sonde) ozone values by MLS data at 100 hPa is observed, even if one can argue that the large estimated errors in MLS ozone at this level can explain the differences. This overestimate is even larger than in the high northern latitude (Gardermoen) case, and a factor of two difference exists here in the average profiles (for September 1992), about 1.5 ppmv for MLS versus 0.7 ppmv for the sondc, as seen in Fig. 38. This is caused in part by the occurrence of unrealistic ozone "bulges" at 100 hPa in some of the MLS profiles, where 100 hPa ozone values are larger than tile 46 hPa values. Such features arc not observed in the ozonesonde data and the MLS retrievals need a systematic improvement in this respect at 100 hPa, regardless of the non-negligible noise level of individual retrievals at this height. We arc investigating this issue to assess whether this might be related to poor knowledge of "contaminant" species (such as $H_2O$, $N_2O$, or $HNO_3$) in this region at this time. However, it is worth noting that the standard deviations of the differences arc smaller, for McMurdo than for other sites considered shove (especially at 10 hPa), indicating good tracking between the two datasets, regardless of any biases.

*Summ ary*

Fig. 39 summarizes data from the 6 ozonesonde sites mentioned above, as compared to MLS ozone, in terms of average values at 100, 46, 22, and 10 hPa, along with average and rms differences in ppmv and percent. Even though the time periods of observation are not identical, this indicates how latitude variations from averaged ozonesonde data are reproduced by MLS coincident profiles. Even at 100 hPa, the average trends with latitude look encouraging. Sensitivity tests with latitude-independent a priori ozone indicate that the retrieved latitudinal variation is to a large degree unaffected by the choice of a priori, even at this pressure level (the variation observed by MLS is not - to first order - "caused" by the a priori, because of poorer measurement Sensitivity). in some instances (especiall y at high latitudes), an MLS overestimate of ozone at 100 hPa exists, although we note that only half of the datasets used in the comparison here show this as a significant problem. The general development of the ozone hole ant] the springtime recovery is well followed by MLS data, iu accord with average colu mn ozone comparisons versus TOMS in the polar region (see *Froidevaux et* al., 1994). However, given the biases as well as the random errors, MLS ozone (Version 3 data) at 100 hPa cannot be considered reliable for detailed scientific analyses. At 46 hPa, there is a tendency for MLS data to lie below the ozonesonde measurements by a few tenths of a ppmv (except at Gardermoen, where the bias is reversed in sign). Some of the above differences may be related to closure problems in the simulations (see discussion of section *4).* At 10 and 22 hPa, mean differences arc systematically close to 5%, with MLS ozone values higher than the sonde data; rms differences generally vary between 5 and 1570. Temporal variations observed in the sonde data (as displayed in previous plots) arc generally well tracked by the MLS 205 GHz ozone retrievals, from 46 to 10 hPa.

**Comparisons with ozone data from balloon flights**

We now present a summary of comparisons between MLS ozone data and ]nid-latitude measurements obtained from large balloon flights bet ween fall 1991 and spring 1994. The two datasets discussed here arc the UV photometer (in situ) results (8 flights total), aud the Submillimeter Limb Sounder (SLS) data - remote sensing similar to the M 1,S technique. These two datasets were chosen primarily because they contain a significant number of profiles, even though it is clear that the frequency of these flights cannot match that of ozonesonde launches. The balloon flights were made either from Daggett, California (34.3 N latitude, 256,4 E longitude) or from Fort Sumner, Ncw Mexico (34.9 N latitude, 243.2 E longitude), and wc present average results for statistical reasons (and for brevity). Time-series plots arc not appropriate in this case, given the relatively poor temporal

coverage of balloon flights. However, equinox conditions at rnid-latitudes have the advantage of providing a relatively static stratosphere, so that differences due to atmospheric variability can be minimized.

*UV photometer data*

The UV photometer is generally considered among the most accurate for ozone profile measurements (*Hilsenrath et* cd., 1986). We have combined 8 profiles from a UV in situ instrument launched aboard large balloons (which can reach somewhat higher altitudes than ozonesondes). Individual MLS and UV photometer ozone values (6 of which are for profiles measured within ~ 300 krn of each other, and all of which arc within 900 km) are not shown here, but compare quite well, *i.e.* essentially always within the estimated combined rms accuracies - of order 7% at best. A small bias emerges, however, between the two datasets, as seen from the average comparison profiles of Fig. 40, and the bias accounts for a significant part of the rms differences between 22 and 5 h] 'a. The MLS ozone values are, as in the comparisons with ozonesondes, slightly higher than the UV data (by about 5%), near the ozone peak - from 5 to 22 hPa. Agreement at 46 and 100 hPa is Letter than 0.1 ppmv, but even such a small overestimate by MLS (versus the in situ data) can amount to ~20% at 1 00 h] 'a, where the mixing ratios arc small (less than 0.5 ppmv). Rms differences for these comparisons are of order 0.5 ppmv at all heights, which amounts to 5-20% between 4.6 and 46 hP'a. For the estimated precision of the UV photometer, we have used 2% here, which would correspond better to the observed rms variability (at balloon float altitude for example) than the 5% canonical number used above for ozonesondes. The standard deviation of the differences in Pig. 40 arc reasonably consistent with (but generally somewhat higher than) the estimated precision of the combined datasets.

*SLS data*

Ozone is measured by the S1,S experiment (*Stachnik et* al., 1992) from emission at 625 GHz, as the FOV scans through the atmosphere from the balloon at float altitude (~ 38 km); some information is also retrieved about the ozone abundance above this altitude, albeit with poorer accuracy. The S),S ozone profile averaged over the 5 rnid-latitude flights (all near equinox) is displayed in Fig. 41, along with the corresponding average MLS profile, and the sets of difference values. The differences are very small throughout the stratosphere, i.e. a few percent systematic difference (not really significant, given the relatively small number of coincident profiles), with the M 1S values generally on the high side. We expect this small difference to be reduced when the newer MLS software - with updated $0_2$ spectroscopy - is used, since a few % reduction in ozone (at least above 10 h} 'a) is then likely (see section 8). The standard deviations of the differences between M 1.S and S1,S are as small as any others presented above, and are consistent with the combined error estimates shown; however, these estimates include values whit}] represent accuracy (one sigma) rather than precision for the S1,S data aud the actual precision for the SLS profiles (which represent averages of many single profiles) is undoubtedly lower than the 5 % assumption made here. The main point, however, is that the average M 1,S and SLS profiles presented in Fig. 41 are remarkably consistent.

## Comparisons with lick data

*Table* Mountain Facility *(TMF)*

The Table Mountain Facility lidar has acquired a large continuous ozone database since 1988 (see *McDermid,* 1993), and for this reason, we focus here on comparisons of this dateset with MLS ozone (205 GHz band) for the first, 2 years of MLS operations. *Redaelli et* al., 1994 have discussed sample comparisons between MLS data and lidar data from l'Aquila, and comparisons with other lidar systems are presented in G'rose and *Gille* (1994).

Time series comparisons from MLS aud TMF lidar data are displayed in Fig.42, and average profile comparisons are shown in Fig.43. As we see from these two figures, the IO hPa comparisons give results which are in better agreement (on average) than the other datasets shown above; namely, there is excellent agreement between the TMF lidar data aud MLS ozone at this level, whereas a small but systematic 5% offset was evident in the other dataset comparisons. If the ozonesonde data and UV results are considered as "truth", this would imply that both the TMF lidar and MLS values are biased high (by about 5 %) near 10 hPa. Fig. 42 shows excellent tracking of the annual cycle at 10 hPa for MLS and lidar values, and Fig. 43 gives rms differences close to 5% at this level. Comparisons are nearly as good for the 4.6 hPa pressure surface. Systematic differences between the TMF lidar and MLS data begin to appear in the upper stratosphere, where the lidar values become sol[]e-

what larger than the MIS data, especially at the top level of 1 h] 'a, where the bias is of order 15%. The standard deviations of the differences between MLS and lidar profiles increase with altitude, reaching 20% at 1 hPa; this could be in part because of larger atmospheric variability at the uppermost levels, and also because of the reduced sensitivity of both instruments in that region. Finally, we note from Fig. 42 that there is a time period, namely during April and May 1992, when comparisons are significantly worse than average; in these months, the lidar data exhibit somewhat more scatter than at other times and generally lie significantly higher than the M 1,S values. Preliminary investigations indicate that some of this could arise as a result of the transformation of lidar profiles from altitude to pressure coordinates, but this will require further research. Comparisons with other datasets may also help resolve the systematic differences discussed above.

### Other datasets

The purpose of this section is to mention other ozone datasets for which wc know some comparisons with MLS data exist; this can help place the above discussions in a broader context. First, a large number of profile comparisons between MLS ozone (from the 205 GHz band) and SAGE 11 ozone data have been performed and presented in *Cunnold et al.* (1994a). The general conclusion of that work is that MLS (Version 3) ozone values arc about 5% larger than the SAGE II data, for the stratospheric values compared (down to about 30 hPa); this result is (to first order) not latitude or height dependent. This would tend to agree with a good fraction (but not all) of the comparisons shown in this paper for 10 and 22 h] 'a. However, the TMF lidar and MLS ozone comparisons (pressures of 1 to 10 hPa) do not show such a bias. This could be because the TMF lidar data also have a slight positive bias (with respect to "truth"); indeed, there arc indications that those data arc on the high side of other lidar and grou~ld-based microwave ozone data (see *Grose and Gille*, 1994), but it is not clear that a sufficiently extensive study has been performed. Based 011 some of the analyses discussed in *Grose and Gille* (1 994) and other comparisons (J. Gleason, private communication, 1994), MLS ozone zonal mean values arc generally larger than the Solar Backscatter Ultra Violet (SBUV/2) mean data, by about 10 to 15%, with the amplitude of temporal variations larger in the M 1,S dataset than in the SBUV/2 data (possibly in relation to the different, vertical resolutions); an understanding of these differences will require further study. Another set of ozone profiles of interest is the dataset from the Atmospheric Trace Molecule Spectroscopy (ATMOS) experiment aboard the Space Shuttle (ATLAS missions); very encouraging comparisons are emerging from such studies (M. Abrams, private communication, 1994). Further comparisons of UARS ozone datasets can be found in *Cunnold et* al. (1994b). Also, validation work of interest would involve the comparison of mapped products at a given pressure. General features certainly look similar among various instrument results (UARS and SBUV/2 global data), but there arc some differences (see *e.g. Grose* and *Gille*, ]994) which still need to be fully understood.

## i'. Precision and Accuracy of Version 3 Data

The evidence presented in this paper, arid the references to other comparisons mentioned here, indicate that the MLS ozone data can be most reliably used in the 22 to 0.5 hPa region. Comparisons with some datasets which can be considered accurate to about 5% (i.e. UV photometer, ozonesonde, and SAGE II data) give 5 to 10% (or better) agreement. MLS data in this region tend to be about 5 '‰ larger than most of the correlative values . We will see in the next section that this bias is likely to be reduced with a future MLS software version.

WC have derived estimated accuracy values as a function of height by using the root sum square of the estimated systematic uncertainties and the a priori contributions given in section 5. Even though the a priori error contribution, or smoothing error (see *Marks and Rodgers*, 1993) is treated as a random component in a theoretical sense (Rodgers, 1990), wc include it here as part of the accuracy figures, since averaging many MLS ozone profiles in an altitude region of poor measurement sensitivity (e.g. at or above 0.1 hPa for 205 GHz ozone data) would - in the extreme case - give a climatological value with error quite possibly larger than the systematic uncertainty. By using this approach, one is kept aware of the fact that there arc regions where the measurements should not be considered reliable. For ozone data from the 205 GHz band, rounded-off values arc c1osc to 0.3 ppmv from 22 to 0.5 h} 'a, and slightly under 0.6 ppmv at 46 h] 'a; the estimated accuracy at 100 hPa for the current retrievals is best expressed as being of order 50 % or larger, given the wide relative range of pos-

sible ozone mixing ratios (from tropics to poles) at this altitude, We choose to round the estimates off (generally on the high side) because these numbers are estimates with probably one only significant digit (past the decimal point). If wc compare these values to typical residual errors, we find good agreement and see no reason to change the estimates based on the radiance fits. Based on the comparisons given in section 6 and the overall biases noted there, wc also see little reason to change our estimates of accuracy (except at 46 hPa, sec below). Indeed, these are to be used as "one sigma" estimates, and the biases (and certainly the rms differences) between M 1,S and other datasets provide at best an upper limit to the MLS accuracy (since the other datasets do not have perfect knowledge and true atmospheric variability affects the rms differences). In fact, we believe that the estimated accuracy is too large at 46 hPa, given the comparisons of section 5 (where the absolute differences at 46 hPa are not typically worse than at other pressures). Therefore, in the tabulated recommendations for 205 GHz ozone accuracy (see "1'able 3a), we have used a value of ().4 ppmv (not 0.6 ppmv) at 46 hPa (or 20%) as a guide. Indeed, this Table is to be used as a guide, and the reader can look at the latitude dependence of the comparisons in section 6 for further information on likely accuracy. We note, furthermore, that while these Tables are not inconsistent with the quality of simulation results discussed in section 4, wc cannot convey all the information from that section or the comparison results in onc Table. in terms of precision, comparisons with other datasets and repeatability estimates for the MLS data indicate that the measurement noise contribution estimates of section 5 arc reasonable; wc believe that atmospheric variability and non-colocation of measurements accounts for the additional variability in the differences between M LS and other datasets.

For 183 GHz ozone data, the estimated values from a priori and systematic error contributions given in section 5 provide the basis for the tabulated accuracies in 'J'able 3b. Given the agreement (within the combined precision of the two ozone datasets) generally found between the 205 and 183 GHz ozone data, the actual accuracy of the 183 GHz data is probably better than given in the Table. However, the adjustment to the FOV pointing alignment for the 183 GHz radiometer contains a scwii-empirical component, and there is no doubt that - without other sources of information - the 183 GHz data is intrinsically lcss accurate than the 205 GHz data. Also, the existence of larger radiance residuals supports this assertion. Typical residual errors would appear to be slightly lower than the tabulated values, but not overwhelmingly so (see discussion at end of section 5).

With the information contained in this paper on possible small biases in the current M 1,S ozone values, keeping in mind again that "truth" is not rigorously known at much better than the 5% level of uncertainty, the user can hopefully decide the level of significance to attach to results obtained with this dataset. It is not easy to assign a possible systematic error at the 5% level to one particular cause, and a combination of factors could play a role, given the error sources discussed in section 5. 'l'he most likely sources of this kind of potential 5 % bias (based on the comparisons in section 6), particularly since it appears to occur in the upper stratosphere where contaminant species play a negligible role, would arise from small errors in tangent pressure registration (an error in the $0_2$ 63 GHz linewidth and/or an error in FOV direction for the 205 GHz radiometer) or in the 205 GHz ozone linewidth itself. We also saw that the likely sources of systematic error for the 183 GH z ozone retrievals include the above factors (with FOV direction errors accounting for an even larger contribution than in the 205 GIJz radiometer case), along with a significant uncertainty in the knowledge of sideband ratios. It is possible that the reason for an apparent disagreement between the FOV misalignment estimate obtained from moon scan analyses and the estimate obtained from a comparison between 205 and 183 GHz ozone datasets is because of a compensating error in the sideband ratio values for the 183 GHz radiometer. Such issues may be difficult to resolve completely, but continued investigations arc planned.

## 8. Plans for Further Work

A test version of software with recent updates is briefly discussed here in terms of expected changes in the future. One of the main changes involves retrievals of $HNO_3$ using the band 4 radiances (also used for retrievals of the 205 GHz ozone data); updated spectroscopic data for this molecule have also been obtained (E. Cohen, private communication, 1994). In addition to providing $HNO_3$ data, this provides some improvement in the ozone radiance residuals, and should give somewhat improved ozone values, particularly in the lower stratosphere. The other main change is the inclusion of updated spectroscopic

data for hand 1(63 GHz $O_2$ linewidth data), based on *Liebe et al.* (1992), which amount to a 6 % narrower linewidth. Other minor changes deal with better modeling (in the forward model) of the sideband ratio gradients within channels, a radiance interpolation scheme for the use of radiance values at a tangent point pressure of 100 hPa (for slightly better information content in that region), and a smoother a set of priori ("climatological" ) values for the mixing ratios - to fill in some gaps. Fig.43 gives a summary of ozone results from this updated software (for a one day run ). We observe a small decrease in ozone above 10 hPa, increasing from O% (at 10 hPa) to a maximum of 6% in the upper stratosphere, with very little latitude dependence; this is a result of the lower (by about 200 m) tangent altitudes retrieved using the newer $O_2$ spectroscopy (see *Fishbein et* al,, 1 994). Increases in ozone are observed in the lower stratosphere, reaching *20* % at 46 hPa, with some latitude dependence in the amount of increase; this is largely caused by the inclusion of $HNO_3$ in the retrievals. For the 183 GHz ozone retrievals, the $HNO_3$ retrievals play no role, and the newer software predicts a decrease of order 5 to 10'%0 in most regions, with only a small (1 %) increase at 22 h? 'a. However, we observe a significant improvement in the radiance fits (values of $\chi^2_{ma}$ drop from about 14 to 4, on average), with similar improvements in band 5 (I $I_2O$ retrievals), with the newer software, which gives us some added confidence in the updated $0_2$ spectroscopy and resulting tangent pressures. The bottom panel of Fig. 43 gives the percent difference between the 183 and 205 GHz ozone data for this newer software. Most of the differences are not significant (given the uncertainties), hut the systematic difference at 46 h Pa (of order 30%, with 183 GHz retrievals producing lower values) will require further investigation. The accuracy of ozone values at 100 hPa has not been improved by this newer software, and more work is needed to resolve the existence of artifacts noticed in that altitude region in particular (see section 4). Significant improvements in this region will require better modeling/knowledge of the lower stratospheric continuum' and contaminant species - including better $H_2O$ retrievals - and a non-linear retrieval scheme (for optimum usc of all channels, especially at 183 GHz).

Finally, the vertical resolution of the retrieval grid can be improved, even though the precision at a given level would be degraded. Fig.44 shows the trade-off between vertical resolution and precision, for the 205 GHz ozone retrievals, assuming the current a priori errors (mentioned in section 3). An optimum retrieval grid spacing of shout 3 ktn appears to exist, although it may be more desirable to retrieve on the actual UARS Level 3 grid points, which arc only slightly closer in spacing. We intend to explore these options further for future upgrades to the software.

## 9. Conclusions

The MLS ozone data have been discussed from the point of view of their internal consistency (radiance closure), as well as in comparison to other reliable datasets. Precision and accuracy estimates for both the 205 GHz and 183 GHz data (MLS Version 3 files) have been given, and likely sources of error have been presented.

We find that the vertical range of usefulness for the Version 3 (205 GHz) data is 46 to 0.46 hPa, with 100 hPa retrievals not yet consistently reliable. The rms precision is of order 0.2 ppmv throughout 1 nest of the stratosphere, with estimated (rms) accuracy of order 0.3 ppmv (~ 3% to more than 50% - at 100 hPa -). A large part of the radiance closure problems in the lower stratosphere wilt be remedied, it seems, by the inclusion of $HNO_3$ retrievals; better knowledge of other contaminant species (such as $1\,1_20$ and $N_20$) and tangent pressure will also help. Also, revised $0_2$ spectroscopic parameters should help reduce the slight (5% or so) MLS overestimate of ozone which may exist in the mid-to upper stratosphere (through more accurate retrievals of tangent pressure). At the sub-5% level, it becomes difficult to rigorously demonstrate that one dataset is the closest one to "truth".

For M 1.S Version 3 ozone values retrieved from the 183 GHz radiometer data, the stronger line can lead to more precise measurements in principle; however, radiance closure analyses and absolute mixing ratios after launch pointed to the existence of larger systematic effects in this dataset, most likely as a result of poorer calibration knowledge. The optimum usc of all channels in the future should improve the situation, especially in the mid-to lower stratosphere, and tile stronger line and relative lack of contaminant species are an advantage for this dataset. The currently recommended vertical range of usefulness is 46 to 0.046 hPa for 183 GHz ozone results, but we recommend the 205 GHz data for the stratosphere and the 183 GHz data for the mesosphere (because of the larger signal-to-noise). Significant improvements in closure arc known to occur when updated $O_2$ spec-

troscopy is used.

Future iterative retrievals will produce improved UARS MLS datasets. Other engineering issues, like increasing the spectral bandwidth, will improve future lower stratospheric measurements planned for the Earth Observing System (EOS) MLS; note that the UARS MLS instrument was not originally designed for the lower stratosphere, when chlorine-catalyzed ozone depletion was thought to be mainly an upper stratospheric issue. The information and caveats in this paper shou]d allow for a more informed group of researchers to appreciate the quality of currently available MLS ozone data, and to proceed in their analyses with more confidence (or more caution in some cases). We look forward to providing even better datasets from MLS in the future, with optimum use of this instrument's capabilities.

*Acknowledgments*

Contributions from the entire MLS team (at the Jet l'repulsion Laboratory and in the United Kingdom) are gratefully acknowledged. We are indebted to various persons from the UARS }'reject and elsewhere for the compilation of data and model values which make up the "UARS Climatology File", used as a priori information in the MLS retrieval process; in particular, we acknowledge the efforts of R. Seals and 1'. Connell. Wc also thank M. Allen for the default model profiles (from the Caltech/JPL model) used as part of this procedure. Early simulations of MLS retrievals also benefited greatly from the availability of 3-D model results, made possible by W. 1.. Grose, G. Lingenfelser, and others at the Langley Research Center. For correlative data, we thank V. Brackett for his help regarding the Ascension island and Brazzaville ozonesonde data, and D. Walsh for his assistance on TMF lidar data. We thank W. A. Lahoz for his comments 011 this manuscript. This research was sponsored by NASA's Upper Atmosphere Research Satellite Project and was performed at the Jet Propulsion Laboratory, California Institute of Technology, under contract with the National Aeronautics and Space Administration.

## Appendix: Combination of a priori and measurement information

Starting with measurements y with error covariance $\boldsymbol{E}$, and an assumed linear relation (via weighting functions $\boldsymbol{K}$) to state vector $\boldsymbol{x}$ (or more accurate] y, a linear relation between departures of these quantities from true or a priori values), the well known weighted least-squares solution for $\boldsymbol{x}$ and its error covariance S is:

$$\hat{\boldsymbol{x}}_{LS} = (\boldsymbol{K}^T \boldsymbol{E}^{-1} \boldsymbol{K})^{-1} \boldsymbol{K}^T \boldsymbol{E}^{-1} \boldsymbol{y}, \quad \text{(A1)}$$

$$\hat{\boldsymbol{S}}_{LS} = (\boldsymbol{K}^T \boldsymbol{E}^{-1} \boldsymbol{K})^{-1} \quad \text{(A2)}$$

The above solution minimizes the sum of the squared residuals $(\boldsymbol{y}-\boldsymbol{K}\boldsymbol{x})^T \boldsymbol{E}^{-1}(\boldsymbol{y}-\boldsymbol{K}\boldsymbol{x})$. Also, given 2 estimates $\boldsymbol{x}_1$ and $\boldsymbol{x}_2$ of quantity $\boldsymbol{x}$, with error covariances $\boldsymbol{S}_1$ and $\boldsymbol{S}_2$, the maximum likelihood (or optimum) estimate of $\boldsymbol{x}$ and its error covariance S can be written as:

$$\boldsymbol{x} = (\boldsymbol{S}_1^{-1} + \boldsymbol{S}_2^{-1})^{-1} (\boldsymbol{S}_1^{-1}\boldsymbol{x}_1 + \boldsymbol{S}_2^{-1}\boldsymbol{x}_2), \quad \text{(A3)}$$

$$\boldsymbol{S} = (\boldsymbol{S}_1^{-1} + \boldsymbol{S}_2^{-1})^{-1} \quad \text{(A4)}$$

If we now replace, in the above 2 equations, $\boldsymbol{x}_1$ and $S_1$ by $\boldsymbol{x}_a$ and $\boldsymbol{S}_a$ (a priori estimates) and $\boldsymbol{x}_2$ and $\boldsymbol{S}_2$ by $\hat{\boldsymbol{x}}_{LS}$ and $\hat{\boldsymbol{S}}_{LS}$ above (based on a set of measurements y), we obtain

$$\hat{\boldsymbol{x}} = (\boldsymbol{S}_a^{-1} + \boldsymbol{K}^T \boldsymbol{E}^{-1} \boldsymbol{K})^{-1} (\boldsymbol{S}_a^{-1}\boldsymbol{x}_a + \boldsymbol{K}^T \boldsymbol{E}^{-1} \boldsymbol{y}) \quad \text{(A5)}$$

$$\hat{\boldsymbol{S}} = (\boldsymbol{S}_a^{-1} + \boldsymbol{K}^T \boldsymbol{E}^{-1} \boldsymbol{K})^{-1} \quad \text{(A6)}$$

This equation (see *Rodgers*, 1976) is the basis for the sequential estimation equations used in the MLS retrievals. indeed, the above equations can be rewritten in a manner more similar to the "scalarized" equations (1) and (2) of section 3, namely

$$\hat{\boldsymbol{x}} = \boldsymbol{x}_a + \boldsymbol{S}_a \boldsymbol{K}^T (\boldsymbol{K} \boldsymbol{S}_a \boldsymbol{K}^T + \mathrm{E})^{-1} (\boldsymbol{y} - \boldsymbol{y}_a^c), \quad \text{(A7)}$$

$$\hat{\boldsymbol{S}} = \boldsymbol{S}_a - \boldsymbol{S}_a \boldsymbol{K}^T (\boldsymbol{K} \boldsymbol{S}_a \boldsymbol{K}^T + \boldsymbol{E})^{-1} \boldsymbol{K} \boldsymbol{S}_a \quad \text{(A8)}$$

where departures from a priori state vector are now expressed as a function of departures from a priori radiances $(\boldsymbol{y}_a^c)$.

## References

Barath, F., M. Chavez, R. Cofield, D. Flower, M. Frerking, M. Gram, W. Harris, J. Holden, R. Jarnot, W. Kloeczeman, G. Klose, G. Lau, M. Loo, B. Maddison, R. Mattauch, R. McKinney, G. Peckham, 11. Pickett, G. Siebes, F. Soltis, R. Suttie, J. Tarsala, J. Waters, and W. Wilson, The Upper Atmosphere Research Satellite Microwave Limb Sounder Instrument, *J. Geophys. Res.*, *98*, 10751-10762, 1993.

Barnes, R. A., A. R. handy, and A. L. Torres, Electrochemical concentration cell ozonesonde accuracy

and precision, *J. Geophys. Res.*, 90, 7881-7887, 1985.

Bevington, P. R., "Data Reduction and error analysis for the physical sciences>', McGraw-Hill Book Company, 1969.

Canziani, P. O., J. R. Holton, E. F. Fishbein, L. Froidevaux, and J. W. Waters, Equatorial Kelvin waves: a UARS-MLS view, *J. Atmos. Sci.*, *51*, 3053-3076, 1994.

Cunnold, D., et al., *J. Geophys. Res.*, to be submitted, 1994a.

Cunnold, D., et al., *J. Geophys. Res.*, to be submitted, 1994b.

Elson, L. S., and L. Froidevaux, The use of Fourier transfcn-ills for asynoptic mapping: early results from the Upper Atmosphere Research Satellite Microwave Limb Sounder, *J. Geophys. Res.*, *89*, 23039-23049, 1993.

Elson, L. S., G. L. Manney, L. Froidevaux, and J. W. Waters, l,argc-scale variations in ozone from the first two years of UARS MLS data, *J. Atmos. Sci.*, 51,2867-2876,1994.

Fishbein, E. V., R. E. Cofield, L. Froidevaux, R. F. Jarnot, "1'. A. Lungu, W. G. Read, Z. Shippony, .1. W. Waters, 1. S. McDermid, T. J. McGee, 11. Singh, M. Gross, A. Hauchecorne, and M. E. Gelman, Validation of UARS MLS temperature/pressure measurements, *J. Geophys. Res.* (special issue on UARS data validation), to be submitted, 1994.

Froidevaux, L., J. W. Waters, W. G. Read, L. S. Elson, D. A. Plower, and R. II'. Jarnot, Global ozone observations from UARS MLS: an overview of zonal mean results, *J. Atmos. Sci.*, *51*, 2846-2866, 1994.

Grose, W., and J. Gille, *eds.*, Upper Atmosphere Research Satellite Validation Workshop 111 Report: Temperature and Constituents, NASA Ref. Pub., in preparation, 1994.

Hilsenrath, E., W. Attmannspacher, A. Bass, W. Evans, R. Hagemeyer, R. A. Barnes, W. Komhyr, K. Mauersberger, J. Mentall, M. Proffitt, D. Robbins, S. Taylor, A. Torres, and E. Weinstock, Results from the Balloon Ozone Intercomparison Campaign (BOIC), *J. Geophys. Res.*, *91*, 13137-13152, 1986.

Jarnot, R. F., R. E. Cofield, J. W. Waters, and G. E. Peckham, Calibration of UARS MLS, *J. Geophys. Res.*, submitted, 1994.

Keating, G. M., M. C. Pitts, and D. F. Young, Ozone reference models for the middle atmosphere (New CIRA), in Middle Atmosphere Program Handbook for MAI', G. M. Keating, editor, *Vol. 31*, pp. 1-36, 1989a.

Keating, G. M., M. C. Pitts, and C. Chen, Improved reference models for middle atmosphere ozone, in Middle Atmosphere Program Handbook for MAP, G. M. Keating, editor, *Vol. 31*, pp. 37-49, 1989b.

Lahoz, W. A., M. R. Suttie, L. Froidevaux, R. S. Harwood, C. 1,. Lau, 'l'. A. Lungu, G. E. Peckham, 11. C. Pumphrey, W. G. Read, Z. Shippony, R. A. Suttie, and J. W. Waters, Validation of UARS MLS 183 GHz $H_2O$ Measurements, *J. Geophys. Res.* (special issue on UARS data validation), submitted, 1994.

Liebe, H. J., P. W. Rosenkranz, and G. A. Hufford, Atmospheric 60-GHz oxygen spectrum: new laboratory measurements and line parameters, *J. Quant. Spectrosc. Radiat. Transfer*, *48*, 629-643, 1992.

Manney, G. 1,., L. Froidevaux, J. W. Waters, L. S. Elson, E. F. Fishbein, R. W. Zurek, R. S. Harwood, and W. A. Lahoz, The evolution of ozone observed by UARS MLS in the 1992 late winter southern polar vortex, *Geophys. Res. Lett.*, 20, 1279-1282, 1993.

Marks, C. J., and C. D. Rodgers, A retrieval method for atmospheric composition from limb emission measurements, *J. Geophys. Res.*, 98, 14939-14953, 1993.

McDermid, 1. S., A 4-year climatology of stratospheric ozone from lidar measurements at 'J'able Mountain, 34.4N, *J. Geophys. Res.*, *98*, 10509-10515, 1993.

Marks, C. J., and C. D. Rodgers, A retrieval method for atmospheric composition from limb emission measurements, *J. Geophys. Res.*, 98, 14939-14953, 1993.

McDermid, 1. S., A 4-year climatology of stratospheric ozone from lidar measurements at Table Mountain, 34.4N, *J. Geophys. Res.*, *98*, 10509-10515, 1993.

Oh, J. J., and E. A. Cohen, Pressure broadening of ozone lines near 184 and 206 GHz by nitrogen and oxygen, *J. Quant. Spectrosc. Radiat. Transfer*, *48*, *405-408*, 1992.

Pickett, H. M., R. L. Poynter, and E. A. Cohen, Submillimeter, Millimeter and Microwave Spectral

Line Catalog, Technical Report 80-23, Revision 3, Jet l'repulsion laboratory, 1992.

Ray, E., J. R. Holton, E. F. Fishbein, L. Froidevaux, and J. W. Waters, The tropical seniannual oscillation (SAO) in temperature and ozone observed by the Microwave Limb Sounder (MLS), *J. Atmos. Sci., 31, 3045-3052, 1994.*

**Read, W. G., L. Froidevaux, and J. W. Waters, Microwave Limb Sounder (MLS) measurements of $SO_2$ from Mt. Pinatubo volcano, *Geophys. Res. Lett.*, 20, 1299-1302, 1993.**

Read, W. G., J, W. Waters, 1,. Froidevaux, D. A. Flower, R. F. Jarnot, D. L. Hartmann, R. S. Harwood, and R. B. Rood, Upper tropospheric water vapor from UARS MLS, *Bull. Amer. Met. Soc.*, to *be* submitted, 1994.

Reber, C. A., and F. T. Huang, The UARS Level 3B grid ding algorithm, *J. Geophys. Res. (special issue on UARS data* validation), to be submitted, 1994.

Redaelli, G., 1,. Lait, M. Schoeberl, P. A. Newman, G. Visconti, A. D'Altorio, F. Masci, V. Rizi, L. Froidevaux, J. Waters, and J. Miller, UARS M 1.S $O_3$ soundings compared with lidar measurements using the conservative coordinates reconstruction technique, *Geophys. Res. Lett.*, 21, 1535-1538, 1994.

Ricaud, P., J. de La Not, B. J. Connor, L. Froidevaux, J. W. Waters, R. S. Harwood, 1. A. MacKenzie, and G. E. Peckham, Diurnal variability of mesospheric ozone as measured by UARS MLS: theoretical and ground-based validations, *J. Geophys. Res.* (special issue on UARS data validation), to be submitted, 1994.

Rodgers, C. D., Retrieval of atmospheric temperature and composition from remote measurements of thermal radiation, *Rev. Geophys, and Space Phys., 14*, 609-624, 1976.

Rodgers, C. D., Characterization and error analyses of profiles retrieved from remote sounding measurements, *J. Geophys. Res.*, 95, 5587-5595, 1990.

Santee, M.],., W. G. Read, J. W. Waters, I,. Froidevaux, G. ],. Manney, D. A. Flower, R. F. Jarnot, R. S. Harwood, and G. E. Peckham, Interhemispheric differences in polar stratospheric $HNO_3$, $H_2O$, ClO aud $O_3$ from UARS M 1.S, *Science*, submitted, ]994.

Stachnik, R. A., J. C. Hardy, J. A. Tarsala, J. W. Waters, and N. R. Erickson, Submillimeter wave heterodyne measurements of stratospheric ClO, HCl, $O_3$, and $HO_2$: First **results, *Geophys. Res. Lett.*, 19, 1931-1934, 1992.**

Waters, J. W., Microwave limb-sounding of Earth's upper atmosphere, *Atmospheric Research*, 23, 391-410, 1989.

Waters, J. W., Microwave limb sounding, in *Atmospheric Remote Sensing by* Microwave Radiometry, Janssen, M. A., editor, chapter 8, J. Wiley & Sons, New York, 1993.

Waters, J. W., L. Froidevaux, G. I,. Manney, W. G. Read, and 1,. S. Elson, Lower stratospheric ClO and $0_3$ in the 1992 southern hemisphere winter, *Geophys. Res. Lett.*, 20, 1219-1222, 1993.

Waters, J. W., W. G. Read, 1,. Froidevaux, T. A. Lungu, V. S. Perun, R. A. Stachnik, R. F. Jarnot, R. E. Cofield, E. F. Fishbein, D. A. Flower, J. R. Burke, J. C. hardy, 1,. ],. Nakamura, B. P. Ridenoure, Z. Shippony, R. }'. Thurstans, 1,. M. Avallone, D. W. Toohey, R. L. deZafra, and D. T. Shindell, Validation of UARS MIS ClO Measurements, *J. Geophys. Res.* (special issue on UARS data validation), submitted, 1994.

This preprint was prepared with the AGU LaTeX macros v3.0. File jgrpaper 1 formatted 1994 November 1.

**Table 1.** State Vector Components in M 1,S Version 3 Retrievals

| Radiance Band | Retrieved Components | Constrained Components |
|---|---|---|
| B1 (63 GHz) | $\boldsymbol{P}_{tan}$, 1, $\boldsymbol{y}_1^{off}$ | $\boldsymbol{f}^{O_2}$, ,0'"0, $\boldsymbol{v}$, $R_E$, $R_S$, $\boldsymbol{B}$ |
| B5 (183 GHz) | $\boldsymbol{f}^{H_2O}$, $\boldsymbol{y}_5^{off}$ | $\boldsymbol{P}_{tan}$, $\boldsymbol{T}$, $\delta\chi'$, $\boldsymbol{v}$, $R_E$, $R_S$ |
| B6 (183 GHz) | $\boldsymbol{f}^{O_3(183)}$, $\boldsymbol{y}_6^{off}$ | $\boldsymbol{P}_{tan}$, $\boldsymbol{T}$, $\boldsymbol{f}^{H_2O}$, $\delta\chi'$, $\boldsymbol{v}$, $R_E$, $R_S$ |
| B4 (205 GHz) | $\boldsymbol{f}^{O_3(205)}$, $\boldsymbol{y}_4^{off}$ | $\boldsymbol{P}_{tan}$, $\boldsymbol{T}$, $\boldsymbol{f}^{H_2O}$, $\boldsymbol{f}^{O^{18}OO}$, $\delta\chi$, $\boldsymbol{v}$, $R_E$, $R_S$ |
| B2/B3 (205 GHz) | f $^{ClO}$, $\boldsymbol{f}^{SO_2}$, $\boldsymbol{f}^{HNO_3}$, $\boldsymbol{y}_{2/3}^{off}$, $\boldsymbol{y}_{2/3}^{lin}$ | $\boldsymbol{P}_{tan}$, $\boldsymbol{T}$, $\boldsymbol{f}^{O_3(205)}$, $\boldsymbol{f}^{H_2O}$, $\boldsymbol{f}^{H_2^{18}O}$, $\boldsymbol{f}^{OO^{18}O}$, $\delta\chi$, $\boldsymbol{v}$, lip;, $R_S$ |

Hold type indicates a vector (like $\boldsymbol{T}$, $\boldsymbol{f}$, $\boldsymbol{v}$, and B), including a quantity which has an updated value for each scan position (like $\boldsymbol{P}_{tan}$, $\boldsymbol{y}^{off}$, and $\boldsymbol{y}^{lin}$. $R_E$ and $R_S$ are updated once per major frame (complete scan) for their effect on radiances, hut once per minor frame (scan dwell position) in the a priori equation for tangent pressure (see description in text). Mixing ratios ($\boldsymbol{f}$) include the appropriate species as a superscript. Other quantities are defined in the text.

**Table 2.** Error Sources Affecting M 1,S Ozone Retrievals

| Error source |
|---|
| 1. Radiance noise |
| 2. Radiance scaling error (includes radiometric, sideband ratio, and line strength errors) |
| 3. Error in filter shapes |
| 4. Error in FOV direction (relative to 63 GHz radiometer FOV) |
| 5. Error in FOV shape (includes spectral dependence) |
| 6. Error in ozone linewidth |
| 7. Retrieval numerics |
| 8. Error contribution from a priori |
| 9. Error in $P_{tan}$ |
| 10. Error in atmospheric temperature |
| 11. Error in dry air continuum |
| 12. Error in knowledge of $H_2O$ |
| 13. Error in knowledge of $HNO_3$ |
| 14. Error in knowledge of $N_2O$ |
| 15. Error in knowledge of $SO_2$ |

Other sources of error exist, but are either implicitly included in this list, or considered to be negligible (see text). The $11N0_3$, $N_20$ and $SO_2$ error sources were only applied to the analysis of 205 GHz ozone.

**Table 3a.** Estimated Precision* and Accuracy of MLS 205 GHz Ozone

| UARS Standard Level | Pressure (hPa) | Precision (ppmv) | Precision (percent) | Accuracy (ppmv) | Accuracy (percent) |
|---|---|---|---|---|---|
| 20 | 0.46 | 0.37 | 20 | 0.3 | 15 |
| 18 | 1 | 0.31 | 10 | 0.3 | 10 |
| 16 | 2.2 | 0.23 | 4 | 0.3 | 5 |
| 14 | 4.6 | 0.2 | 2 | 0.3 | 5 |
| 12 | 10 | 0.18 | 2 | 0.3 | 5 |
| 10 | 22 | 0.16 | 3 | 0.4 | 5 |
| 8 | 46 | 0.22 | 11 | 0.4 | 20 |
| 6 | 100 | 0.55 | ≥50 | | ≥50 |

* Precision given here is for individual profiles.

**Table 3b.** Estimated Precision* and Accuracy of MLS 183 GHz Ozone

| UARS Standard Level | Pressure (hPa) | Precision (ppmv) | Precision (percent) | Accuracy (ppmv) | Accuracy (percent) |
|---|---|---|---|---|---|
| 26 | 0.05 | 0.3 | 55 | 0.5 | ≥50 |
| 24 | 0.1 | 0.26 | 30 | 0.3 | 35 |
| 22 | 0.22 | 0.17 | 17 | 0.2 | 20 |
| 20 | 0.46 | 0.1 | 6 | 0.2 | 10 |
| 18 | 1 | 0.1 | 3 | 0.4 | 15 |
| 16 | 2.2 | 0.1 | 2 | 0.8 | 15 |
| 14 | 4.6 | 0.1 | 1 | 0.9 | 10 |
| 12 | 10 | 0.13 | 2 | 0.9 | 10 |
| 10 | 22 | 0.2 | 3 | 0.8 | 15 |
| 8 | 46 | 0.1 | 6 | 0.8 | 45 |

* Precision given here is for individual profiles.

Figure 1. Main spectral features contributing to the MLS radiances from the 205 GHz radiometer, for typical lower (46 h] 'a) and upper (4.6 hPa) stratospheric mid-latitude conditions. Spectral regions covered for both primary and image sidebands of bands 2 and 3 (for C]()), and band 4 (for ozone) are indicated by vertical dashed lines. Spew.ics with significant emission features are indicated. A similar diagram is given in *Lahoz et al.* (1994), for the $H_2O$ and 183 GHz $O_3$ spectral features measured by MLS.

**Figure 2.** Scheı natic of the UAR S MLS measurement geometry. The UARS M 1,S observations are made from point S, where emission from the earth's atmosphere (*e.g.* points $P_1$ and $P_2$) is received, as the MLS antenna scans through the limb.

**Figure** 3. September zonal mean cross section for climatological ozone (ppmv) used as a priori information (see text) in the ret, rieval algorithms.

**Figure** *4. Error ratio (estimated over a priori)* for M 1,S *ozone* retrievals at 70S latitude (thin lines) and at the equator (thick lines); solid lines are for 205 GHz results, dashed lines are for 183 GHz results (both for September 17, 1992).

Figure **5.** Averaging kernels (see text) of h41,S Version 3 ozone retrievals for (a) 205 GHz and (b) 183 GHz.

**Figure 6.** Simulated radiances and residuals for M 1,S 205 GHz ozone. The simulations use smoothed h41, S retrievals from Sep. 17, 1992 as input ( "truth" ). Average results for a 10 degree-wide latitude bin centered at 40S are shown. Signals are interpolated onto the MLS retrieval pressure grid and shown for tangent pressures from 0.46 hPa (top left panel) down to 100 hPa (bottom right panel). "Observed" radiances (l{) from the synthetic profiles are drawn as solid lines versus frequency from the center channel (in MHz); clashed lines give the "calculated" radiances - based cm retrievals from the "observed" radiances -, although the two radiance curves are often indistinguishable 011 the scale shown. Radiance residuals ("observed" minus "calculated") are displayed about the horizontal "zero line", based on the right-axis scale (expanded relative to radiance scale by a factor of 1 O).

**Figure 'i'.** Same as Fig. 6, but for MLS 183 GHz ozone (with different radiance scale, but still a factor of 10 expanded scale on the right axis for residuals).

**Figure 8.** Contour plots of $\chi^2$ statistics (goodness of fit, ) for radiances in the *205* GHz ozone band (left panels), and the 183 GHz ozone band (right panels), for the simulated data discussed in relation to Figs. *6* and *7*. Panels (a) and (b) give zonal mean values of $\chi^2_{mi}$ (see text) versus tangent pressure. Panels (c) and (cl) give zonal mean values of $\chi^2_{ma}$ (see text) as the solid line, with minimum and maximum values given by dashed lines.

**Figure 9.** Contour plots (versus pressure and latitude) of zonal mean ozone simulations for MLS retrievals from the 205 GHz band. (a) simulated "true" *ozone* (*ppmv*) (b) retrieved *ozone* (ppmv) based on a set of model radiances (with noise), generated from the "true" profiles (c) mean differences (ppmv) - retrieved minus "true" profiles - (d) mean permit differences; large percentage differences exist at 100 hPa partly because mixing ratios can be very small.

**Figure 10.** Maps of ozone (ppmv) for "true ozone" (top row) and retrieved ozone from 205 GHz simulations (bottom row) - with realistic radiance noise - at 46, 10, and 2 hPa (as indicated).

**Figure 11.** Same as Fig. 9, but for zonal mean comparison of simulated ozone from 183 GHz band with "true" ozone (note that pressure scale extends to 0.01 hPa).

**Figure 12.** Radiances and residuals for MLS 205 GHz ozone in the 40S latitude bin on Sep. 17, 1992 (actual data, not a simulation). Format used here is identical to that in Fig. 6.

**Figure Y 3.** Radiances and residuals for MLS 205 GHz ozone in the lowermost stratosphere (46 hPa on the left, 100 hPa on the right), at 10S (top two panels) and 70S (bottom two panels), on Sep. 17, 1992. Format used here is identical to that used for each panel of Fig. 12 (and 6).

**Figure 14** Same as Fig.12, but for MLS 183 GHz ozone.

**Figure 15.** Same as Fig.13, but for MLS 83 GHz ozone, and for 46 and 22 hPa rather than 100 and 46 hPa.

**Figure 16.** Contour plots of $\chi^2$ goodness of fit (radiance) diagnostic for 205 GHz ozone (left panels), and 183 GHz ozone (right panels). Format is identical to that of Fig. 8, but actual data for Sep. 17, 1992 are used here rather than simulated data.

**Figure 17.** Zonally-averaged diagnostic ($\chi^2_{ma}$) as a function of latitude and time, for radiances in the 205 GHz radiometer ozone band (top panels), and the 183 GHz ozone band (bottom panels). Left panels are for the first year of UARS MLS data, and right panels are for the second year (no data beyond mid-April from the 183 GHz radiometer). Color bars on the right give the scale for $\chi^2_{ma}$ values.

**Figure 18.** MLS 205 GHz ozone profiles versus climatological profiles for January and July. The climatological data (see text) are shown for January (solid line) and July (dashed line) at the various latitudes shown in the 5 panels (60N, 30N, 0, 30S, and 60S, top to bottom). MLS ozone values are given by crosses for January, and open circles for July, at the same latitudes (zonal means over a 5 degree wide bin centered at the above latitudes); 4 days of MLS data in mid-January and mid-July 1993 were used here.

**Figure 19.** Mapped field of the MLS-retrieved ozone abundances at 46 hPa minus those at 100 hPa; blue and purple colors indicate a negative difference, *i.e.* a retrieval artifact ("bulge" at 100 hPa), if sustained over a large area - not just a noise effect. These tend to occur at polar and equatorial latitudes. Top panel is for north-viewing conditions on Oct. 12 1991 and bottom panel is for south-viewing conditions on Sep.12 1992.

**Figure 20.** Zonal mean difference (%) between the two MLS ozone retrievals (183 GHz minus 205 GHz ozone). Top panel is for Version 2 data, when the retrievals used pre-launch values for FOV angular offset versus the 63 GHz radiometer; bottom panel is for Version 3 retrievals (see text for discussion of angular offset adjustment).

**Figure 21.** Rms variability about zonal means divided by estimated uncertainty (from MLS Version 3 data files), for 28 Nov. 1992 (a day with minimal variability) for 205 GHz ozone (top panel) and 183 GHz ozone (bottom panel).

**Figure 22.** Error characterization for the MLS 205 GHz ozone data. Rms uncertainty estimates are given for the various error sources listed in Table 1. Top panels give uncertainty in ppmv, and bottom panels give the values as a percentage; results are generally averaged over all latitudes based on sensitivity tests for a full day of MLS retrievals (see text for details). Left panels: uncertainties from radiance noise (solid line), and systematic errors in radiance scaling (dotted line), filter shapes (dashed line) - essentially negligible, only seen as 5% effect at 100 hPa -, FOV direction (dash-dot), and FOV shape (dash-dot-dot). Middle panels: uncertainties from ozone linewidth (solid line), retrieval numerics (dotted line) and a priori error contribution (dashed line). Right panels: uncertainties from systematic error in knowledge of $P_{tan}$ (thick solid line), temperature (dotted line), dry air continuum (dashed line), $H_2O$ (dash-dot), $HNO_3$ (dash-dot-dot), $N_2O$ (long-dashed line), and $SO_2$ (thin line).

**Figure** *23.* Same as Fig. 22, but for ozone from 183 GHz band data. The last three error sources (from $HNO_3$, $N_2O$, and $SO_2$) in Fig. 22 are not present for 183 GHz.

**Figure** *2-1.* Total estimated uncertainty for 205 GHz radiometer ozone. Random (clotted line), systematic (dash-dot line), and a priori error contributions (dashed line), along with total (rss) uncertainties (solid lines connecting squares) are plot ted as a function of pressure. Also, typical (global rms) uncertainty values given, in M LS Version 3 data files are shown as crosses (see text for discussion). Top panel gives values in ppmv, and bottom panel is given in percent (of global rms profile for September 1"7, 1992).

**Figure** 25. Same as Fig. 24, but for 183 GHz ozone.

**Figure 26.** Individual profile comparisons b etween MLS 205 GHz ozone and o zonesonde data from Boulder during 1992. Data were taken on the following dates: (a) January 3 (b) April 17 (c) J~llJ'29 and (d) October 8. Examples of good correspondance between the two data sets are shown (panels (a) through (c)), as well as an example of an unresolved problem in MLS ret rievals at 100 hPa (panel (d)). MI. S data are connect ed solid circles with estimated uncertainties from the (Version 3) data files (see text); correlative sonde data are given by solid line, with a shaded uncertainty of 5% (see trot). Distance (km) and time difference (hr) between the M 1,S retrieved profile and the sonde data are indicated on right side of each panel.

**Figure** 27. 'J'illle-series comparison between MLS ozone mixing ratios (ppmv) at 100, 46, 22, and 10 hPa (bottom panel to top panel) and Boulder ozonesonde data during 1992 (42 coincident profiles total); MI, S data are plus symbols (red) with estimated uncertainties (see text) and sonde data are diamonds (blue) with estimated uncertainties (see text).

**Figure 28.** Statistics of comparisons between M LS ozone profiles and coincident Boulder ozonesonde data presented in Fig. 27. (a) Average MLS ozone profile (ppmv) - solid circles connected by line - and sonde profile - thick line - (b) Average differences (ppmv) at the MLS retrieval grid points (100, 46, 22, and 10 hPa) - squares - and rms differences (ppmv) - crosses, along with the standard deviations of the differences - open circles - and the estimated rms precision of the differences - solid circles (c) Same as in (b), but as a percentage of the mean sonde profile.

**Figure** *29.* Time series comparison between MLS ozone mixing ratios (ppmv) at 100, 46, 22, and 10 hPa (bottom panel to top panel) and Hilo ozonesonde data during 1992 (29 coincident profiles iota]); formatis same as for Fig. 27.

**Figure 30.** Statistics of comparisons between M LS ozone profiles and coincident Hilo ozonesonde data presented in Fig. 29; format is same as for Fig. 28.

**Figure** 31. Time series comparison between MLS ozone mixing ratios (ppmv) at 100, 46, 22, and 10 hPa (bottom panel to top panel) and Ascension Island ozonesonde data during 1991-92 (27 coincident profiles total); format is same as for Fig. 27.

**Figure** 32. Statistics of comparisons between MLS ozone profiles and coincident Ascension Island ozonesonde data presented in Fig. 31; format is same as for Fig. 28.

**Figure** 33. Time series comparison between MLS ozone mixing ratios (ppmv) at 100, 46, 22, and 10 hPa (bottom panel to top panel) and Braz zaville ozonesonde data during 1991-92 (29 coincident profiles total); format is same as for Fig. 27.

**Figure** 34. Statistics of comparisons between MLS ozone profiles and coincident Brazzaville ozonesonde data presented in Fig. 33; format is same as for Fig. 28.

**Figure 35.** Time series comparison between MLS ozone mixing ratios (ppmv) at 100, **46, 22,** and 10 hPa (bottom panel to top panel) and Gardermoen ozonesonde data during 1993-94 (30 coincident profiles total); format is same as for Fig. 27.

**Figure 36.** Statistics of comparisons between M 1,S ozone profiles and coincident Gardermoen ozonesonde data presented in Fig. 35; format is same as for Fig. 28.

**Figure** 37. Time series comparison between MLS ozone mixing ratios (ppmv) at 100, 46, 22, and 10 hPa (bottom panel to top panel) and McMurdo ozonesonde data during August to October, 1992 (17 coincident profiles total); format is same as for Fig. i! 'i.

**Figure** 38. Statistics of comparisons between MLS ozone profiles and coincident McMurdo ozonesonde data presented in Fig. 37; format is same as for Fig. 28.

**Figure** 39. Latitude dependence of the ozone comparisons between M LS 205 GHz band data and ozonesonde data, based on the average data presented in Figs. 28, 30, 32, 34, 36, and 38. Each panel in a given column corresponds to a different pressure level (as indicated above each panel). In the left colu mn, average MLS mixing ratios (pl us symbols) are compared to the average sonde data (open diamonds) for each of the G sonde locatior ıs. Each site is identified by lower case letters (first two letters of site name) in the bottom left panel. The middle column gives average (open squares) and rms (crosses) differences (MLS minus sonde), in ppmv, while the right column shows these differences in percent. We nave omitted the 100 hPa panel on the bottom right, since ozone values get too small to be satisfactorily compared in percent.

**Figure 40.** Statistics of comparisons between h41.S ozone profiles and coincident UV photometer measurements from balloon. Format is same as Fig. 28. Shown are the average profiles and differences, for MLS and UV photometer data obtained near 33 N. Balloon flights occurred on 91 Oct. 1, 92 May 29, 92 Sep. 29, 93 May 31, 93 Sep. 25, and 94 May 22 from near Fort Sumner, New **Mexico,** and **011** 92 **Feb. 20** and 93 Apr. 3 from Daggett, California. MLS data were generally obtained within 12 hours of the flight, except for the 94 May 22 flight, when UARS was not operational; an MLS profile from May 24 was used in this case, which is not unreasonable for this time period of low variability.

**Figure** 41. Average profiles (and difference quantities, as done in previous figu res) for MLS and SLS data from a total of 5 balloon flights from Daggett, Californ ia, and Fort Sumner, New Mexico. The dates are as in Fig. 40, except for the May 1993 and 1994 flights, when the SLS did not participate.

**Figure 42.** Time series corlll)ariso~ll)etw'cell MLS ozone mixing ratios (ppmv) at 10, 4.6, 2.2, and 1 hPa (bottom panel to top panel) and Table Mountain Facility (TMF) lidar data during 1991- 1993, Format is same as Fig. 27.

**Figure 43, Statistics** of comparisons between MLS ozone profiles and coincident lidar data presented in Fig . 42. Format is same as in Fig. 28. Too few lidar profiles exist below 10 hPa to make meaningfu l statistical comparisons, so the differences in the bottom pannels do not include levels below 10 hPa.

**Figure 44.** Comparison of Version 3 MLS data with recently updated software (see text), for Aug. 29, 1992. (a) Zonal mean % differences (new minus old values) for 205 G Hz ozone, (b) 183 GHz ozone, and (c) zonal mean % differences for ozone 183 GHz minus 205 GHz data in the updated software (to be compared to differences shown in Fig. 20 for Version 3 MLS data).

**Figure 45.** Trade-off between vertical resolution (of retrieval grid) and uncertainty in 205 GHz ozone at 46 hPa. Total uncertainty (ppmv), for a 3 ppmv a priori error, is plotted versus retrieval grid resolution (km).

Radiance / K
Frequency / GHz
LO
B4 USB
B2 USB
B3 USB
B2 LSB
B3 LSB
B4 LSB
HNO3
O3(v2)
O3
N2O
46 hPa
97 hPa
O2 18O
HNO33
H2 18O
O3
O17O0
35Cl O
H
O3(v2)
HNO3
O3(v2)
HNO3
O3

Fig. 1

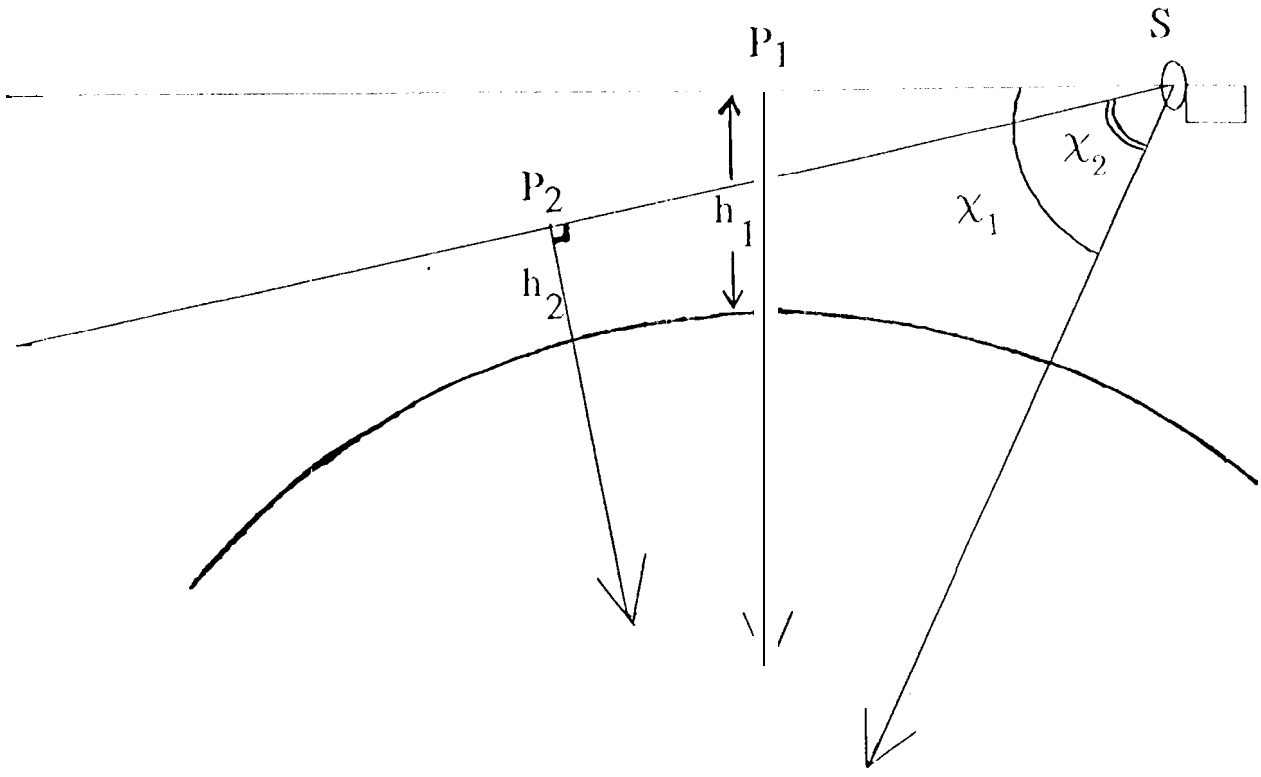


Fig. 2

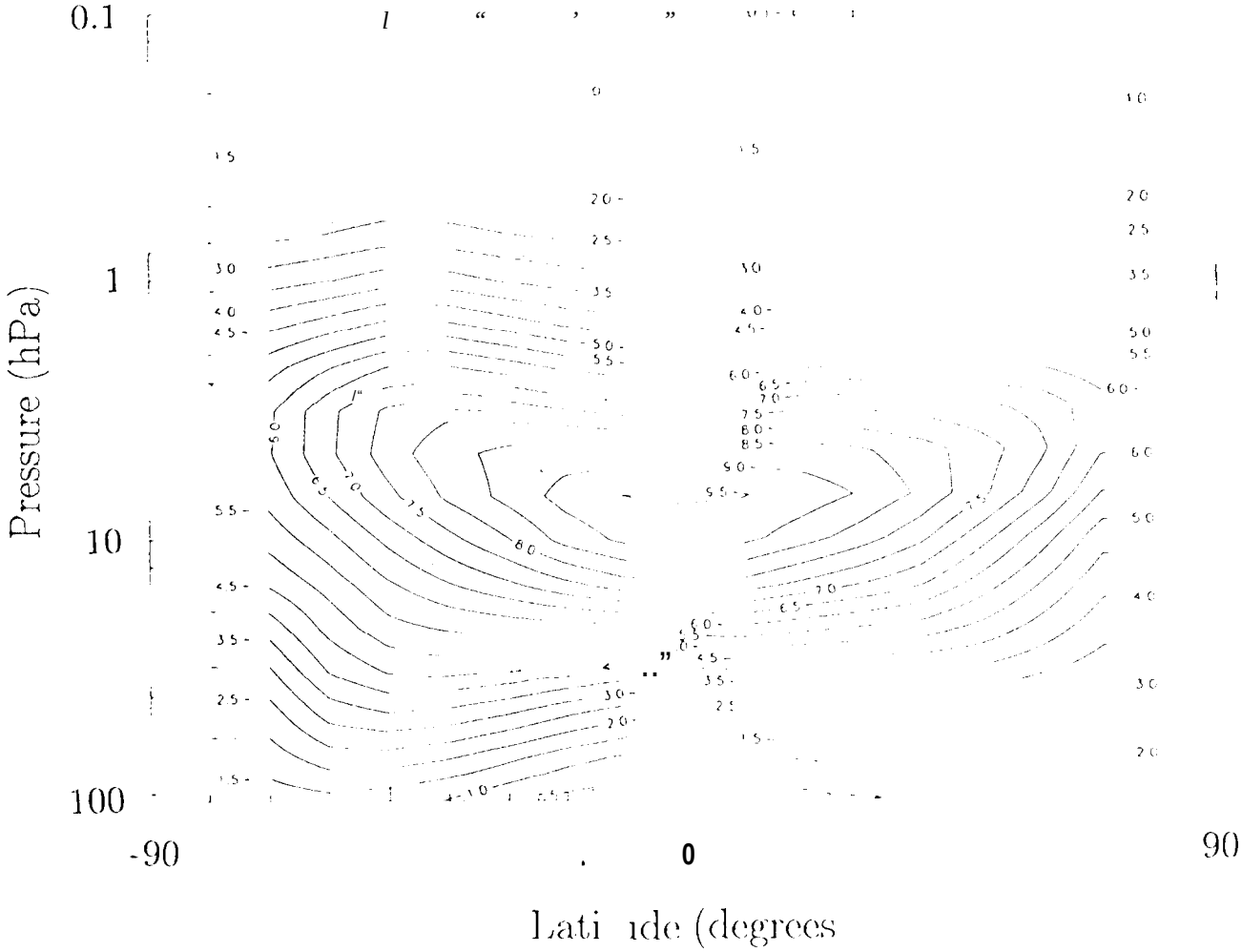


Fig. 3

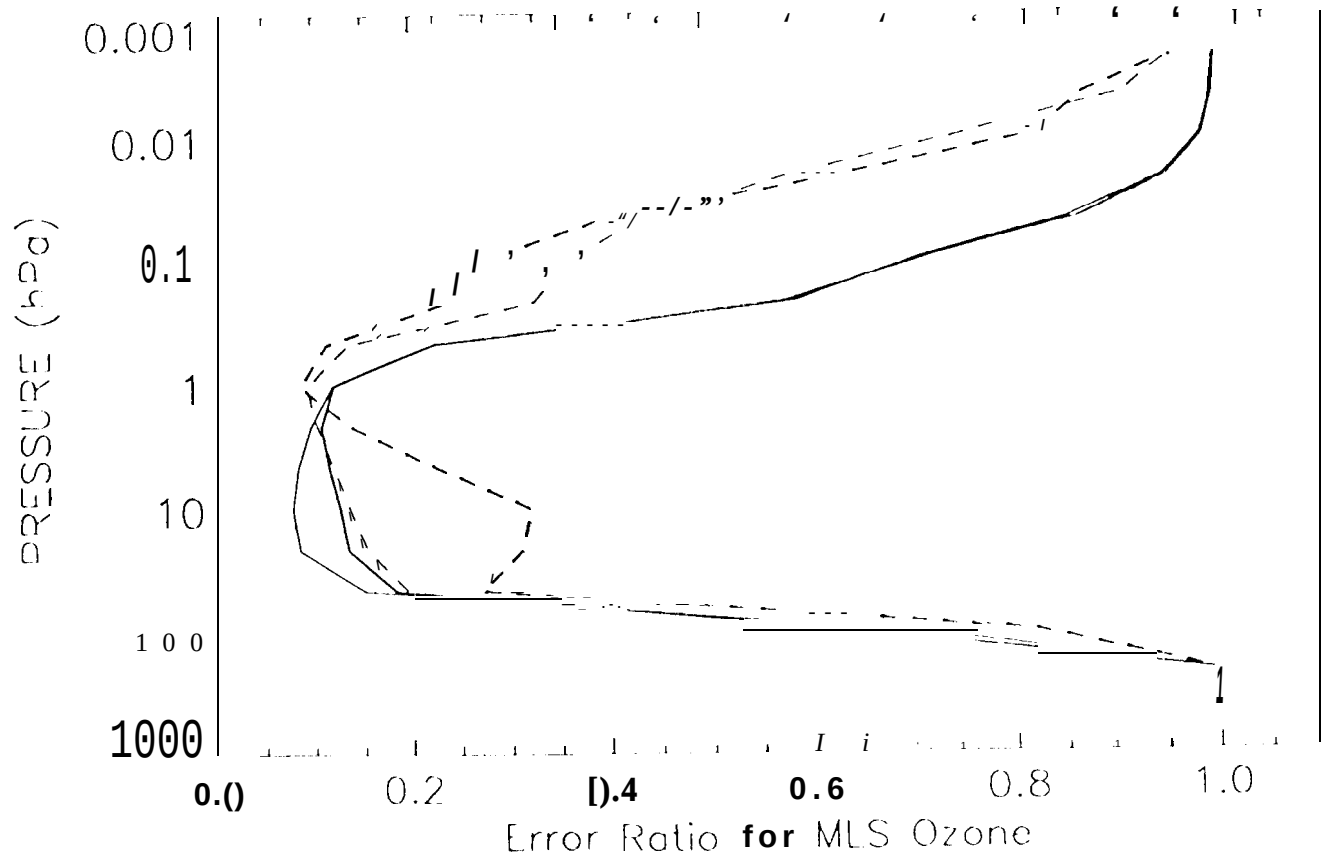
0.001
0.01
0.1
1
10
100
1000
PRESSURE (mb)
0.0
0.2
0.4
0.6
0.8
1.0
Error Ratio for MLS Ozone

Fig. 4

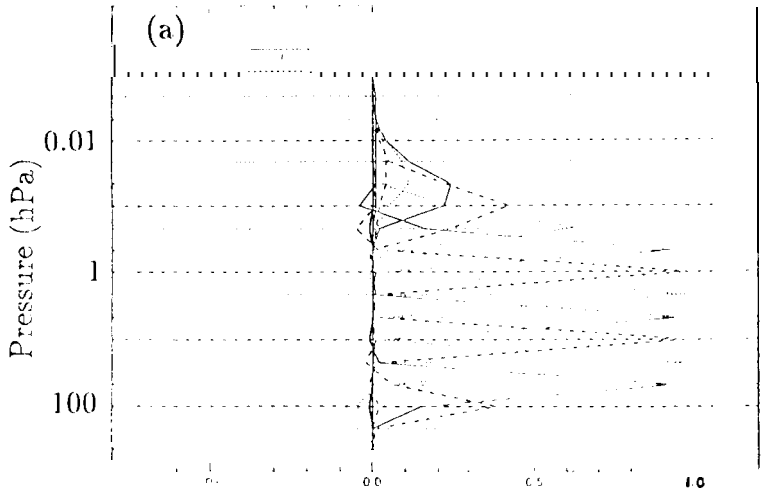
(a)
0.01
1
100
Pressure (hPa)
Averaging Kernel Amplitude

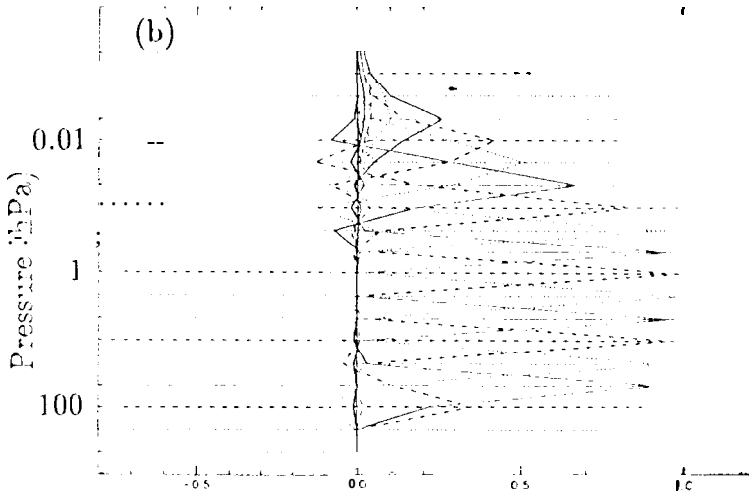
(b)
0.01
1
100
Pressure (hPa)
Averaging Kernel Amplitude

Fig. 5

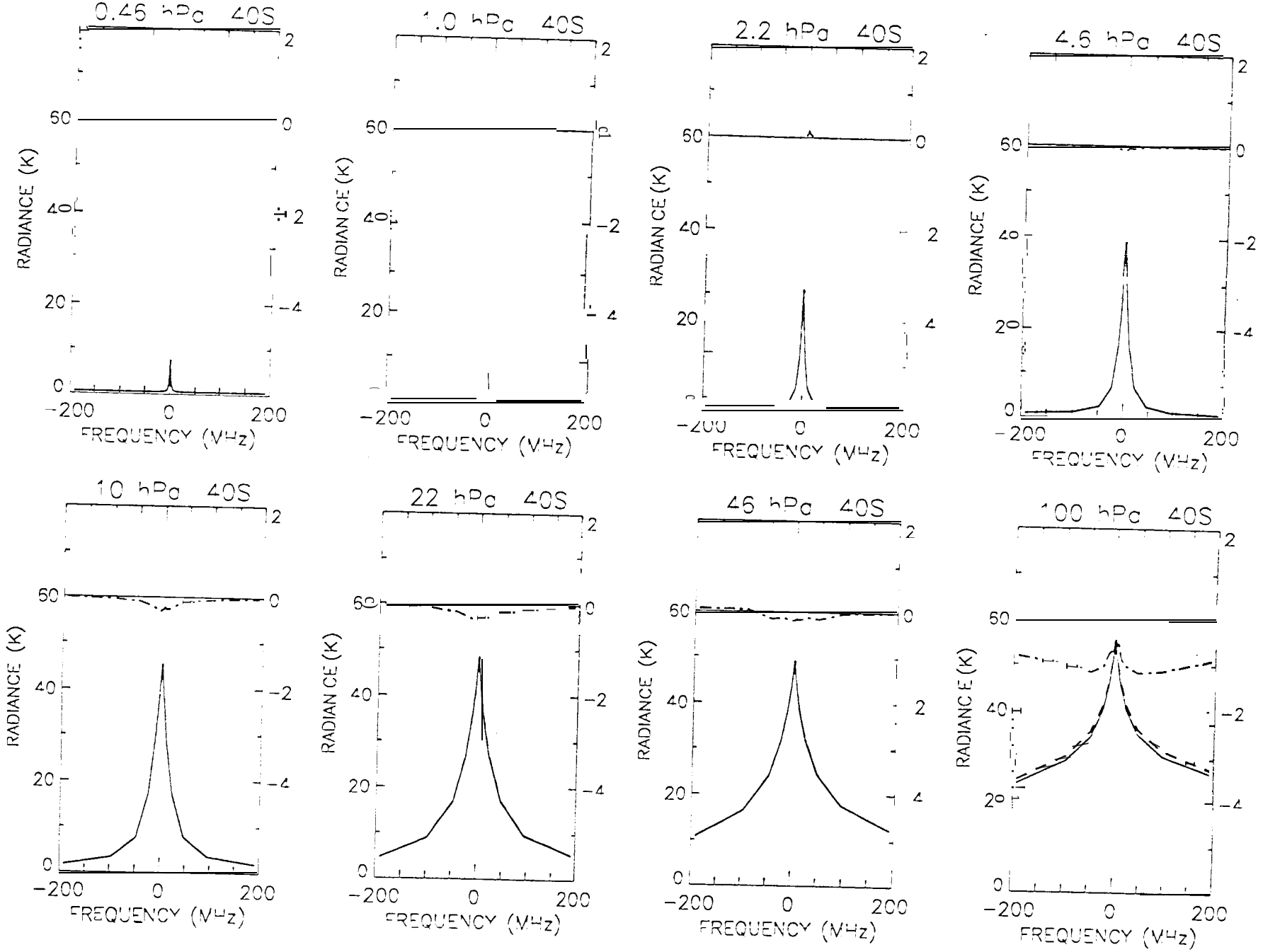
0.46 hPa 40S
1.0 hPa 40S
2.2 hPa 40S
4.6 hPa 40S
10 hPa 40S
22 hPa 40S
46 hPa 40S
100 hPa 40S
RADIANCE (K)
RADIAN CE (K)
FREQUENCY (MHz)
-200
0
200
60
40
20
0
2
0
-2
-4

Fig. 6

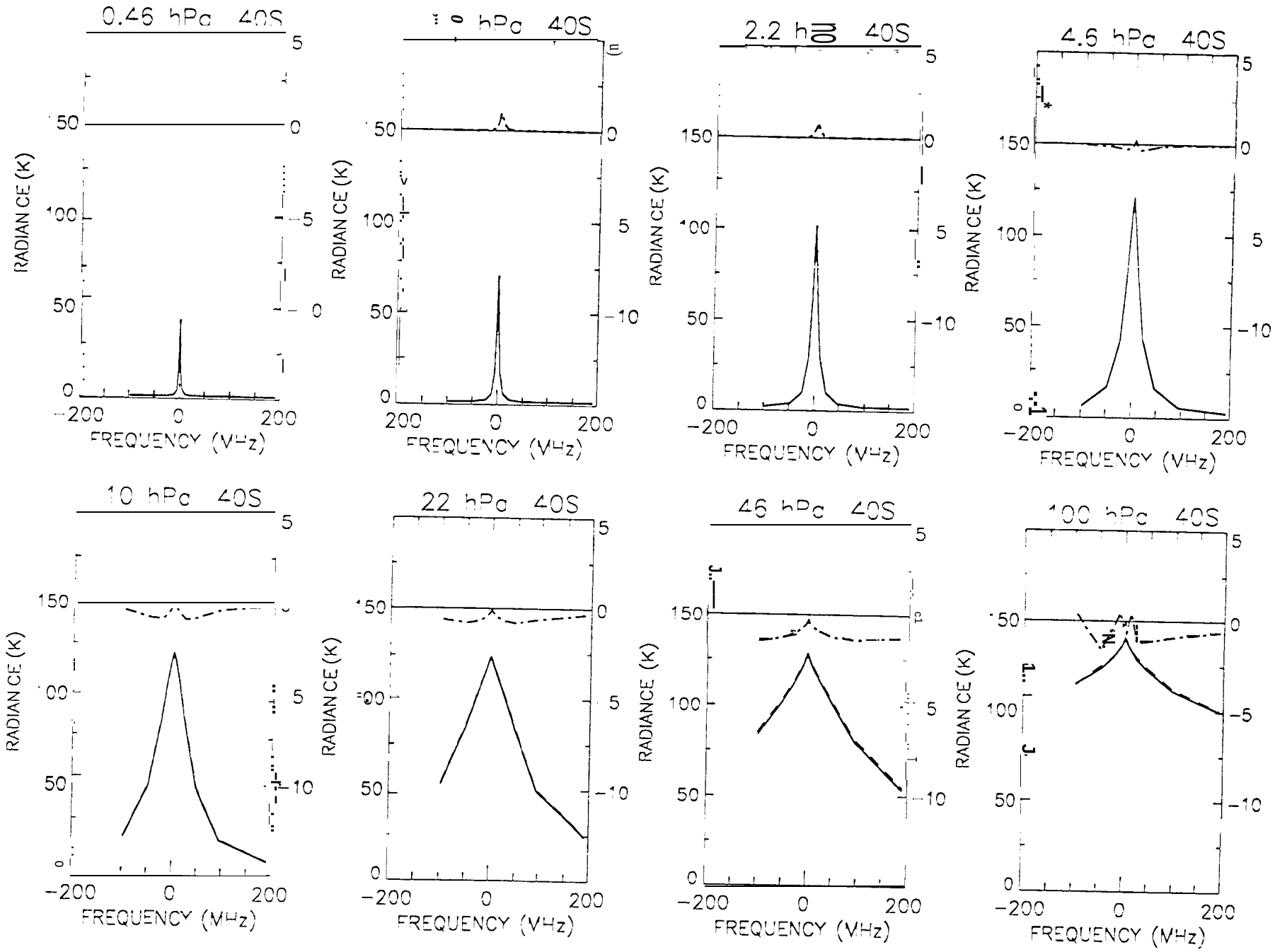
0.46 hPa 40S
RADIAN CE (K)
FREQUENCY (MHz)
2.2 hPa 40S
4.6 hPa 40S
10 hPa 40S
22 hPa 40S
46 hPa 40S
100 hPa 40S
RADIANCE (K)

Fig. 7

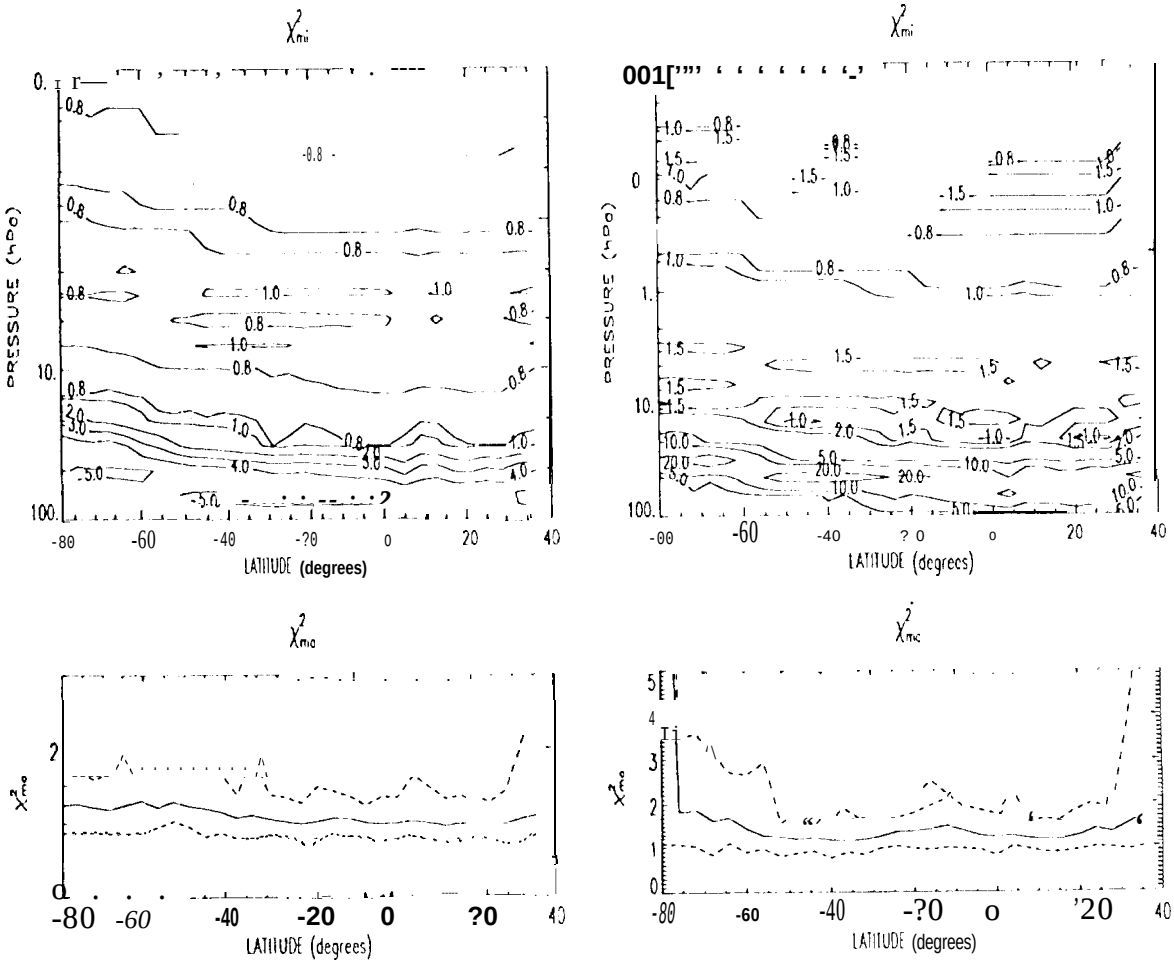
$\chi^2_{mi}$
PRESSURE (hPa)
LATITUDE (degrees)
$\chi^2_{mi}$
PRESSURE (hPa)
LATITUDE (degrees)
$\chi^2_{mo}$
LATITUDE (degrees)
$\chi^2_{mc}$
LATITUDE (degrees)

Fig. 8

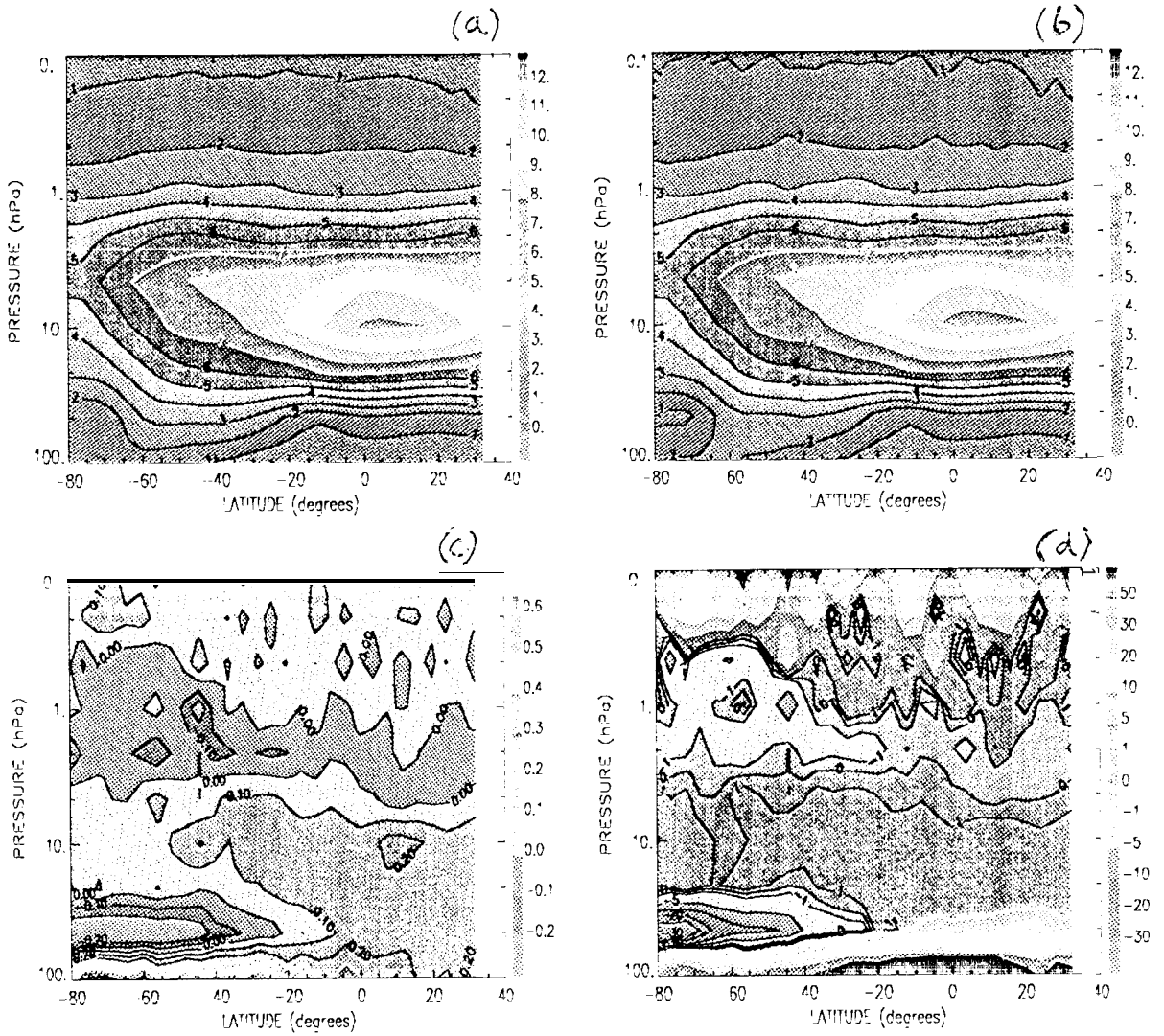


Fig. 9

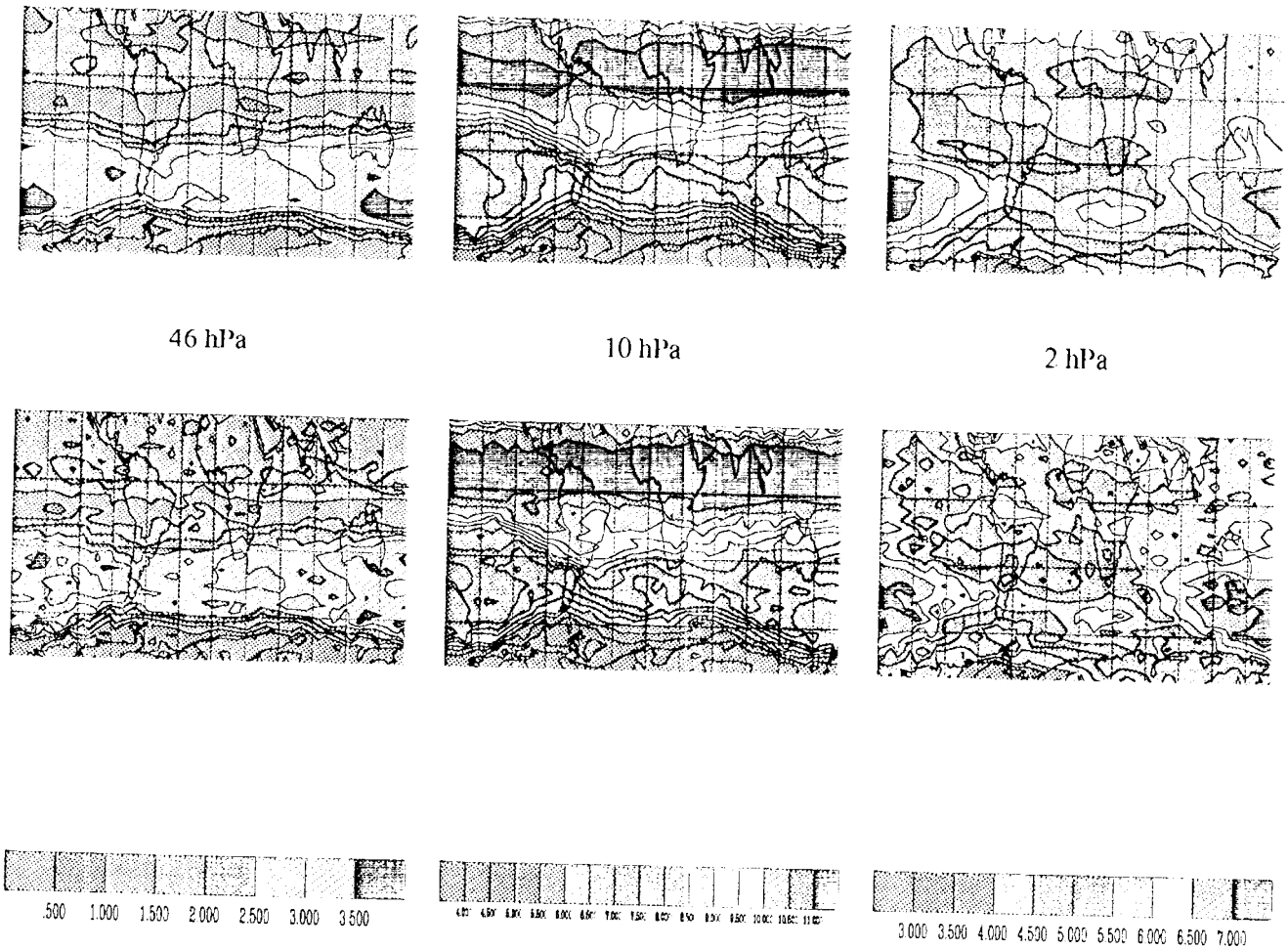
46 hPa
10 hPa
2 hPa
.500 1.000 1.500 2.000 2.500 3.000 3.500
3.000 3.500 4.000 4.500 5.000 5.500 6.000 6.500 7.000

Fig. 10

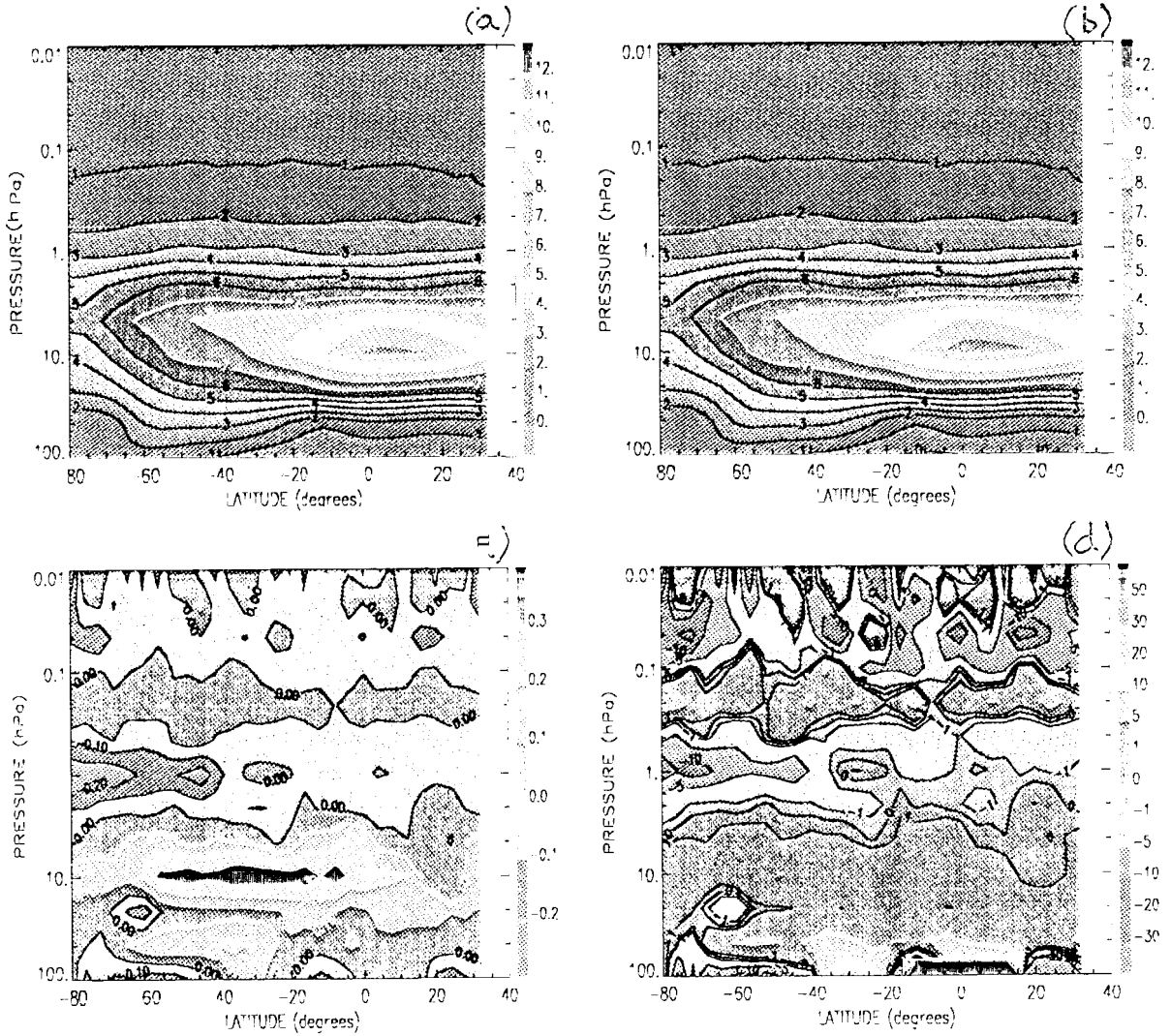
(a)
(b)
(c)
(d)
PRESSURE(hPa)
PRESSURE (hPa)
LATITUDE (degrees)
0.01
0.1
1.
10.
100.
-80
-60
-40
-20
0
20
40

Fig. 11

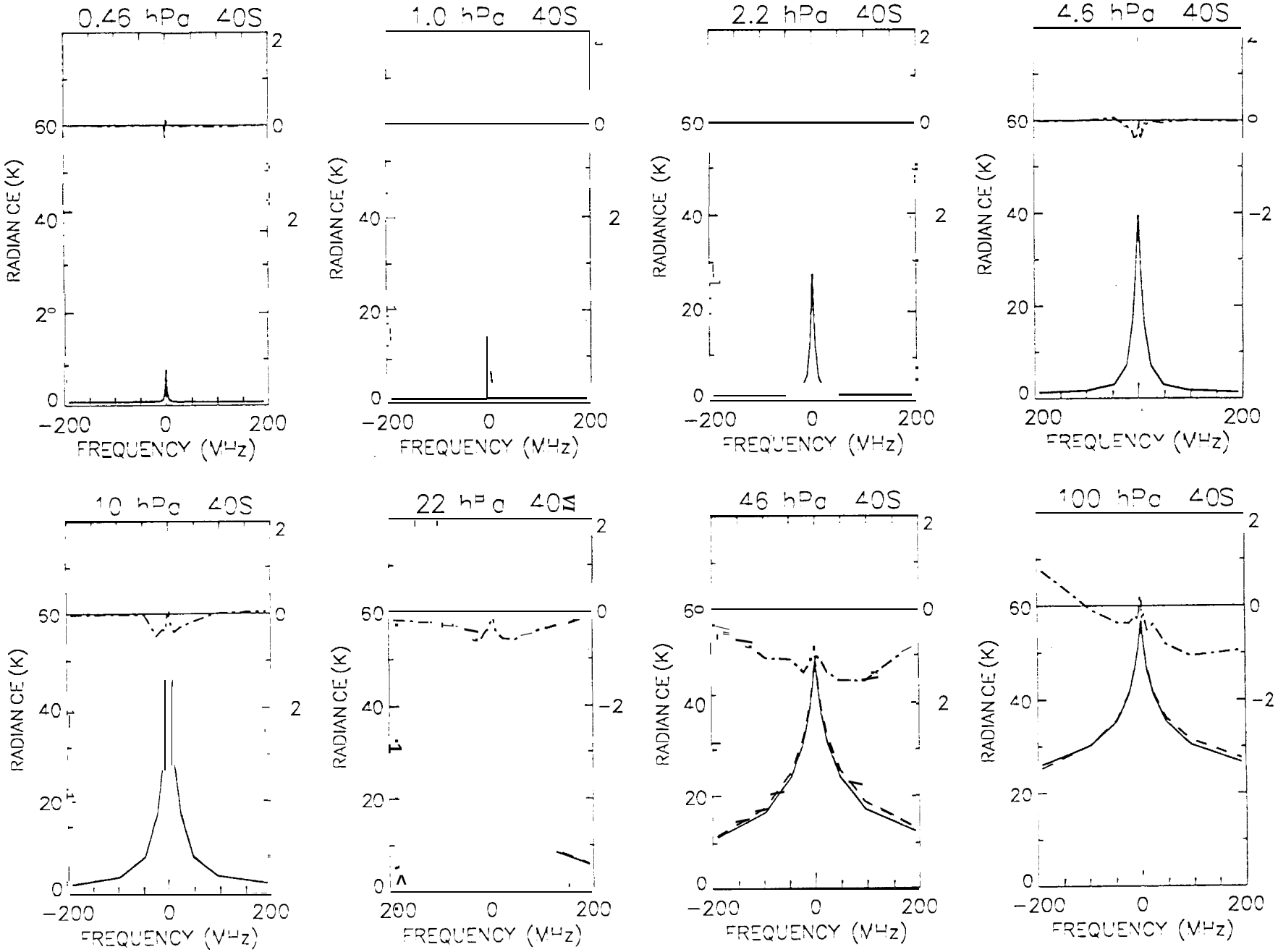
0.46 hPa 40S
1.0 hPa 40S
2.2 hPa 40S
4.6 hPa 40S
10 hPa 40S
22 hPa 40S
46 hPa 40S
100 hPa 40S
RADIAN CE (K)
RADIANCE (K)
FREQUENCY (MHz)
60
40
20
0
2
0
-2
-200
0
200

Fig. 12

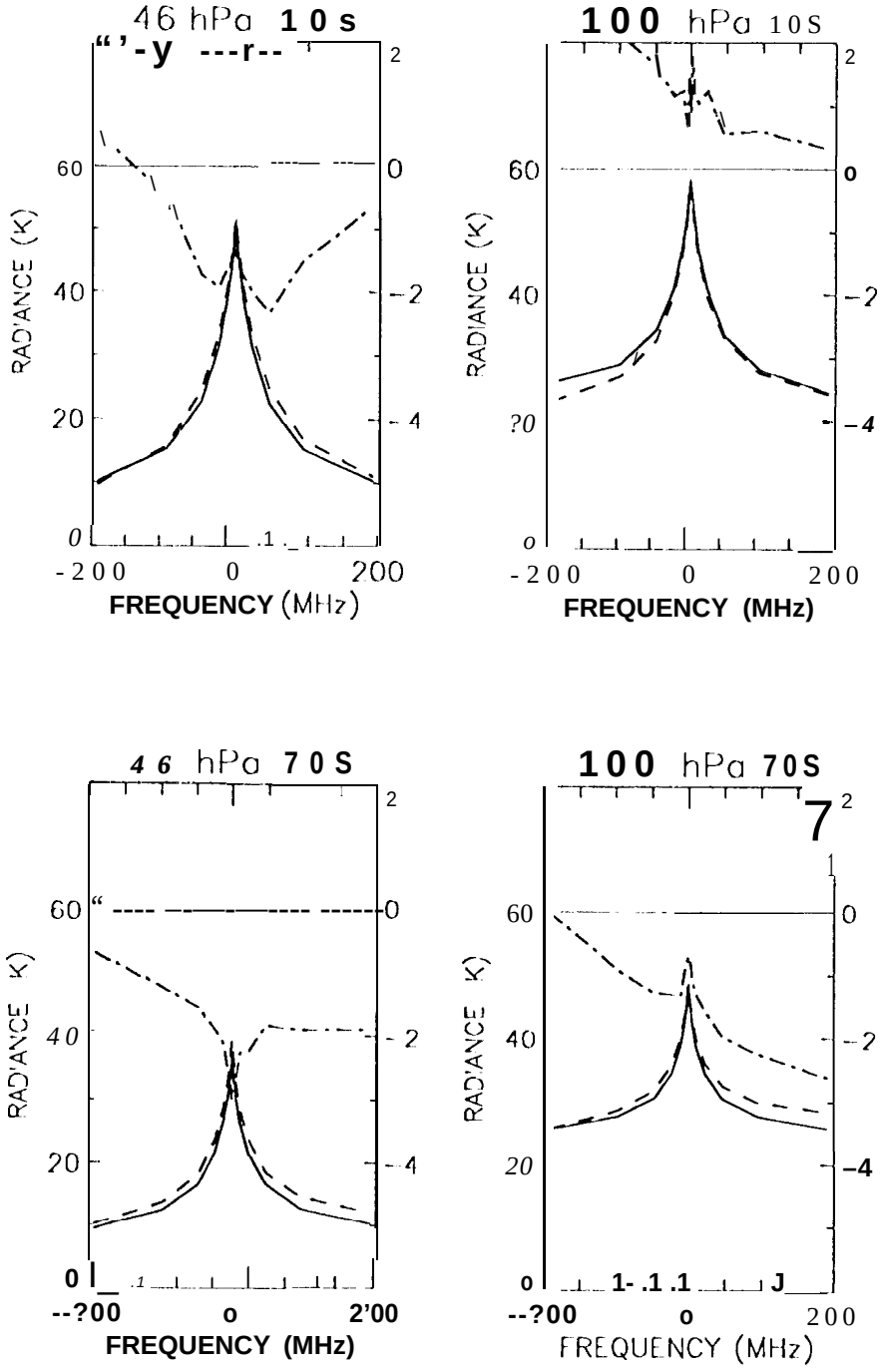
46 hPa 10 s
100 hPa 10S
46 hPa 70S
100 hPa 70S
RADIANCE (K)
FREQUENCY (MHz)
-200
0
200
60
40
20
0
2
-2
-4

Fig. 13

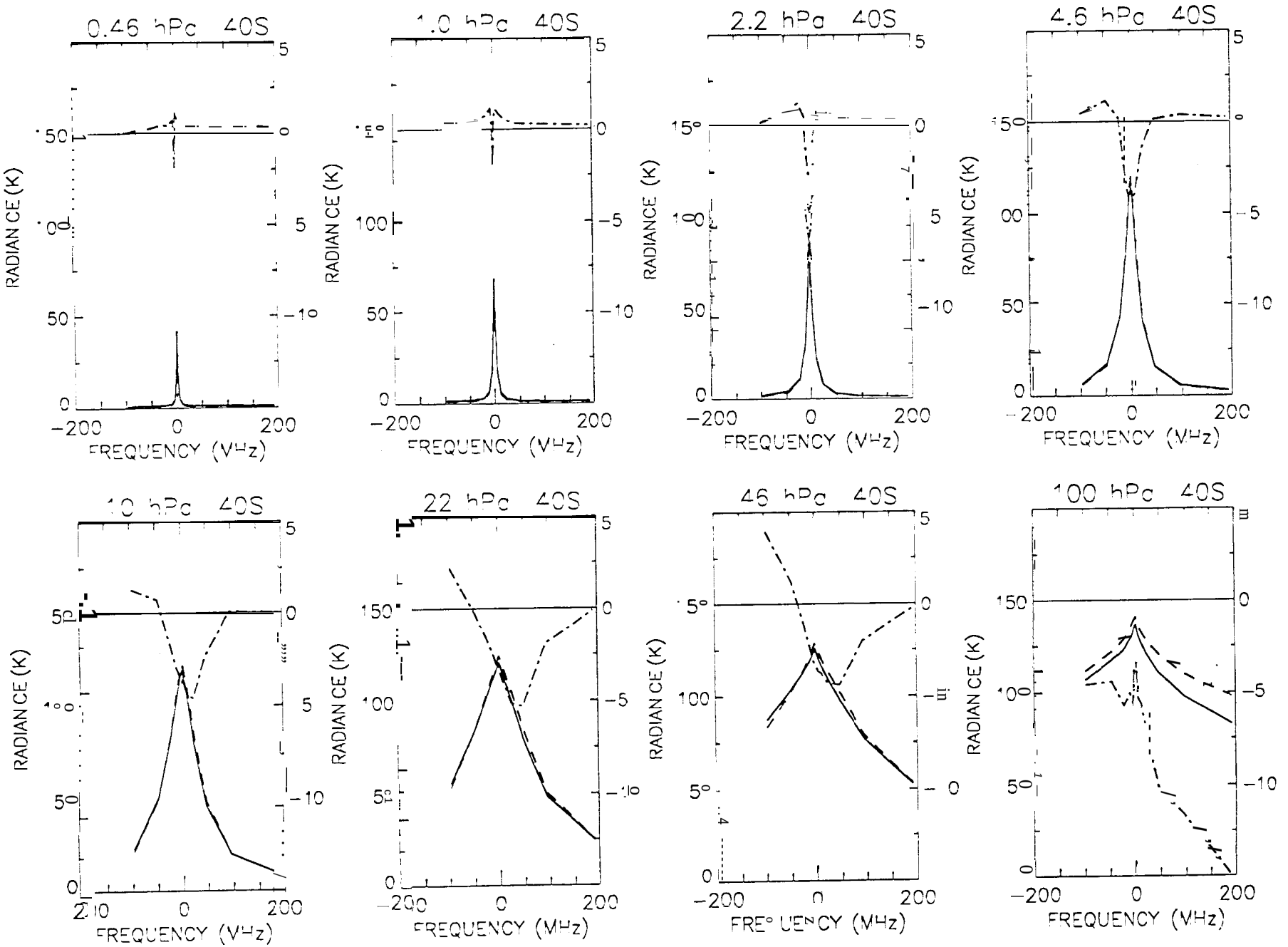
0.46 hPa 40S
1.0 hPa 40S
2.2 hPa 40S
4.6 hPa 40S
10 hPa 40S
22 hPa 40S
46 hPa 40S
100 hPa 40S
RADIAN CE (K)
RADIANCE (K)
FREQUENCY (MHz)
FREQUENCY (VHz)
−200
0
200
5
0
−5
−10

Fig 4

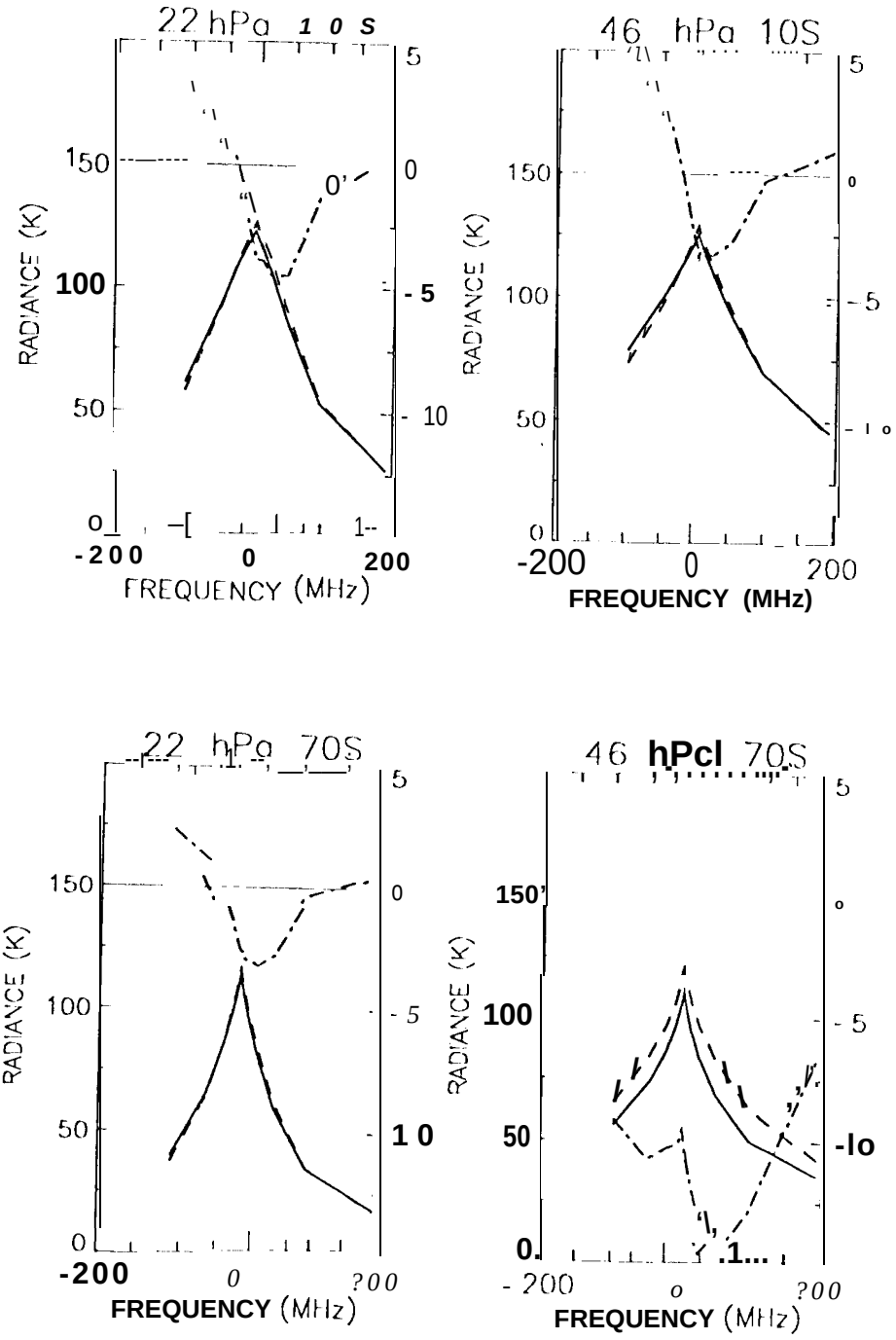
22 hPa 10S
46 hPa 10S
22 hPa 70S
46 hPa 70S
RADIANCE (K)
FREQUENCY (MHz)
-200
0
200

Fig. 15

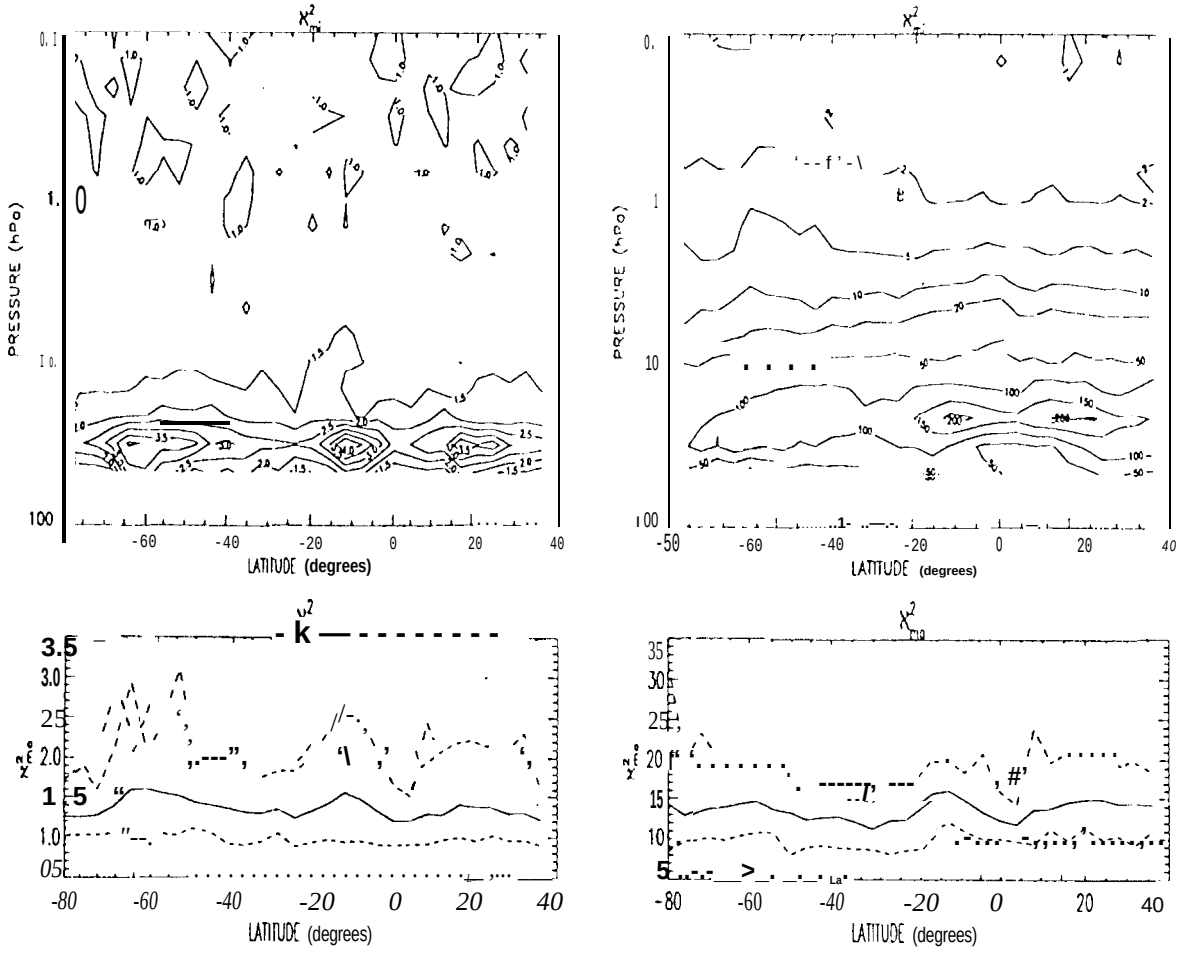
PRESSURE (hPa)
LATITUDE (degrees)
-60
-40
-20
0
20
40
-80
3.5
3.0
2.5
2.0
1.5
1.0
05

Fig. 16

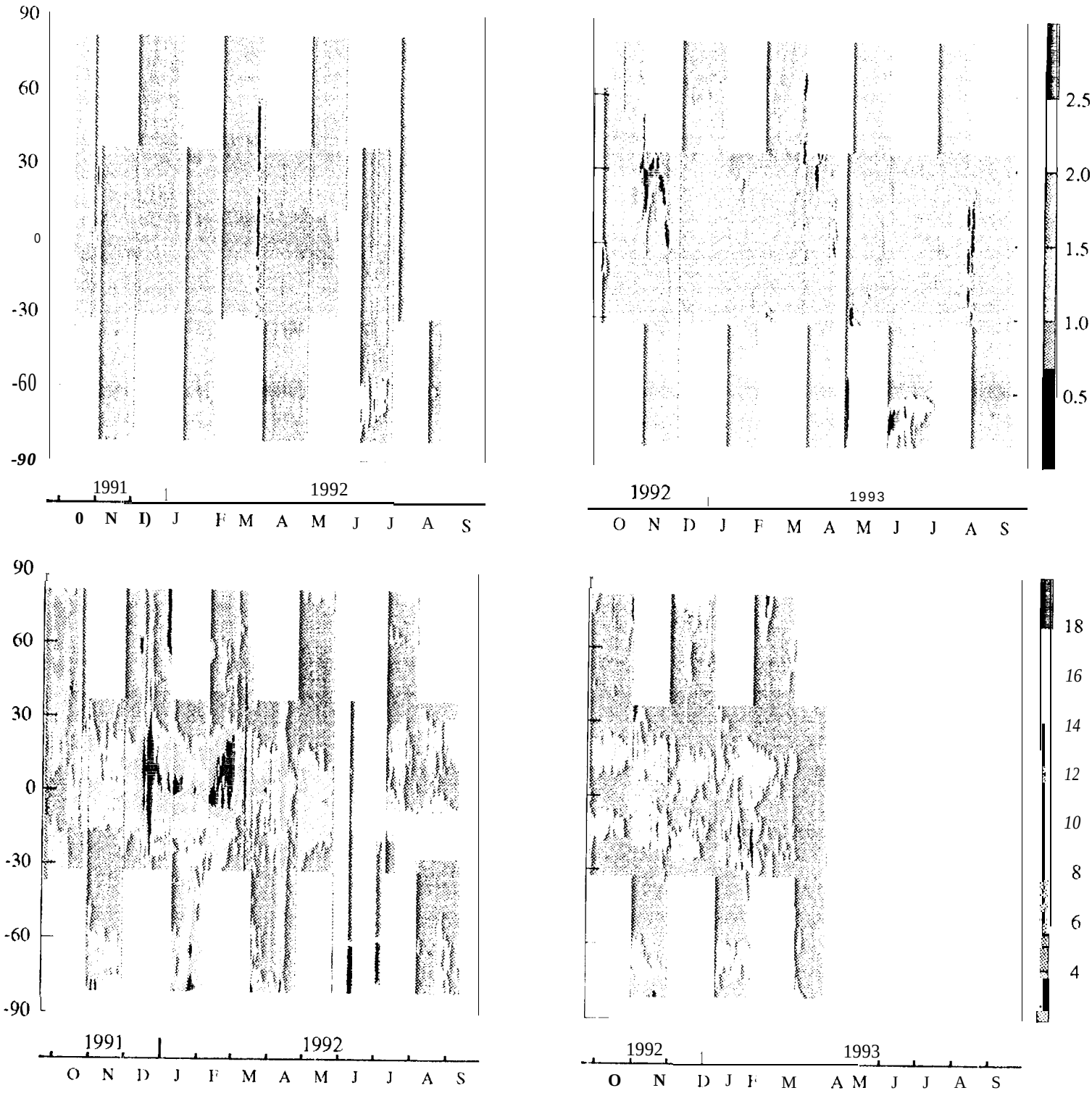
90
60
30
0
-30
-60
-90
1991
1992
O N D J F M A M J J A S
2.5
2.0
1.5
1.0
0.5
1992
1993
O N D J F M A M J J A S
90
60
30
0
-30
-60
-90
1991
1992
O N D J F M A M J J A S
18
16
14
12
10
8
6
4
1992
1993
O N D J F M A M J J A S

Fig. 17

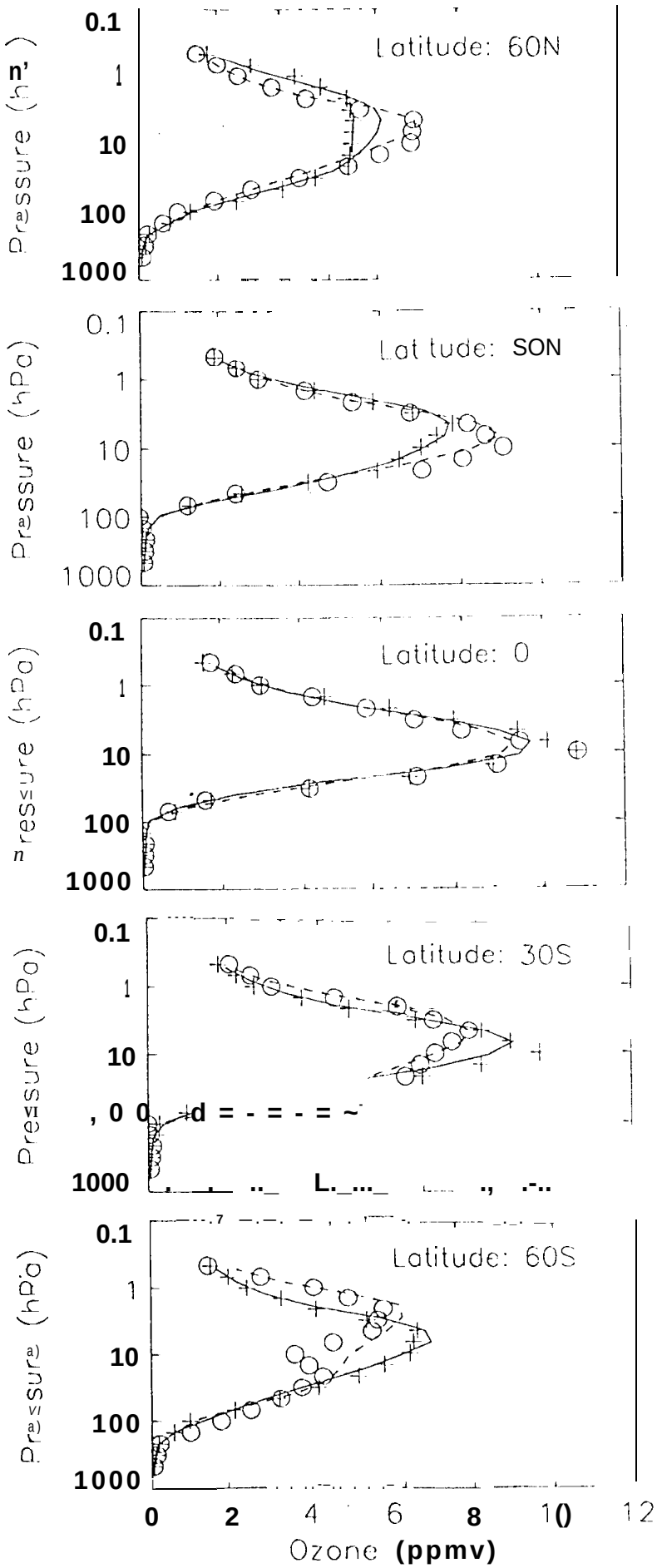
Latitude: 60N
Latitude: SON
Latitude: 0
Latitude: 30S
Latitude: 60S
Pressure (hPa)
0.1
1
10
100
1000
0
2
4
6
8
10
12
Ozone (ppmv)

Fig.18

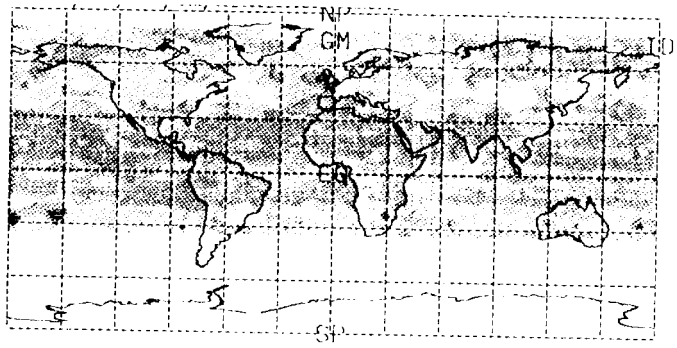


12 Oct 1991

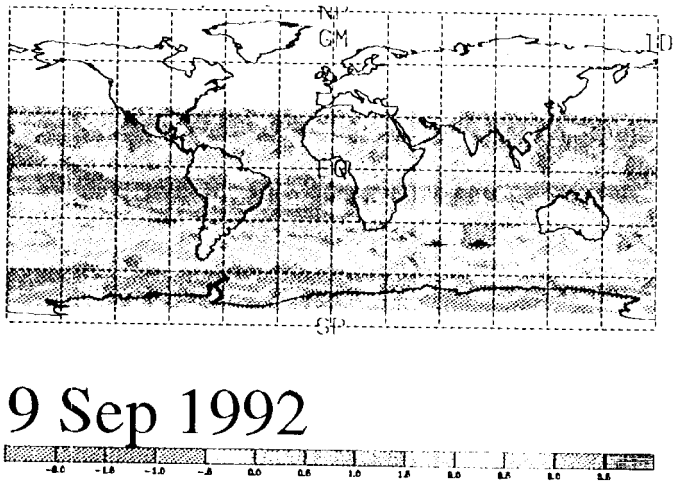


9 Sep 1992

Fig 19

(a)

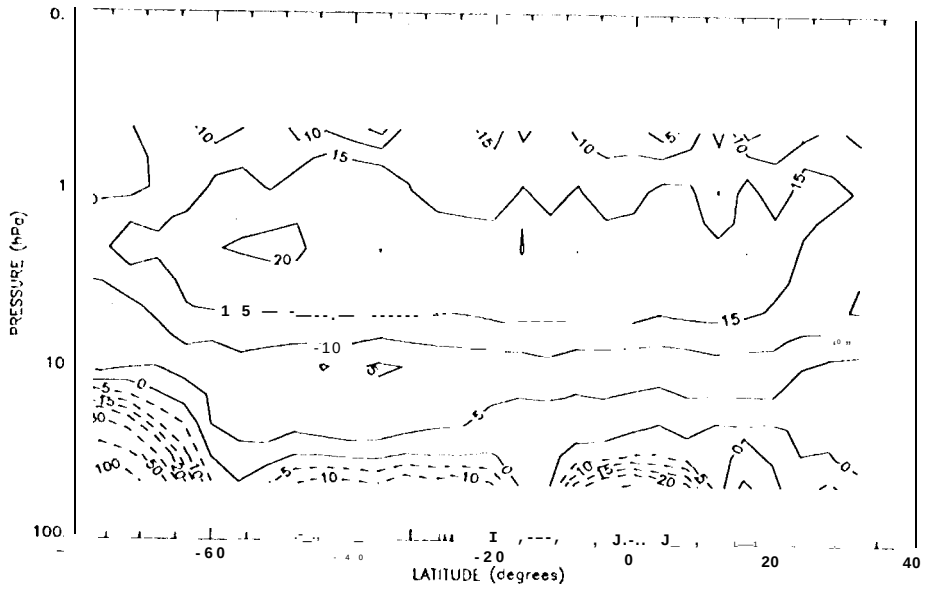
0.
1
10
100
PRESSURE (hPa)
-60
-20
0
20
40
LATITUDE (degrees)

(b)

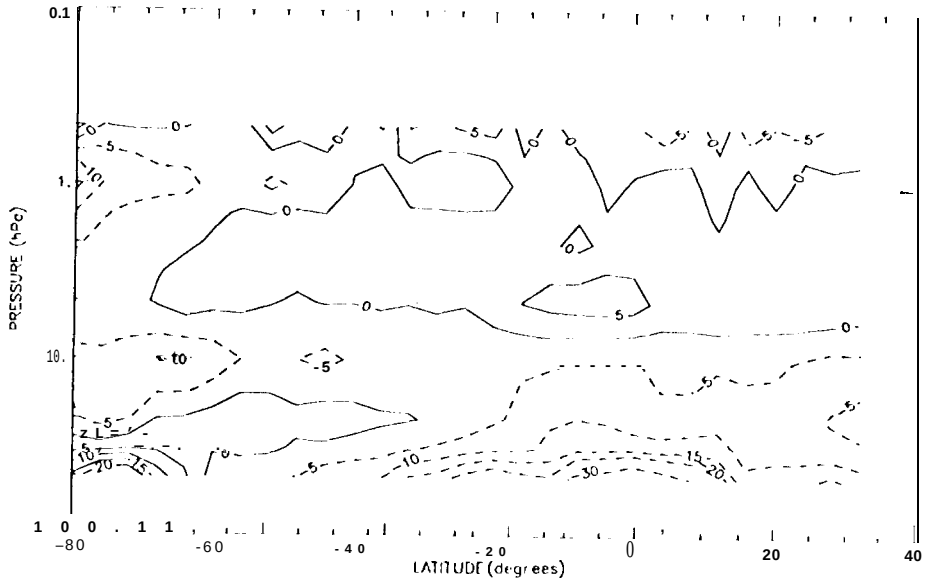
0.1
1.
10.
100.
PRESSURE (hPa)
-80
-60
-40
-20
0
20
40
LATITUDE (degrees)

Fig. 20

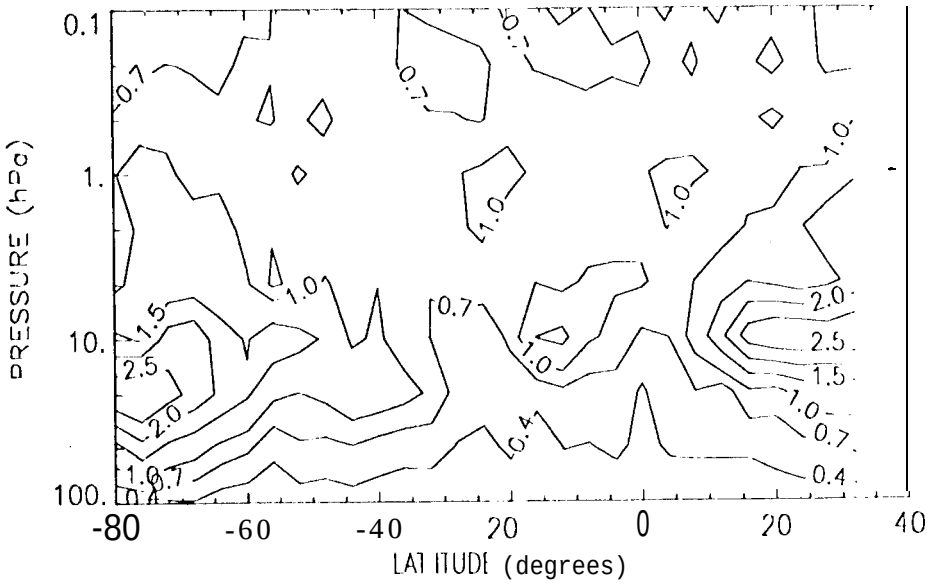
0.1
1.
10.
100.
PRESSURE (hPa)
-80
-60
-40
20
0
20
40
LATITUDE (degrees)

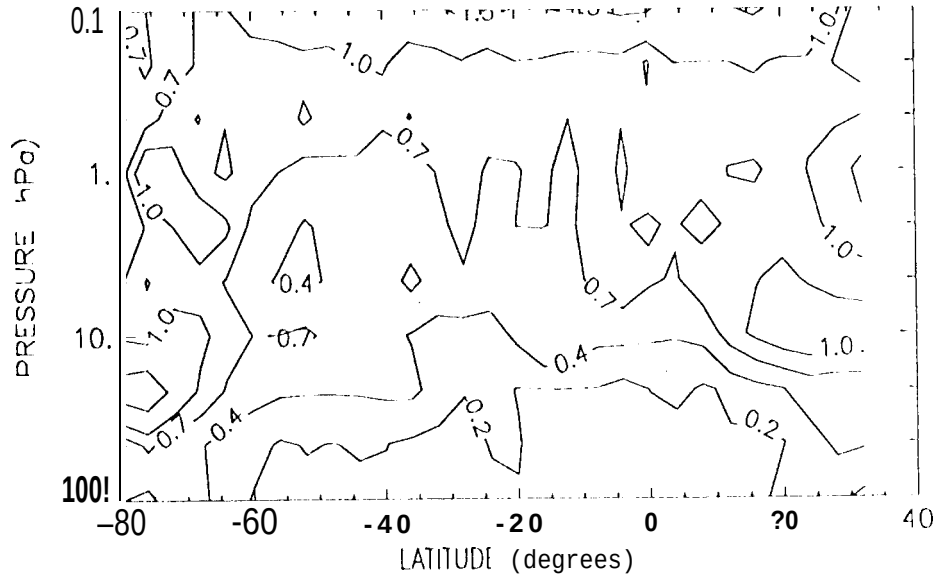
0.1
1.
10.
100!
PRESSURE hPa)
–80
-60
-40
-20
0
?0
40
LATITUDE (degrees)

Fig. 21

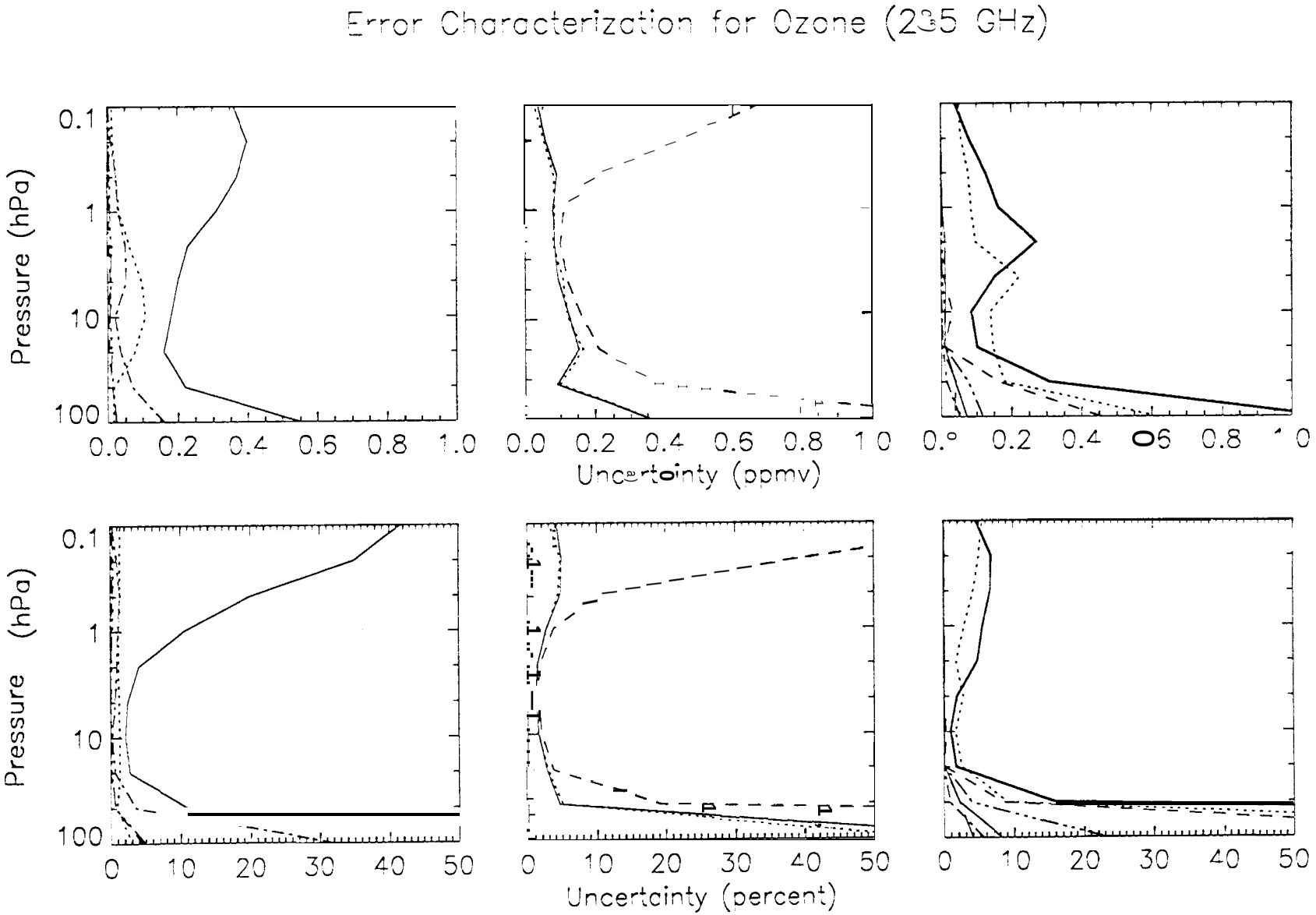
Error Characterization for Ozone (235 GHz)
Pressure (hPa)
0.1
1
10
100
0.0 0.2 0.4 0.6 0.8 1.0
Uncertainty (ppmv)
Pressure (hPa)
0 10 20 30 40 50
Uncertainty (percent)

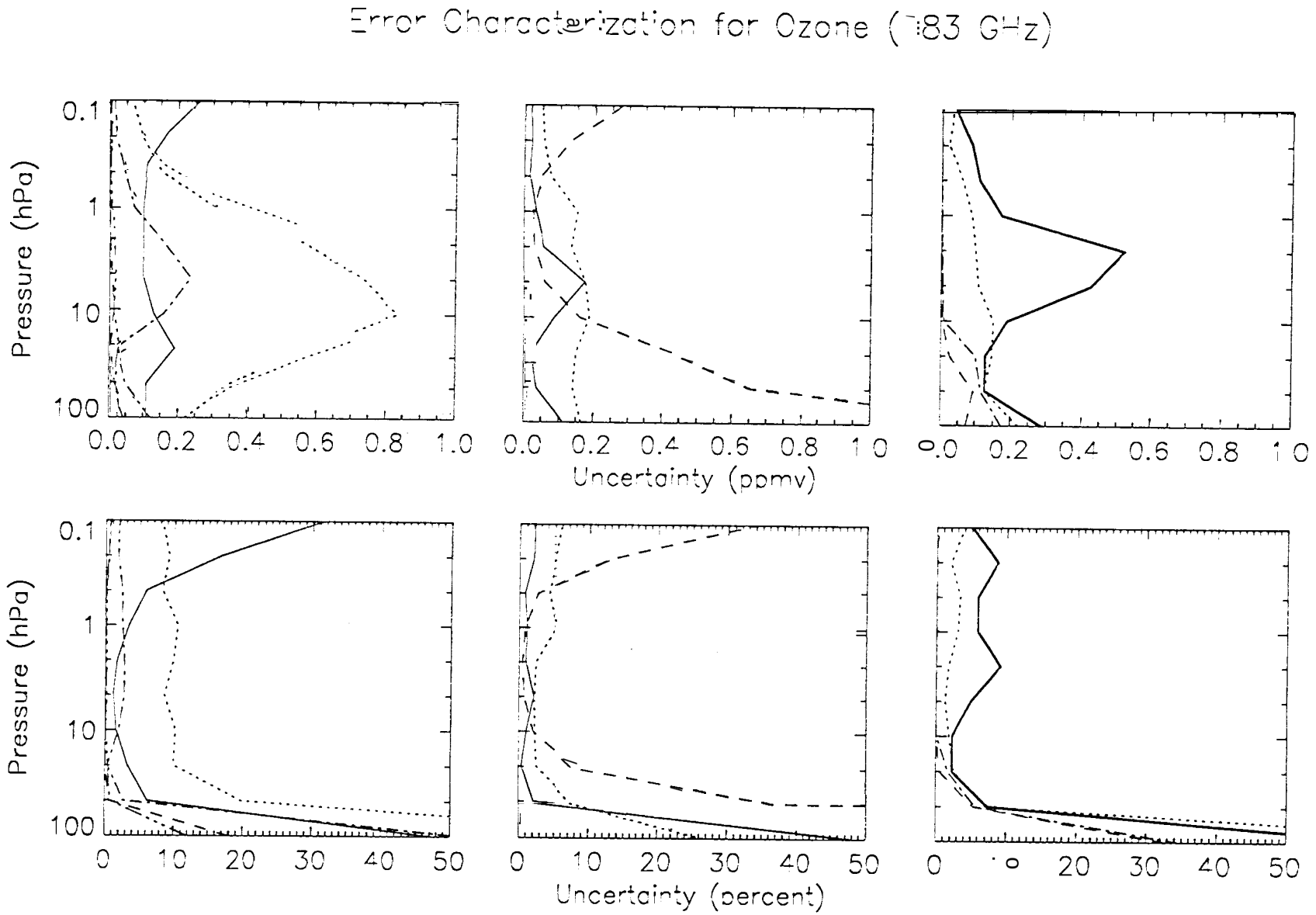
Error Characterization for Ozone (183 GHz)
Pressure (hPa)
0.1
1
10
100
0.0 0.2 0.4 0.6 0.8 1.0
Uncertainty (ppmv)
0 10 20 30 40 50
Uncertainty (percent)

Fig. 23

Error **Characterization** for Ozone (205 GHz)

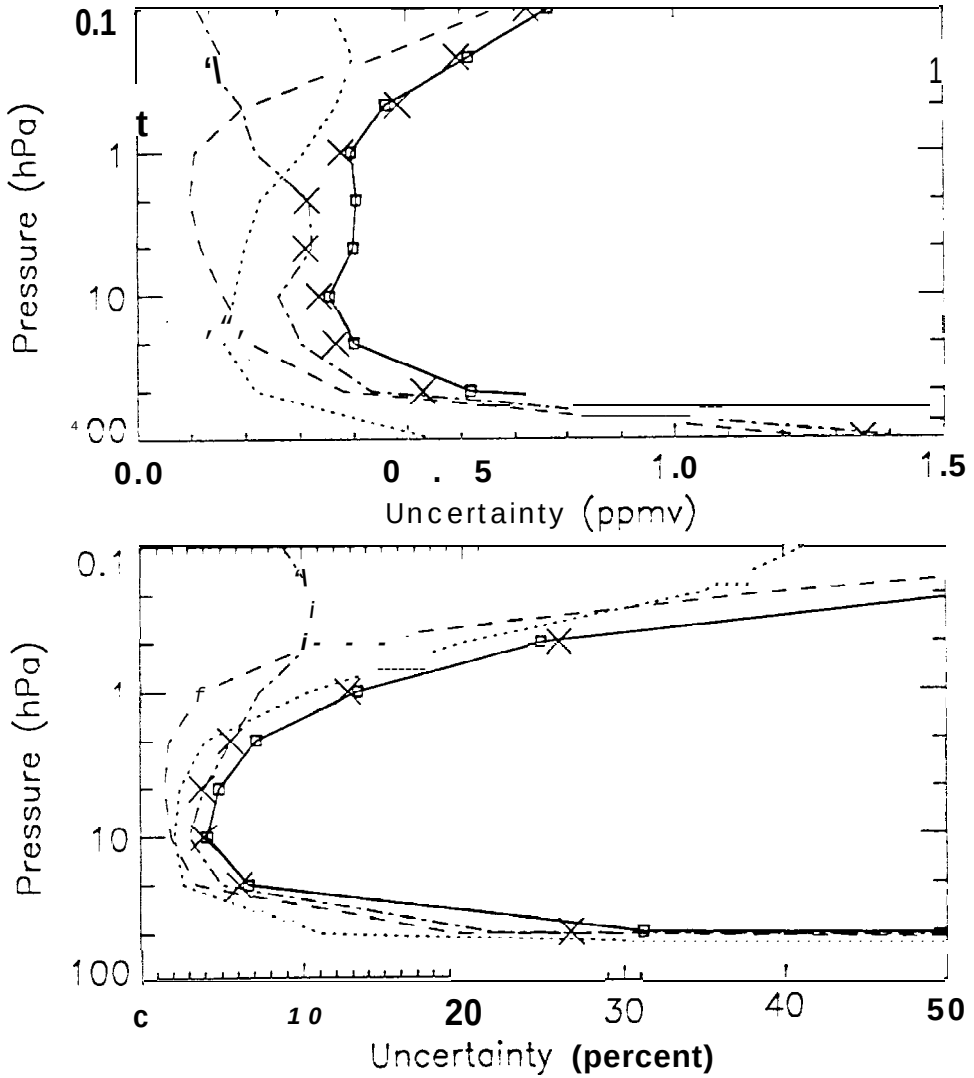


Fig. 24

Error Characterization for Ozone (183 GHz)

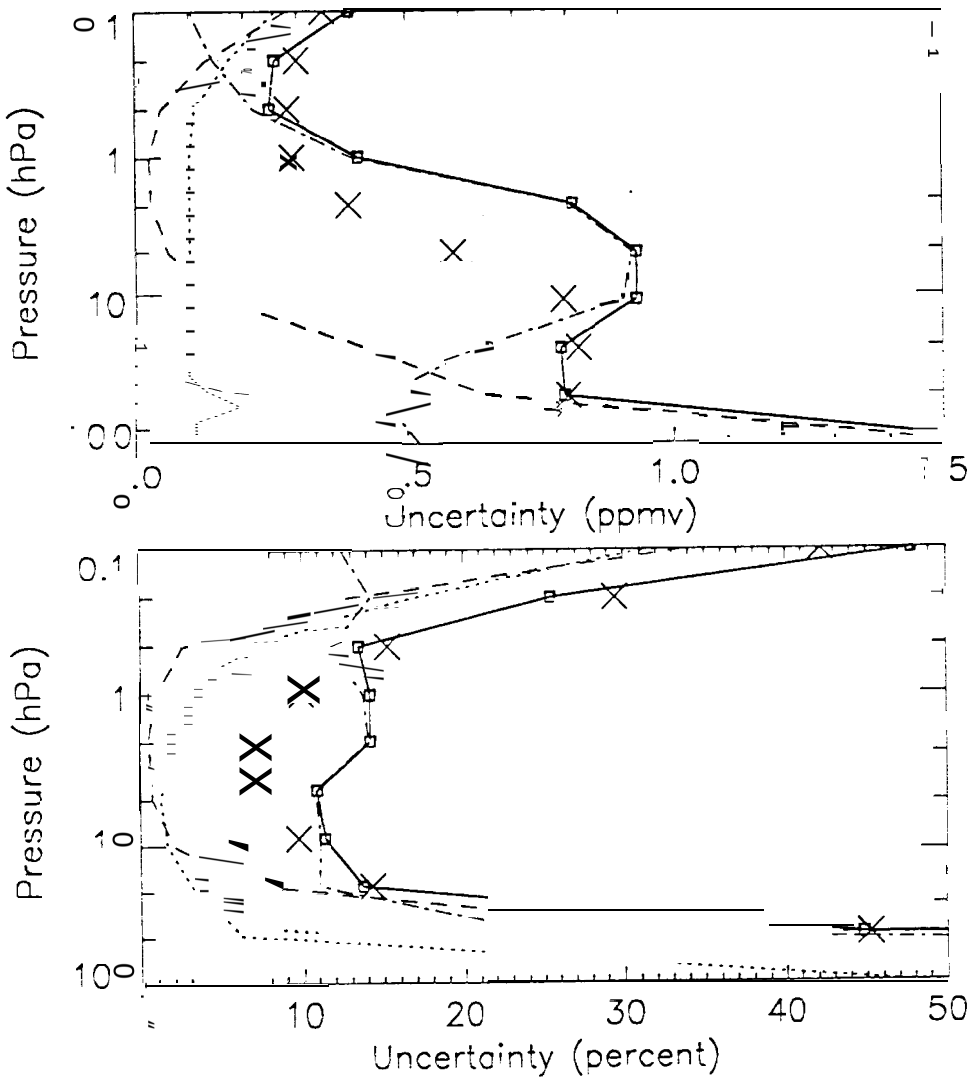


Fig 25

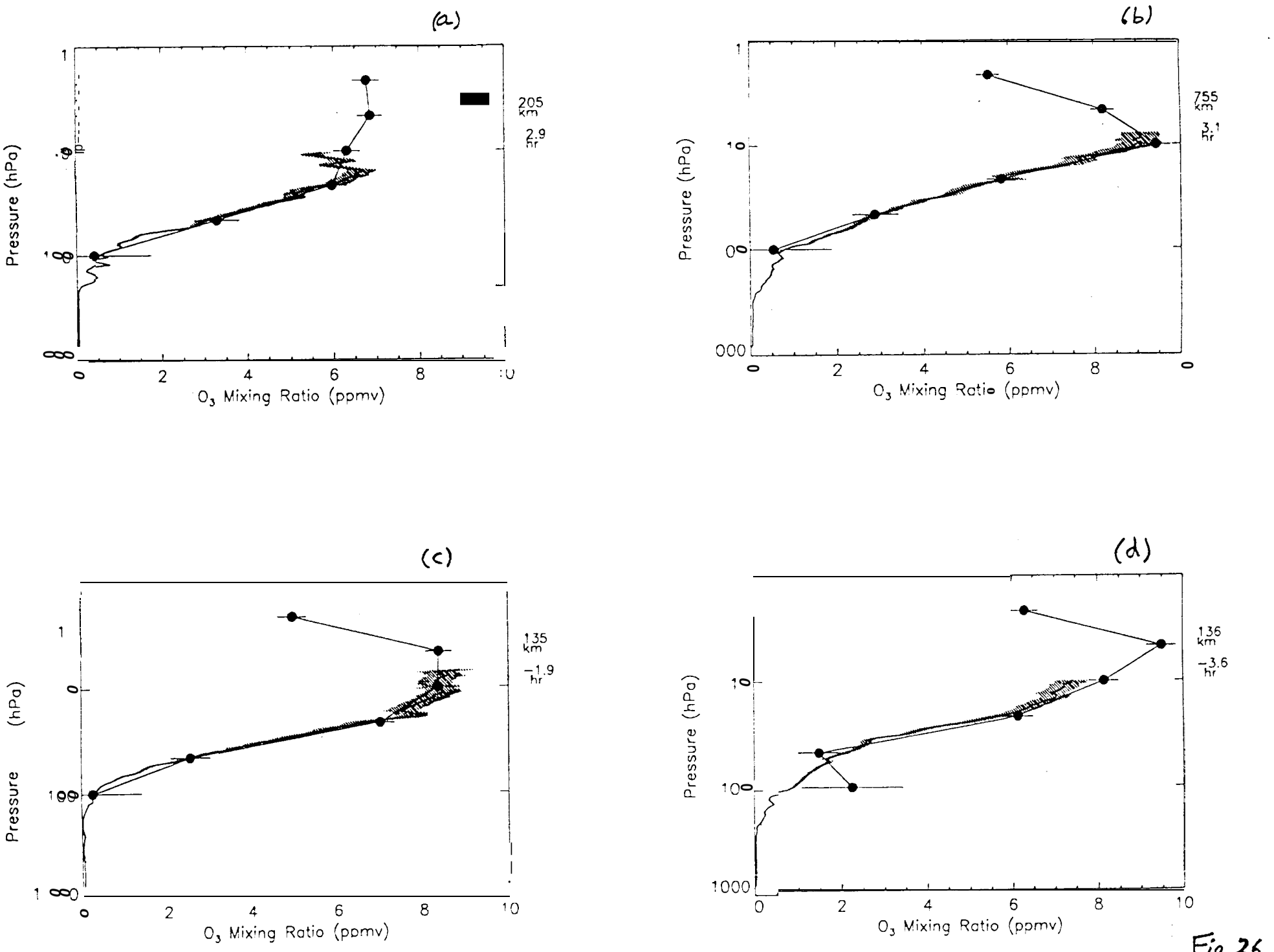
(a)
Pressure (hPa)
1
10
100
1000
205 km
2.9 hr
0
2
4
6
8
10
O3 Mixing Ratio (ppmv)
(b)
Pressure (hPa)
1
10
100
1000
755 km
3.1 hr
0
2
4
6
8
O3 Mixing Ratio (ppmv)
(c)
Pressure (hPa)
1
10
100
1000
135 km
-1.9 hr
0
2
4
6
8
10
O3 Mixing Ratio (ppmv)
(d)
Pressure (hPa)
1
10
100
1000
136 km
-3.6 hr
0
2
4
6
8
10
O3 Mixing Ratio (ppmv)

Fig. 26

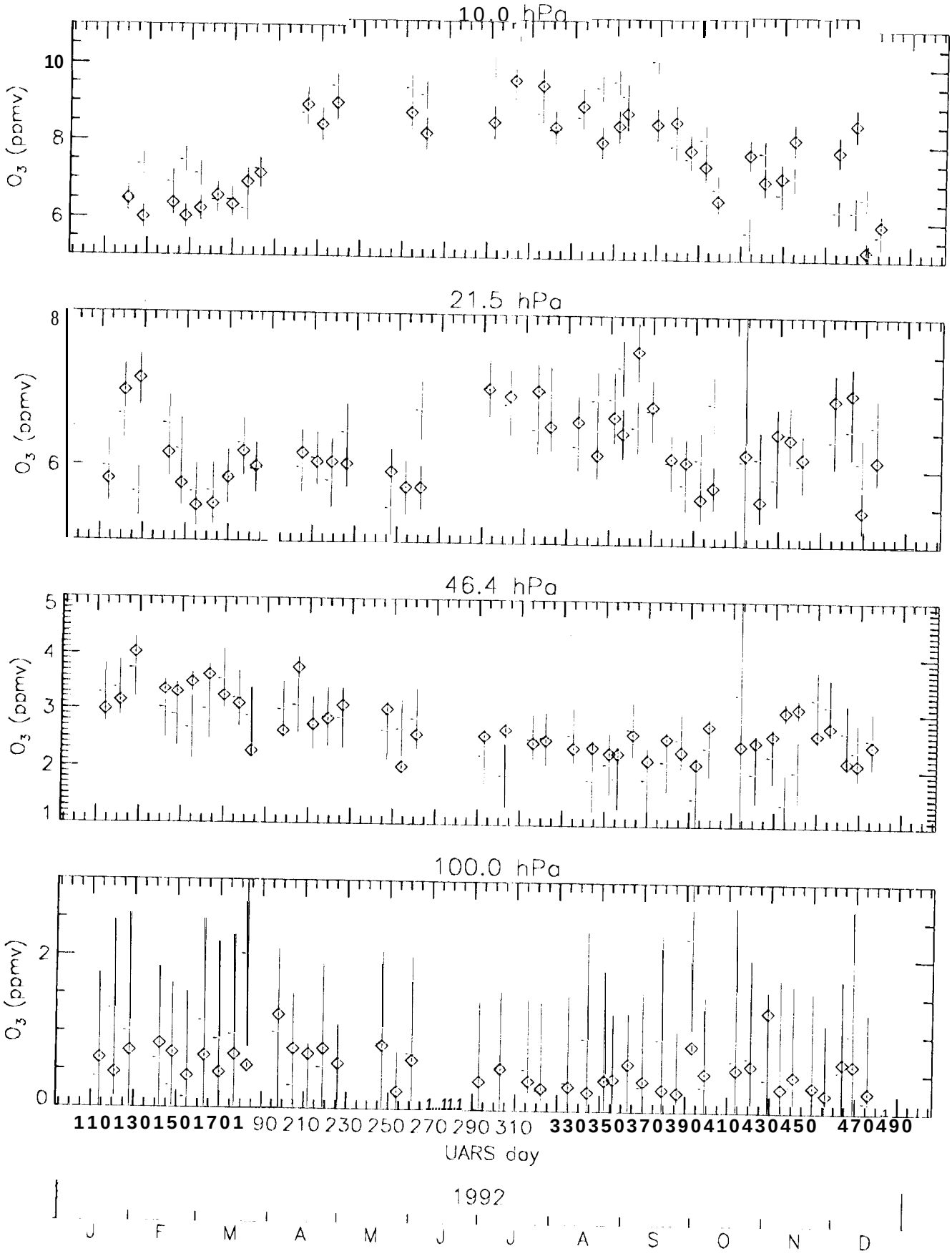
10.0 hPa
21.5 hPa
46.4 hPa
100.0 hPa
$O_3$ (ppmv)
1101301501701 90 210 230 250 270 290 310 330350370390410430450 470490
UARS day
1992
J F M A M J J A S O N D

Fig. 27.

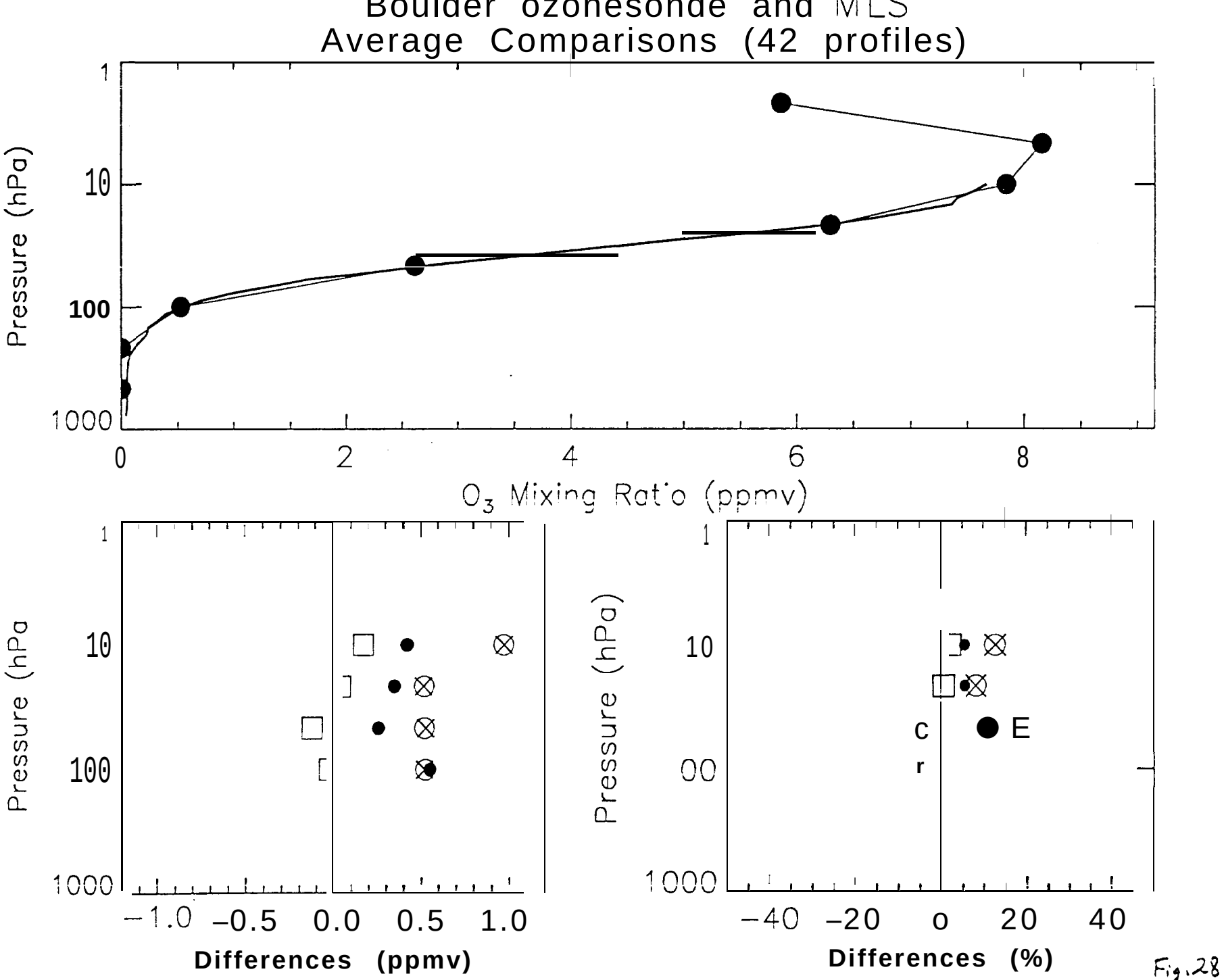
Boulder ozonesonde and MLS
Average Comparisons (42 profiles)
Pressure (hPa)
1
10
100
1000
0
2
4
6
8
O3 Mixing Ratio (ppmv)
Pressure (hPa
−1.0
−0.5
0.0
0.5
1.0
Differences (ppmv)
−40
−20
0
20
40
Differences (%)

Fig. 28

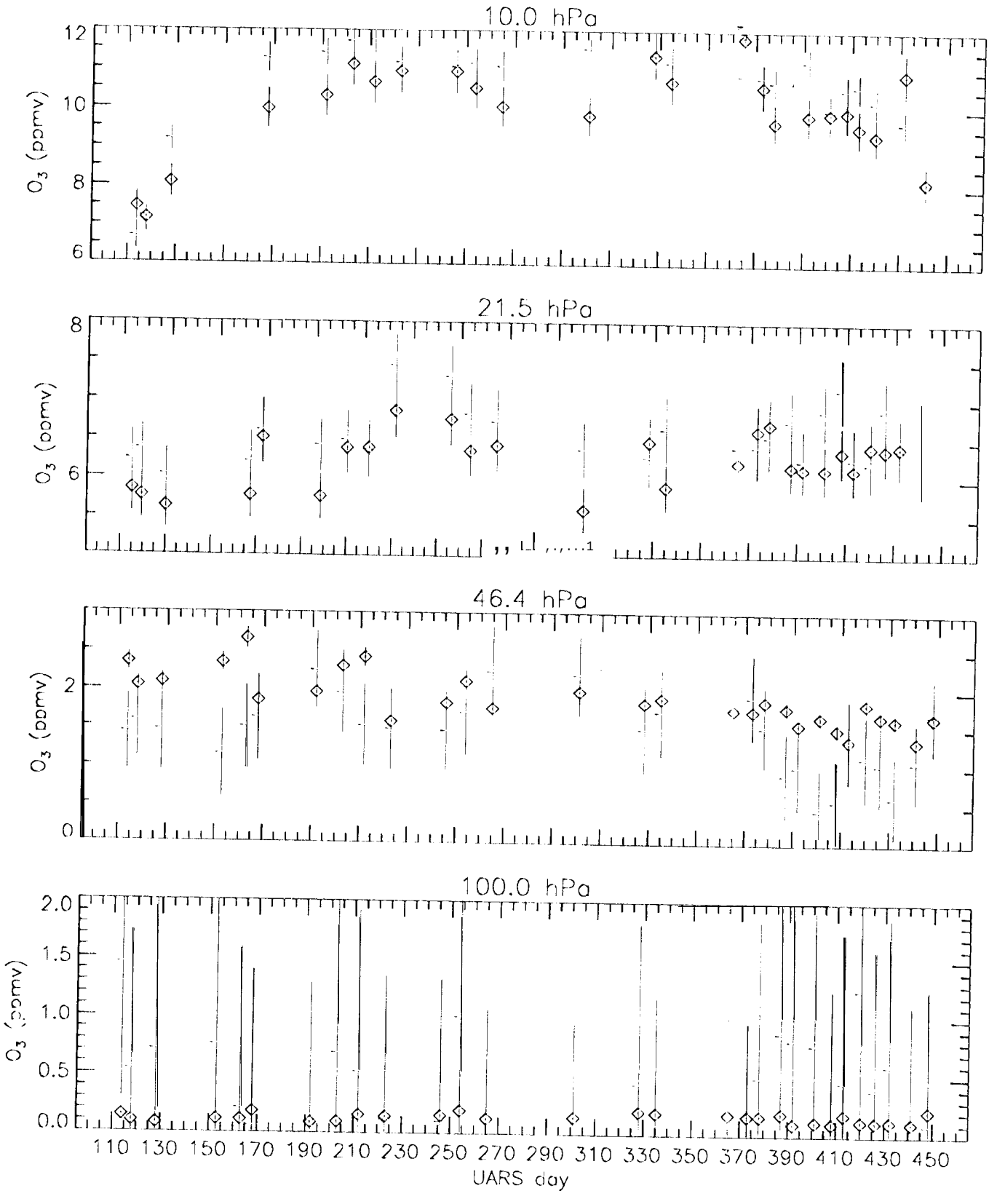
10.0 hPa
12
10
8
6
$O_3$ (ppmv)
21.5 hPa
8
6
$O_3$ (ppmv)
46.4 hPa
2
0
$O_3$ (ppmv)
100.0 hPa
2.0
1.5
1.0
0.5
0.0
$O_3$ (ppmv)
110 130 150 170 190 210 230 250 270 290 310 330 350 370 390 410 430 450
UARS day
1992
J F M A M J J A S O N

Fig. 29

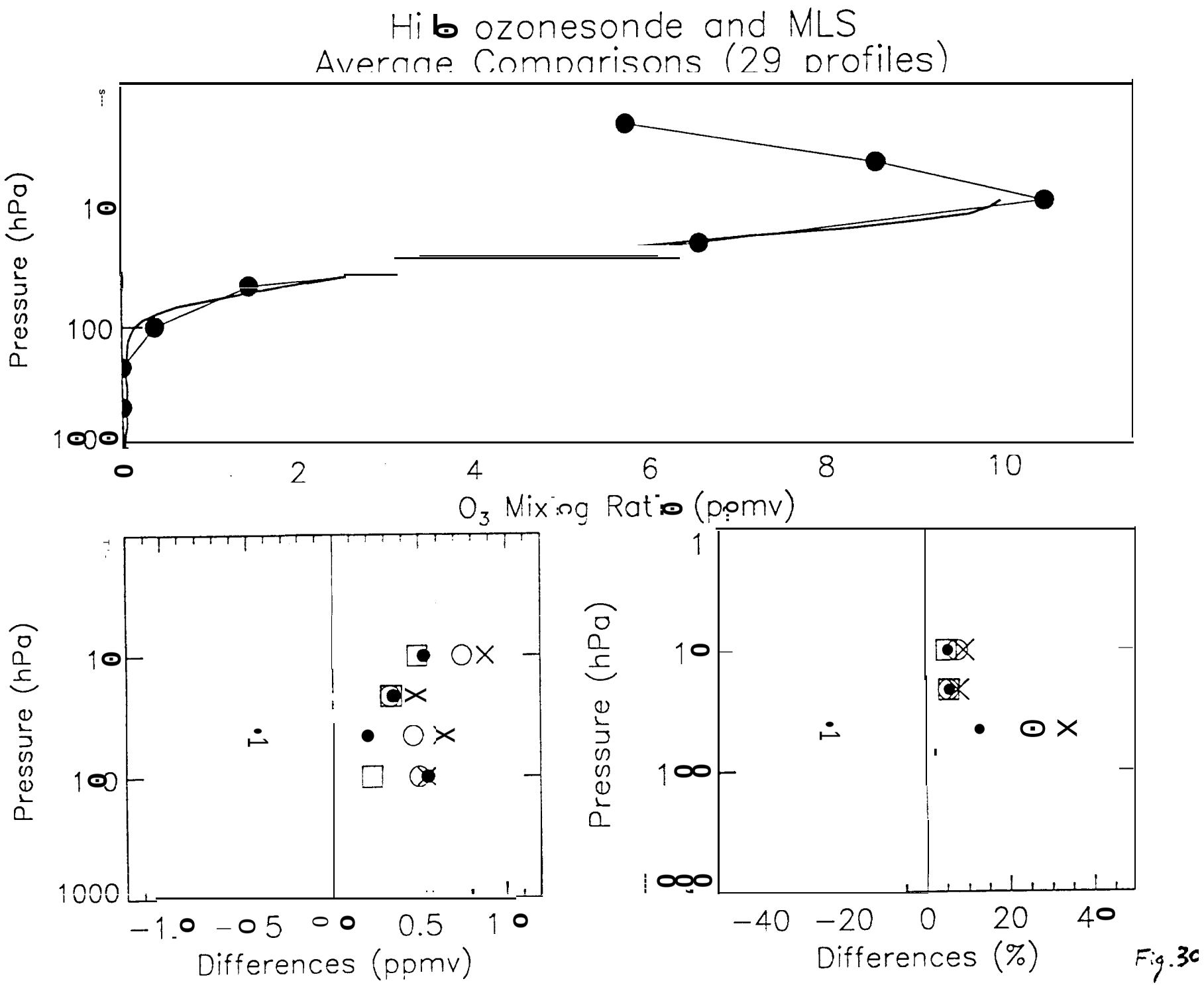
Hilo ozonesonde and MLS
Average Comparisons (29 profiles)
Pressure (hPa)
10
100
1000
0
2
4
6
8
10
O3 Mixing Ratio (ppmv)
Pressure (hPa)
10
100
1000
-1.0
-0.5
0.0
0.5
1.0
Differences (ppmv)
Pressure (hPa)
1
10
100
-40
-20
0
20
40
Differences (%)

Fig. 3c

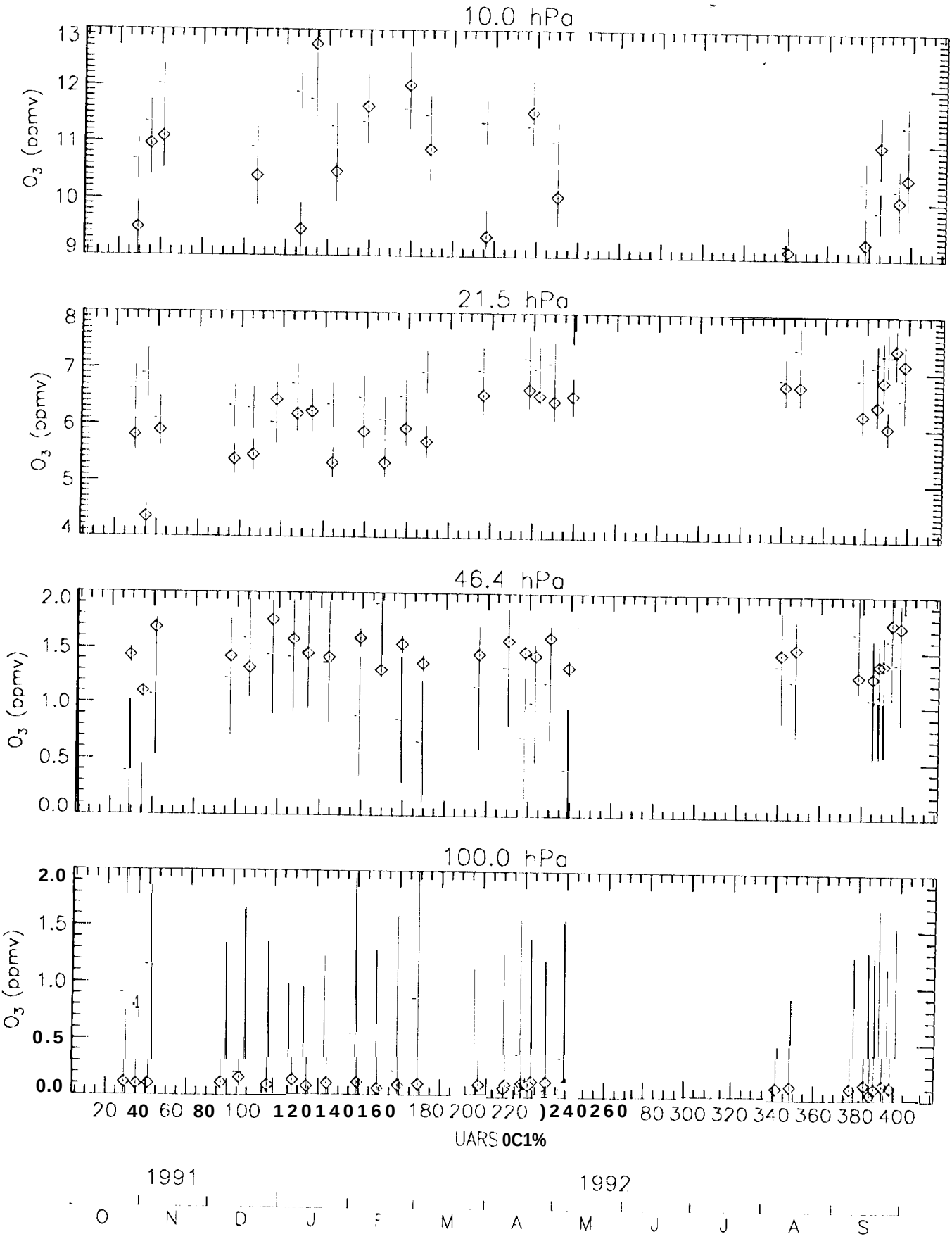
10.0 hPa
21.5 hPa
46.4 hPa
100.0 hPa
O3 (ppmv)
20 40 60 80 100 120140160 180 200 220 )240260 80 300 320 340 360 380 400
UARS 0C1%
1991
1992
O N D J F M A M J J A S

Fig. 31

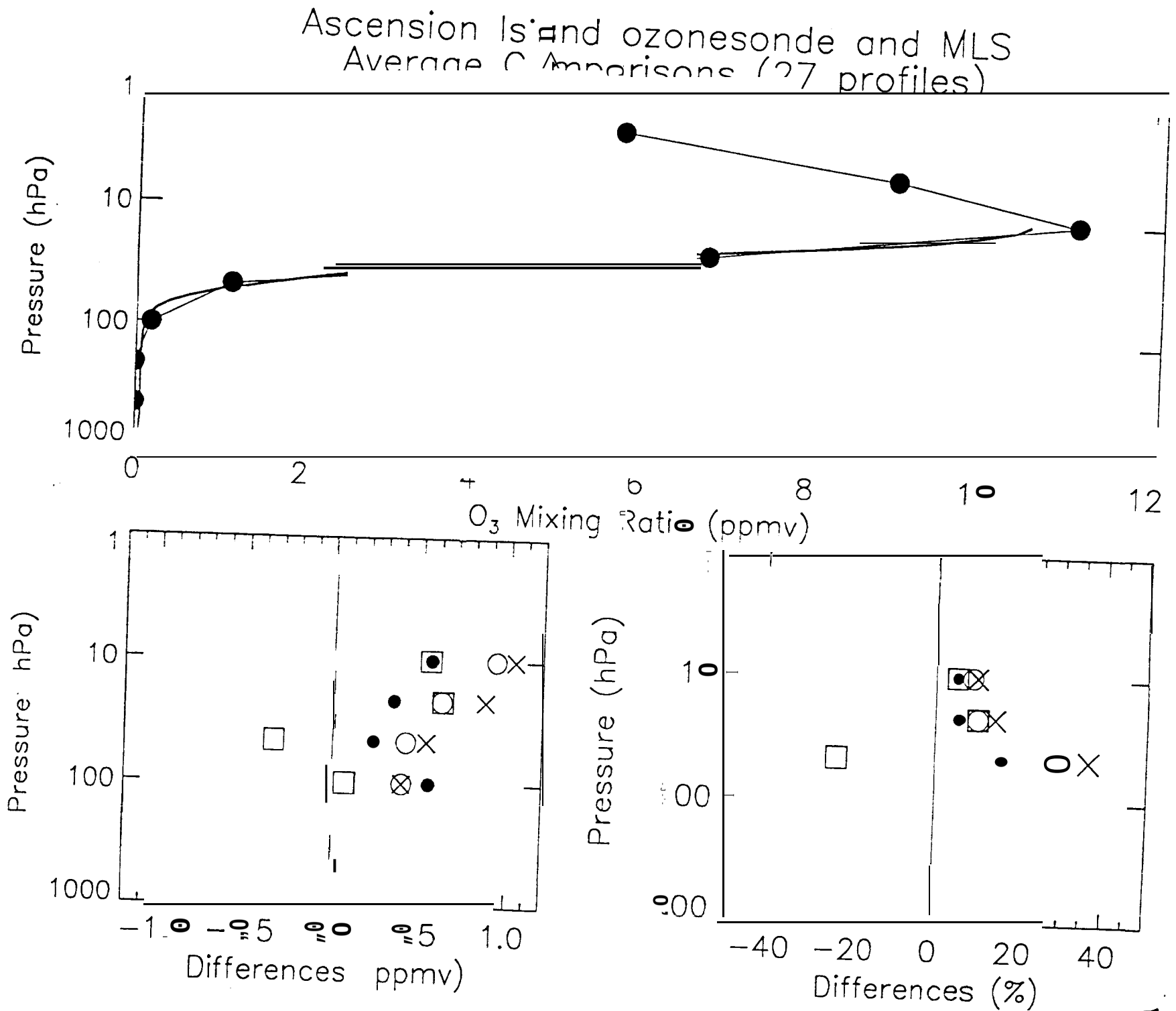
Ascension Island ozonesonde and MLS
Average Comparisons (27 profiles)
Pressure (hPa)
1
10
100
1000
0
2
4
6
8
10
12
O3 Mixing Ratio (ppmv)
Pressure hPa)
Differences ppmv)
-1.0
-0.5
0.0
0.5
1.0
Pressure (hPa)
Differences (%)
-40
-20
0
20
40

Fig 32

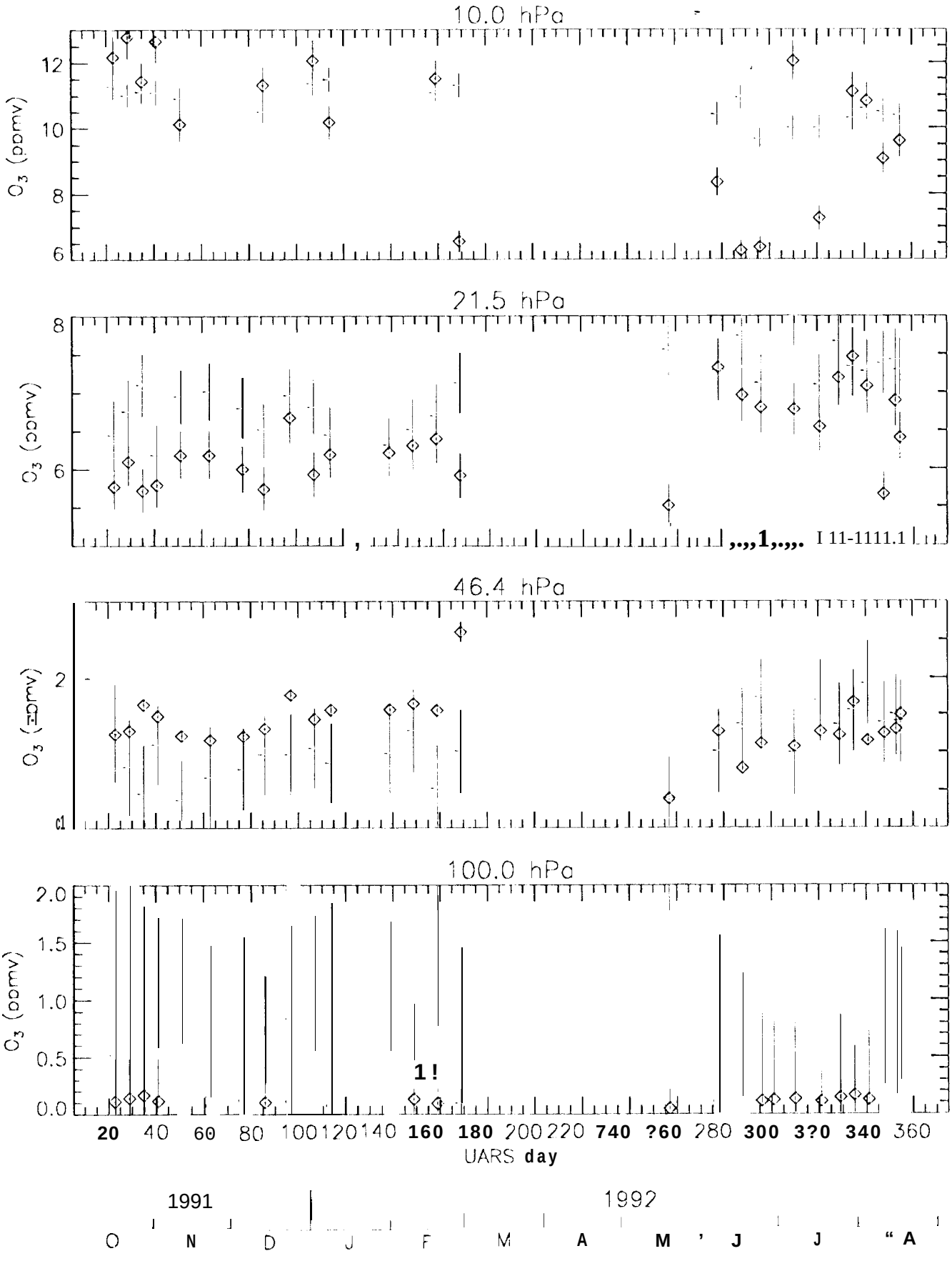
10.0 hPa
21.5 hPa
46.4 hPa
100.0 hPa
O3 (ppmv)
20 40 60 80 100 120 140 160 180 200 220 740 ?60 280 300 3?0 340 360
UARS day
1991
1992
O N D J F M A M ' J J " A

Fig. 33

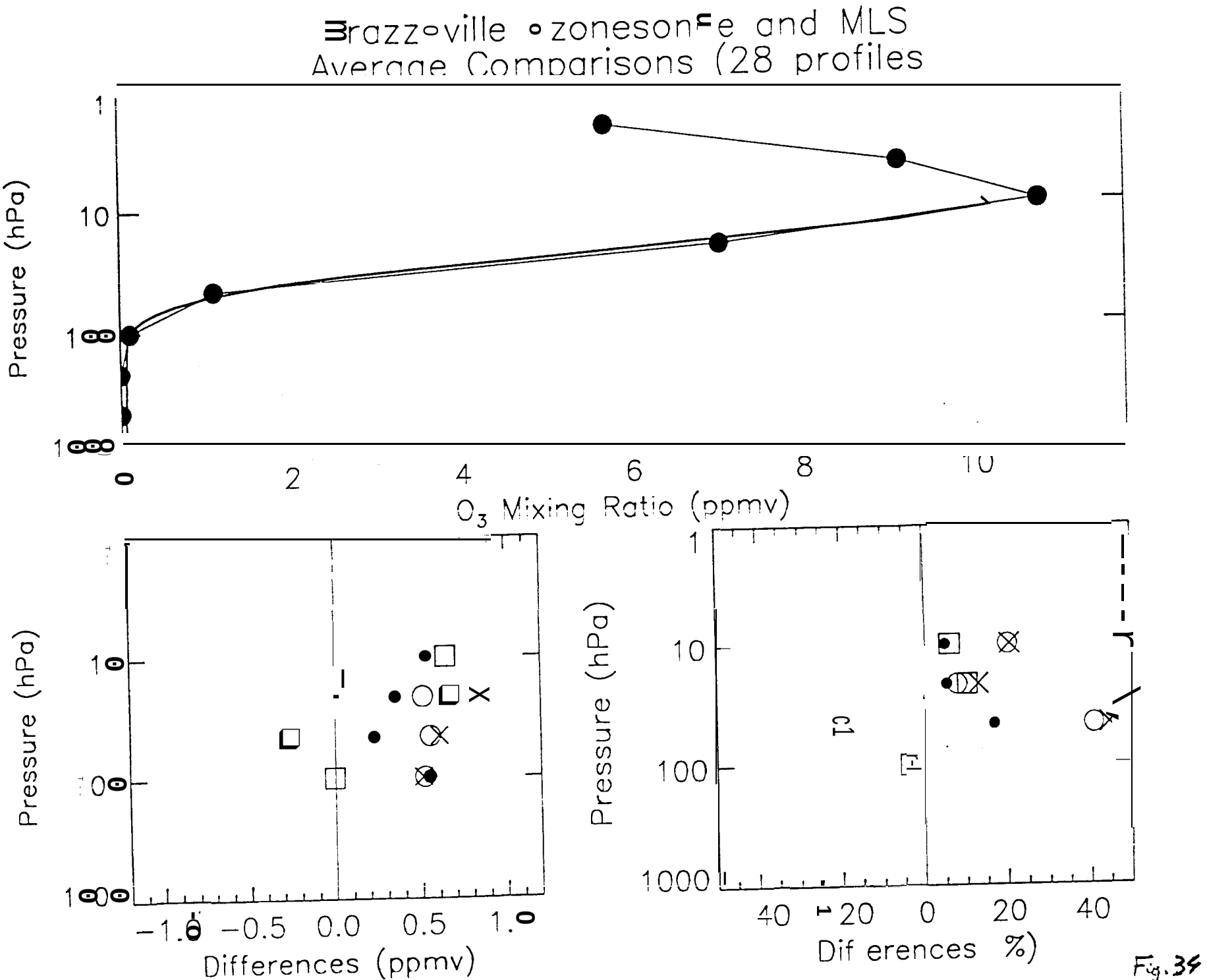
Brazzaville ozonesonde and MLS
Average Comparisons (28 profiles
Pressure (hPa)
1
10
100
1000
0
2
4
6
8
10
$O_3$ Mixing Ratio (ppmv)
Pressure (hPa)
Differences (ppmv)
−1.0
−0.5
0.0
0.5
1.0
Pressure (hPa)
Differences %)
40
20
0
20
40

Fig. 34

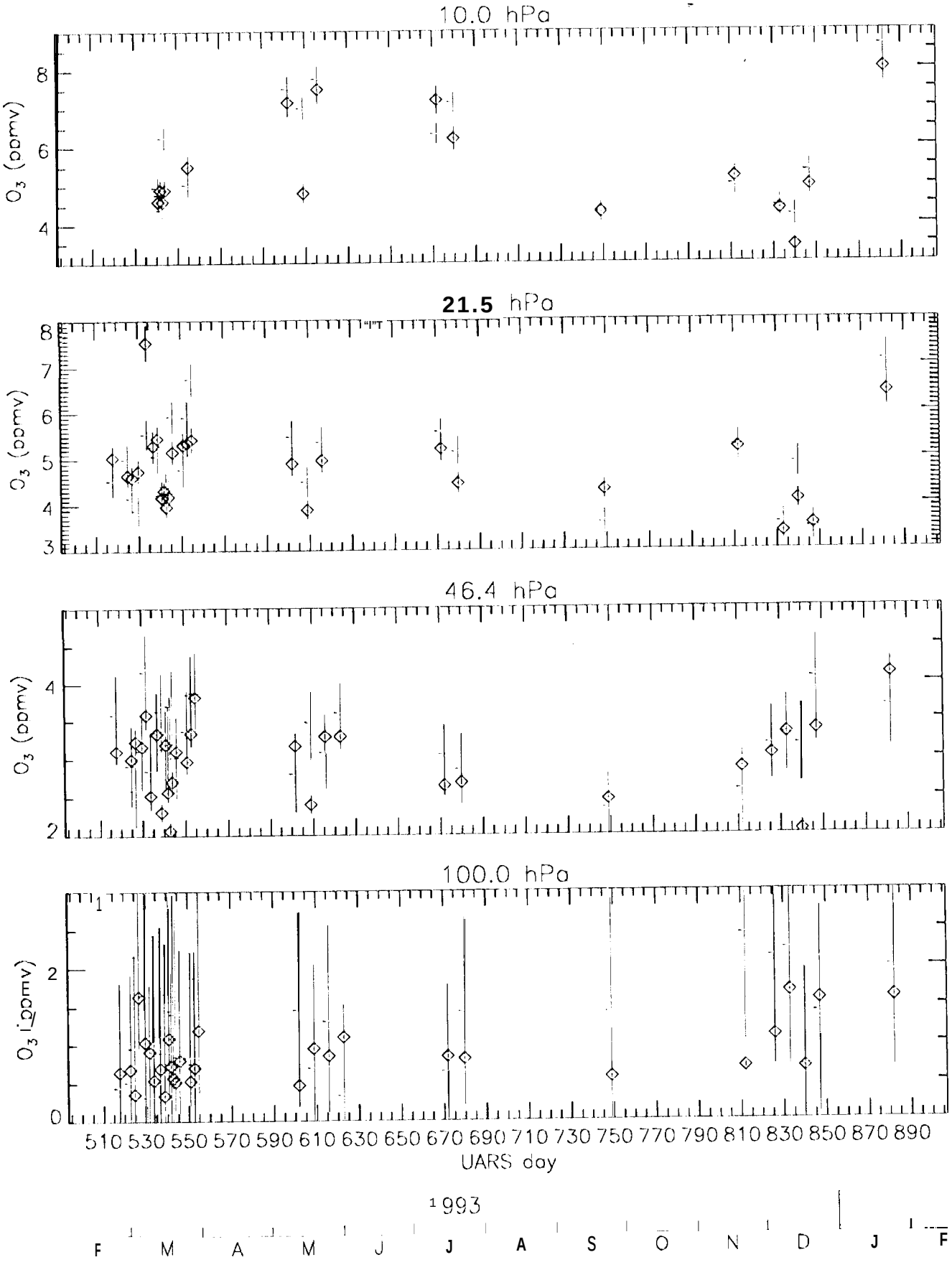
10.0 hPa
21.5 hPa
46.4 hPa
100.0 hPa
O3 (ppmv)
O3 (ppmv)
O3 (ppmv)
O3 (ppmv)
510 530 550 570 590 610 630 650 670 690 710 730 750 770 790 810 830 850 870 890
UARS day
1993
F M A M J J A S O N D J F

Fig. 35

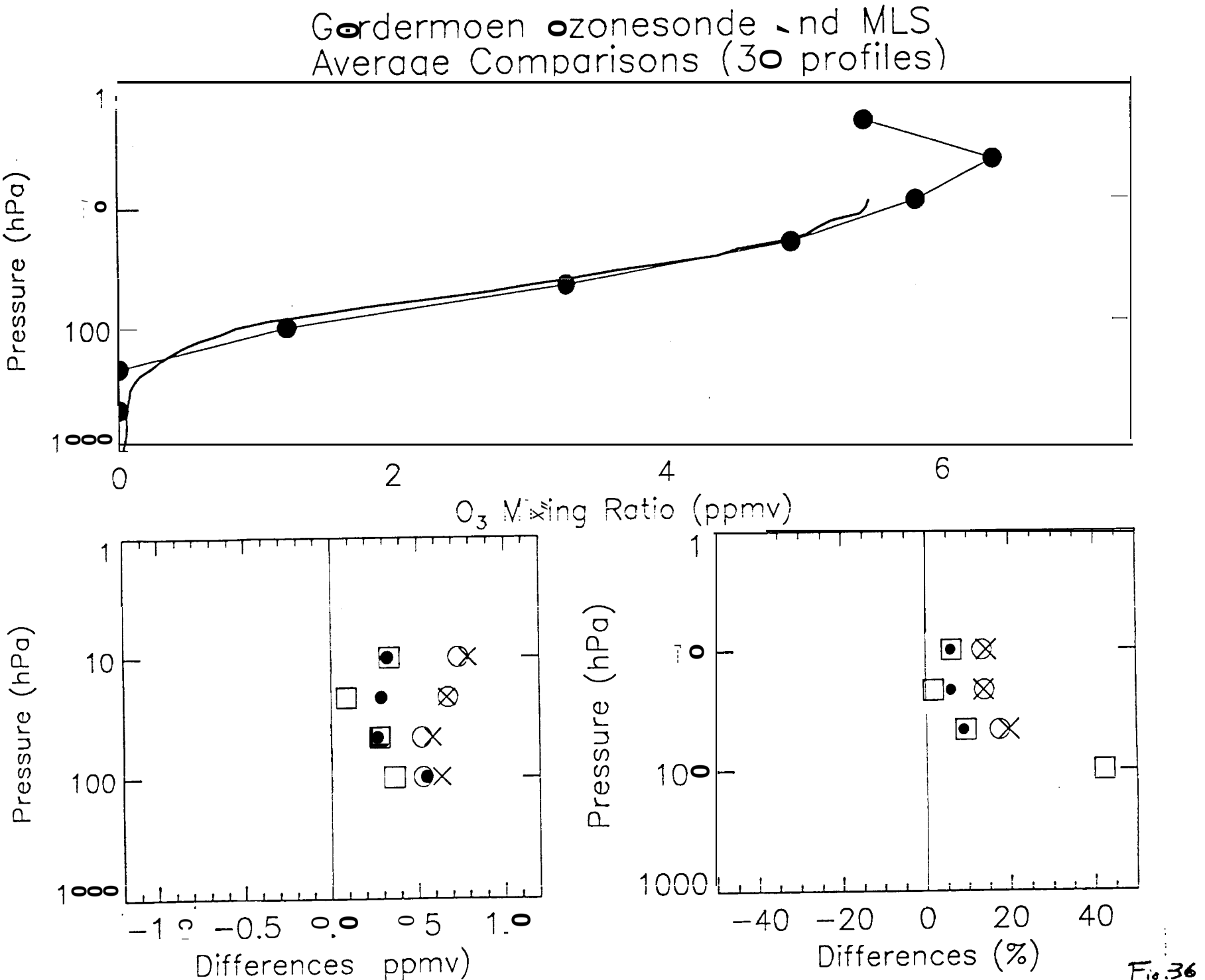
Gardermoen ozonesonde and MLS
Average Comparisons (30 profiles)
Pressure (hPa)
1
10
100
1000
0
2
4
6
O3 Mixing Ratio (ppmv)
Pressure (hPa)
Differences ppmv)
Pressure (hPa)
Differences (%)
-40
-20
0
20
40

Fig. 36

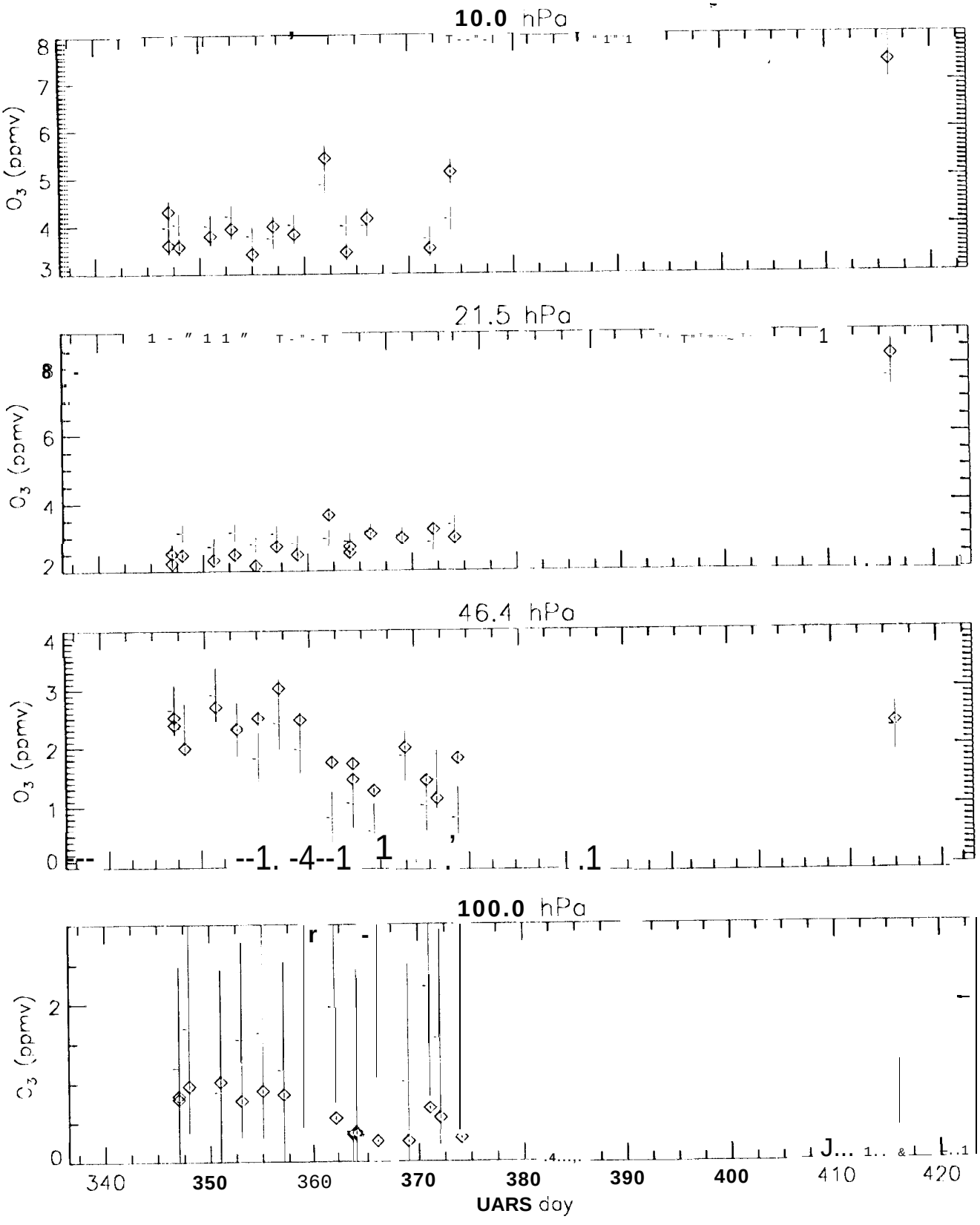


1992

S 0

Fig. 37

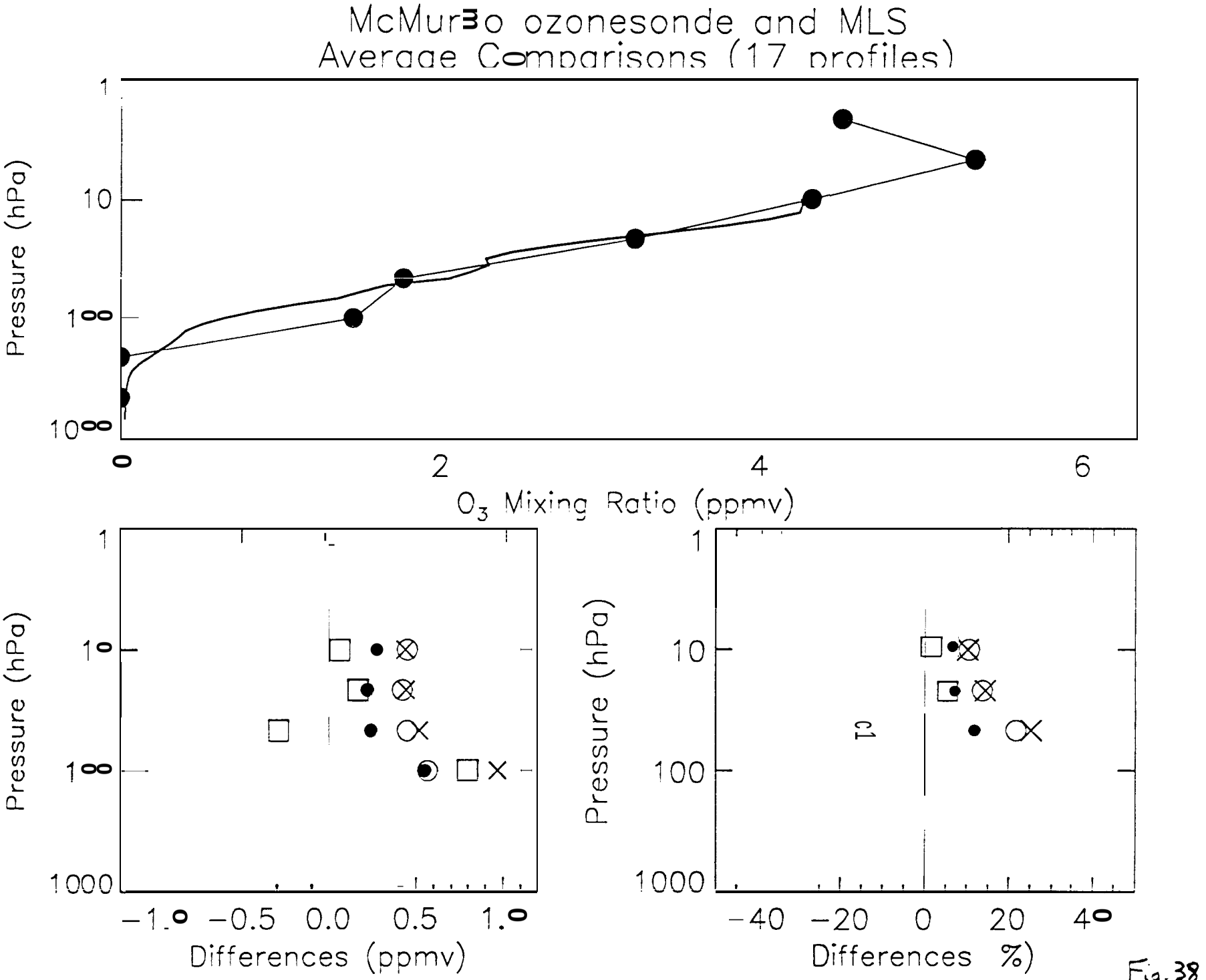
McMurdo ozonesonde and MLS
Average Comparisons (17 profiles)
Pressure (hPa)
1
10
100
1000
0
2
4
6
O3 Mixing Ratio (ppmv)
Pressure (hPa)
−1.0
−0.5
0.0
0.5
1.0
Differences (ppmv)
Pressure (hPa)
−40
−20
0
20
40
Differences %)

Fig. 38

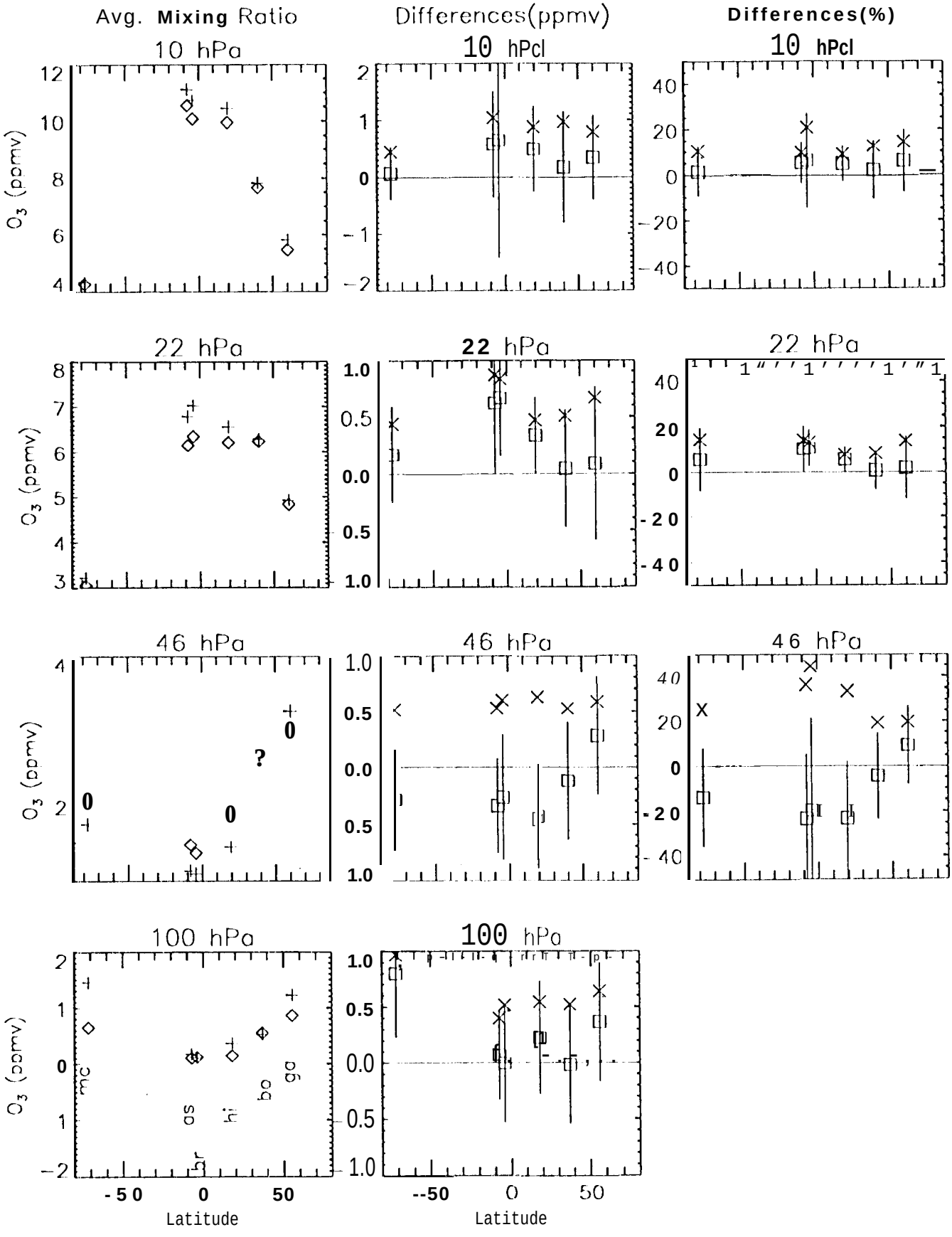
Avg. Mixing Ratio
Differences(ppmv)
Differences(%)
10 hPa
22 hPa
46 hPa
100 hPa
$O_3$ (ppmv)
Latitude
-50
0
50

Fig. 39

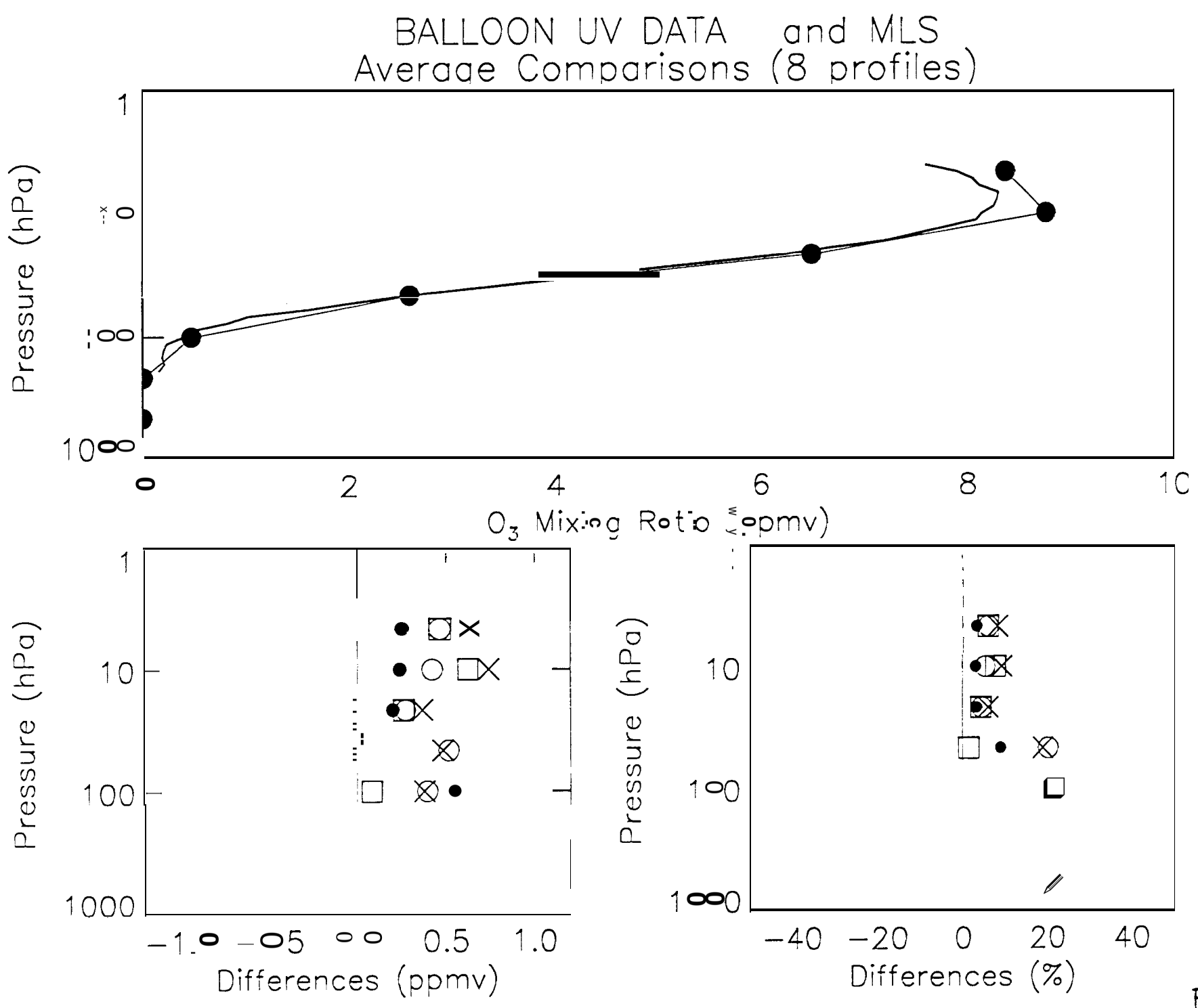
BALLOON UV DATA and MLS
Average Comparisons (8 profiles)
Pressure (hPa)
1
10
100
1000
0
2
4
6
8
10
O3 Mixing Ratio (ppmv)
Differences (ppmv)
-1.0
-0.5
0.0
0.5
1.0
Differences (%)
-40
-20
0
20
40

Fig. 40

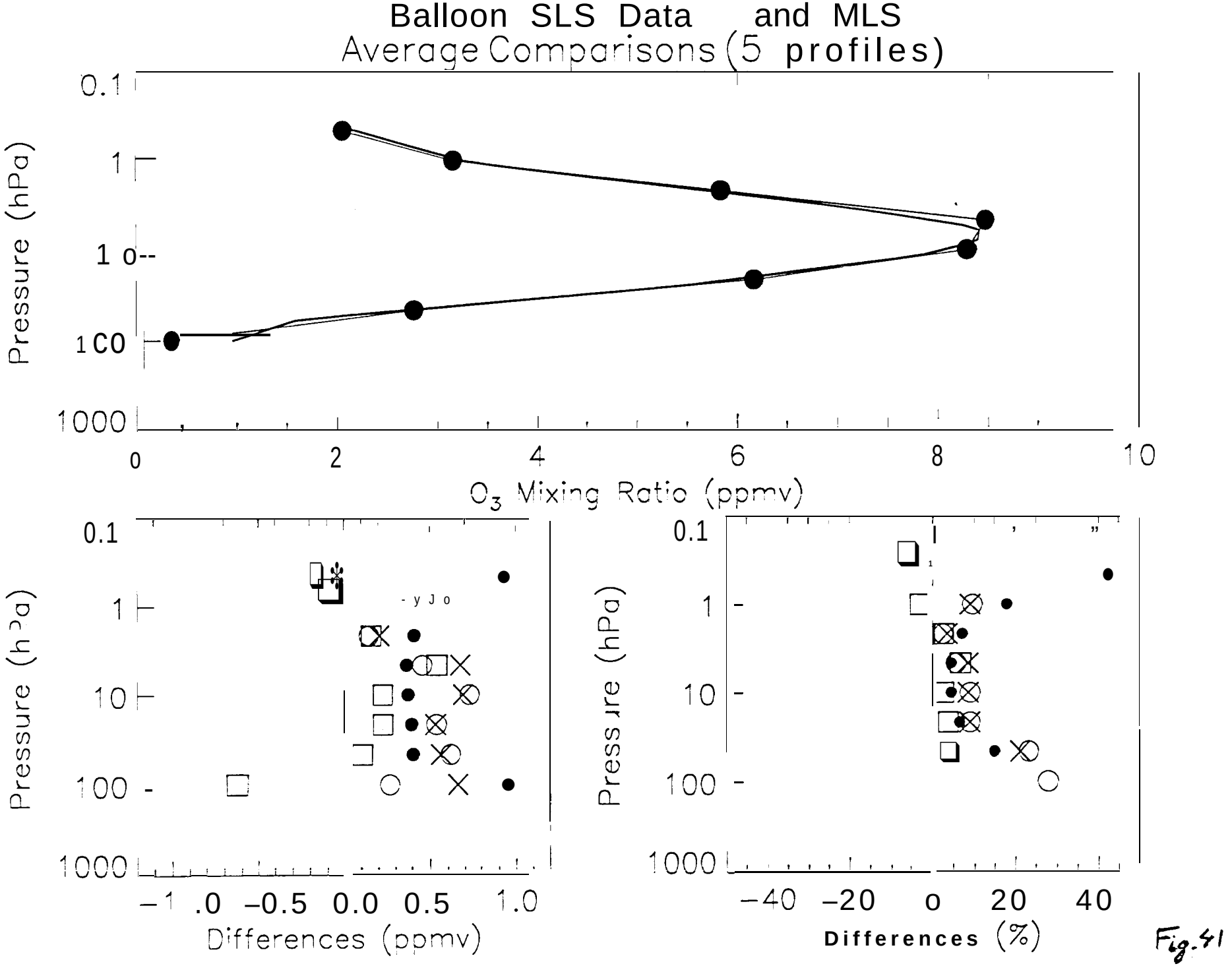
Balloon SLS Data and MLS
Average Comparisons (5 profiles)
Pressure (hPa)
0.1
1
10
100
1000
0
2
4
6
8
10
O3 Mixing Ratio (ppmv)
Pressure (hPa)
0.1
1
10
100
1000
-1.0
-0.5
0.0
0.5
1.0
Differences (ppmv)
Pressure (hPa)
0.1
1
10
100
1000
-40
-20
0
20
40
Differences (%)

Fig. 41

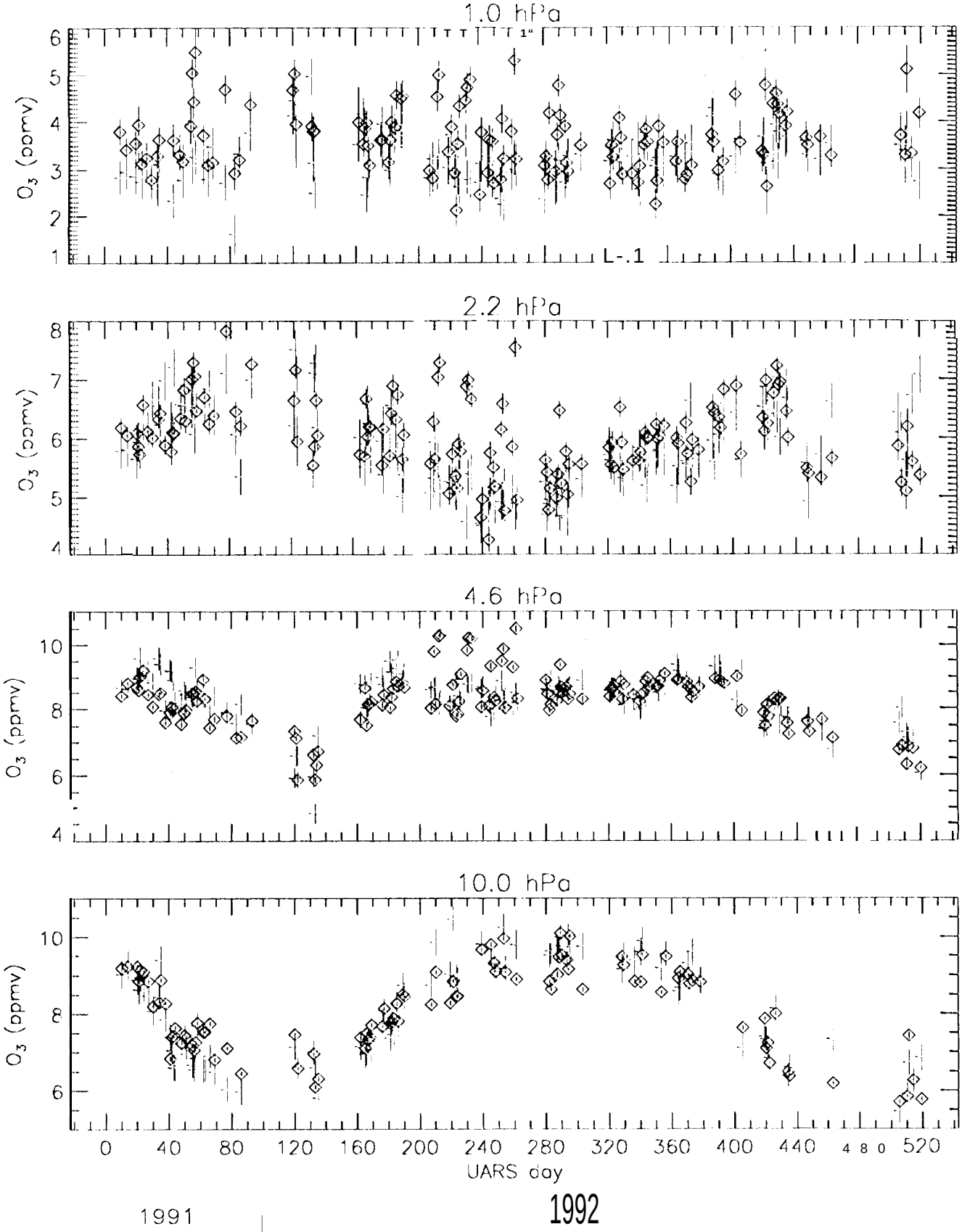
1.0 hPa
2.2 hPa
4.6 hPa
10.0 hPa
O3 (ppmv)
UARS day
0 40 80 120 160 200 240 280 320 360 400 440 480 520
1991
1992
S O N D J F M A M J J A S O N O J

Fig. 42

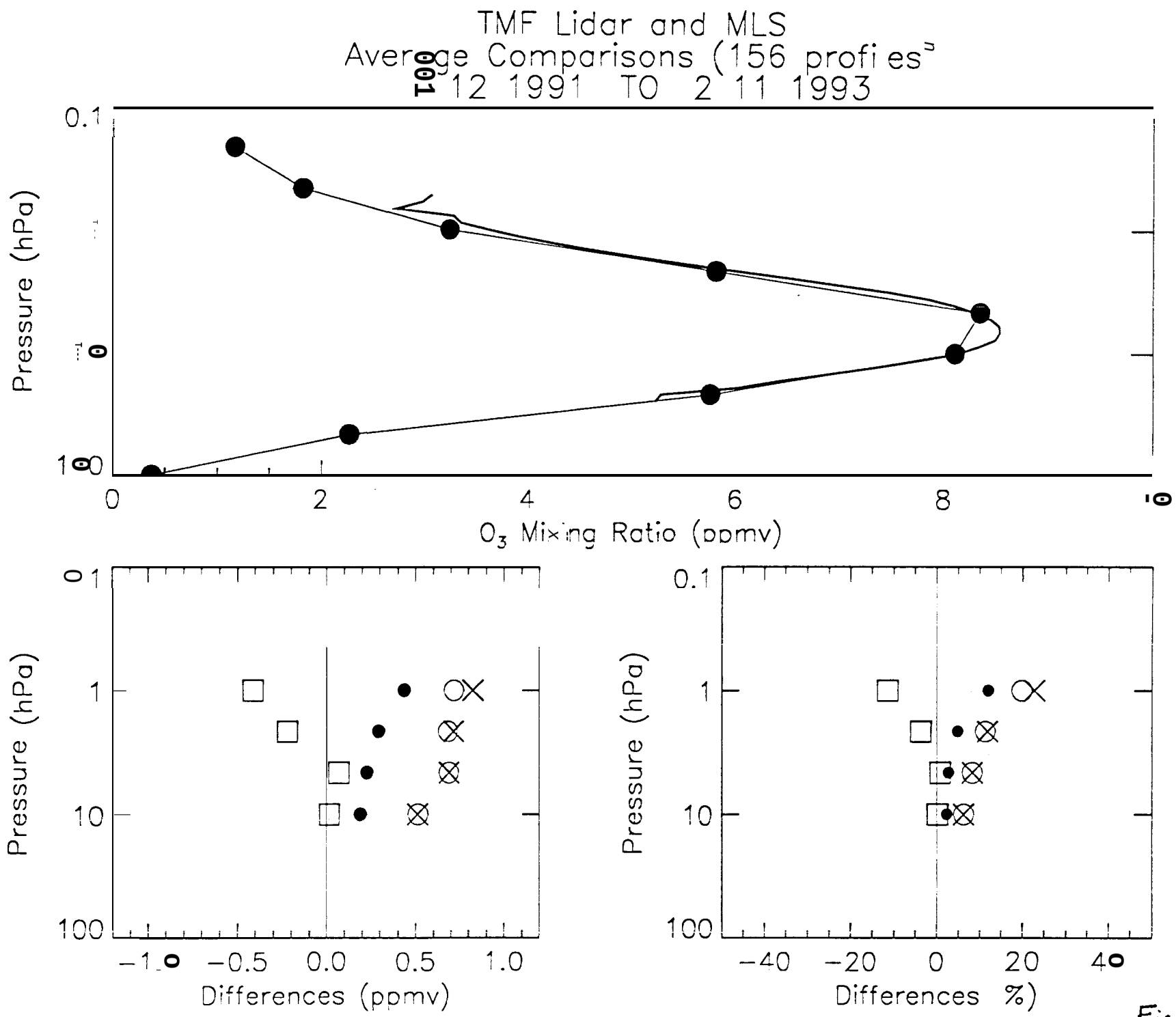
TMF Lidar and MLS
Average Comparisons (156 profiles)
12 1991 TO 2 11 1993
Pressure (hPa)
0.1
1
10
100
0
2
4
6
8
$O_3$ Mixing Ratio (ppmv)
Differences (ppmv)
−1.0
−0.5
0.0
0.5
1.0
Differences %)
−40
−20
0
20
40

Fig 43

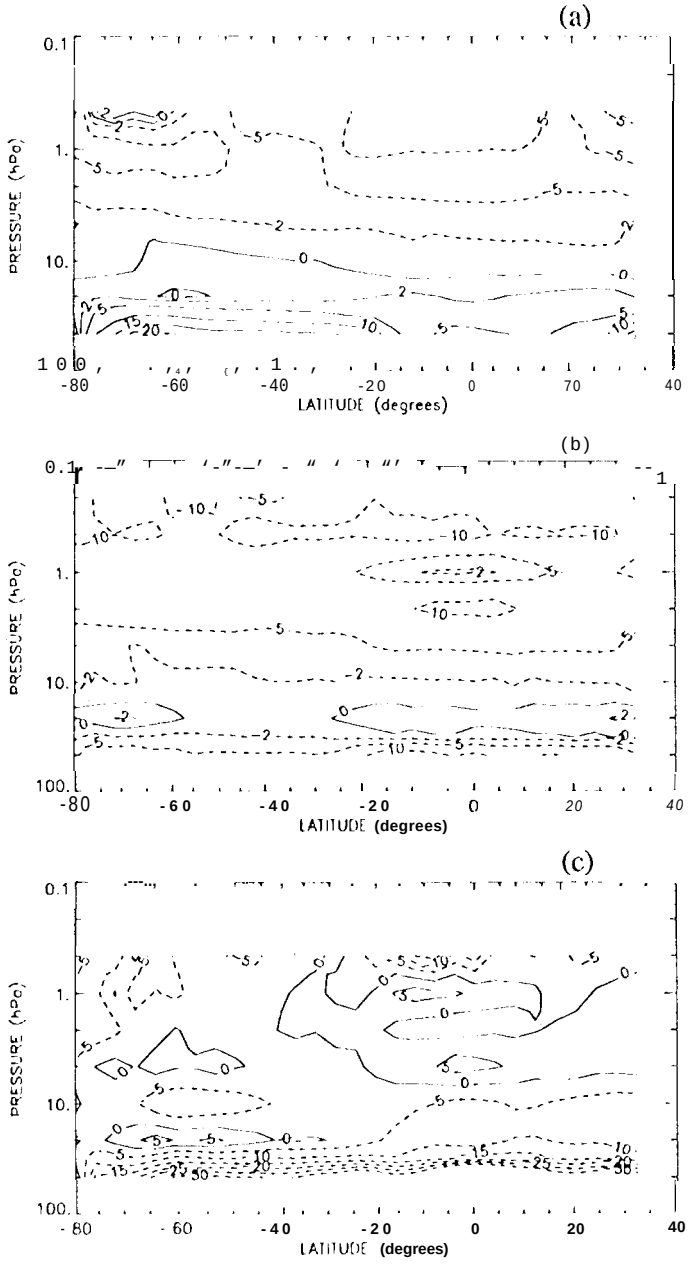
(a)
0.1
1.
10.
100.
PRESSURE (hPa)
-80
-60
-40
-20
0
70
40
LATITUDE (degrees)
(b)
0.1
1
1.
10.
100.
PRESSURE (hPa)
-80
-60
-40
-20
0
20
40
LATITUDE (degrees)
(c)
0.1
1.
10.
100.
PRESSURE (hPa)
-80
-60
-40
-20
0
20
40
LATITUDE (degrees)

Fig. 43

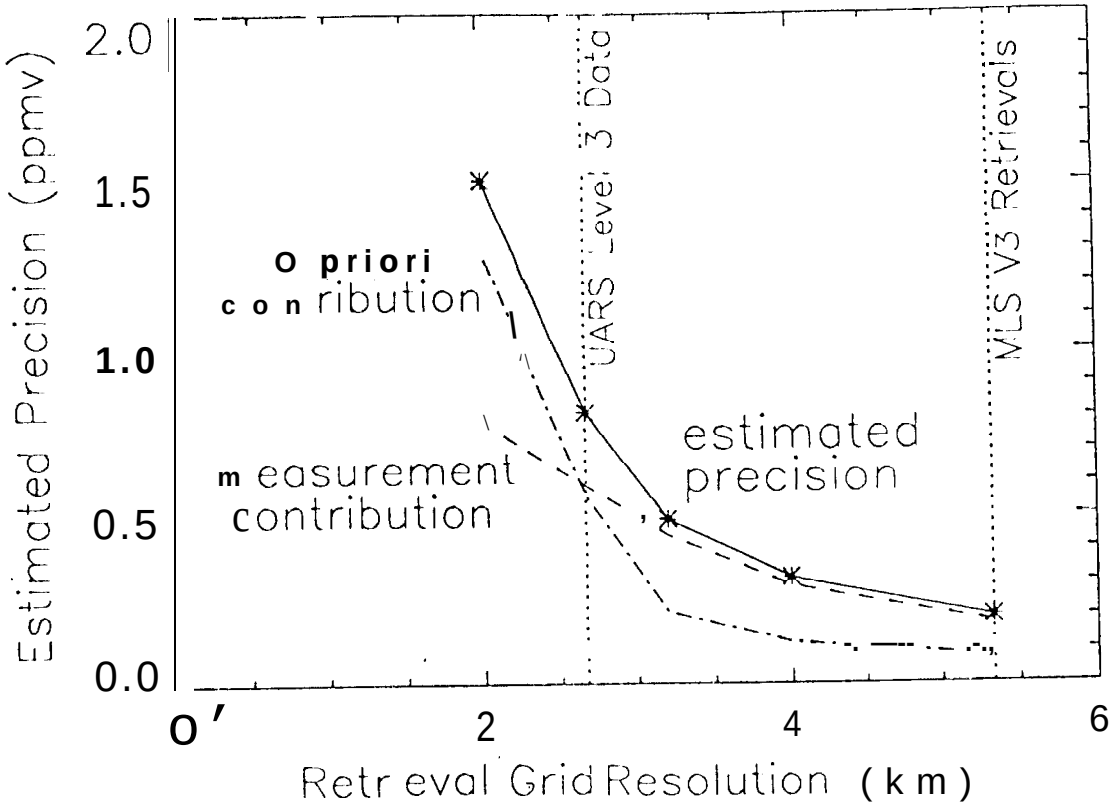
Estimated Precision (ppmv)
2.0
1.5
1.0
0.5
0.0
O priori
contribution
measurement
contribution
estimated
precision
UARS Level 3 Data
MLS V3 Retrievals
O'
2
4
6
Retrieval Grid Resolution (km)

Fig. 45